FINITE ELEMENT ANALYSIS OF

SHOCK AND FINITE-AMPLITUDE WAVES IN

HYPERELASTIC BODIES AT FINITE STRAIN

A THESIS

Presented to

The Faculty of the Division of Graduate

Studies and Research

By

Ronald Burett Fost

In Partial Fulfillment

of the Requirements for the Degree

Doctor of Philosophy

in the School of Engineering Mechanics

Georgia Institute of Technology

April, 1974

FINITE ELEMENT ANALYSIS OF

SHOCK AND FINITE-AMPLITUDE WAVES IN

HYPERELASTIC BODIES AT FINITE STRAIN

Approved:

J. T. Oden, Co-Chairman

C. E. Stoneking, Co-Chairman

R. W. Shreeves

C. V. Smith

Date approved by Chairmen: 4/8/74

To

Ronnie and Richie

ACKNOWLEDGEMENTS

I am deeply indebted to Professor J. T. Oden, who, after

suggesting the subject of this investigation, agreed to serve as the

off-campus thesis advisor and made available the funds which

financed the research. His valuable and untiring guidance, support,

and encouragement is sincerely appreciated.

I want to also express my gratitude to my campus advisor,

Professor C. E. Stoneking, without whose support, advice, and

guidance, my graduate work at Georgia Tech might not have been

possible.

Special thanks are due to J. E. Key who generously denoted his

time and knowledge to the major programming for the membrane

problems. I also appreciate the fine programming of M. Bishop

during the formulation of one-dimensional problems.

I am grateful for the encouragement received from several

faculty members and colleagues during the course of this work. Of

particular benefit were the comments and suggestions of Professors

J. M. Anderson, W. W. King, R. W. Shreeves, C. V. Smith, A. L.

Mullikin, and G. A. Wempner and the valuable discussions with

Dr. J. N. Reddy and L. C. Wellford. Also, I appreciate the support

of the entire Missiles Department personnel at Teledyne Brown

Engineering, particularly R. C. Kolyer, Dr. Manu Patel, and
J. F. Jenkins.

I want to give special acknowledgement to the Aerospace Support
Division Publications Staff at Teledyne Brown Engineering,
particularly Brenda Garlough and Doris Cantrell, who did such a
fantastic job of typing this manuscript.

Lastly, I thank those to whom this thesis is dedicated, who,
when the theory became too deep and the equations too long, took
their daddy out to play.

R. B. F.

TABLE OF CONTENTS

TABLE OF CONTENTS (Concluded)

LIST OF ILLUSTRATIONS

LIST OF ILLUSTRATIONS (Concluded)

NOTATION AND SYMBOL INDEX

Indicial notation and the summation convention are used throughout this work. In general, Greek indices are associated with local coordinate systems and range from 1 to 2. Latin indices range from 1 to 3. All symbols are defined when first introduced into the discussion. The most commonly used symbols are listed below; however, it has not been possible to adhere rigidly to these notations, so that sometimes these same letters are used for quantities other than those shown.

Chapter II

A, A_o	deformed and undeformed area
$\underset{\sim}{A}_\alpha$	vectors tangent to deformed midsurface coordinates X^1, X^2
C, C_o	deformed and undeformed configuration
d, d_o	deformed and undeformed membrane thickness
F_{oi}	components of body force per unit mass
$\underset{\sim}{G}_i$	base vectors tangent to deformed coordinate lines X^i
G_{ij}	components of Green's deformation tensor
h	hydrostatic pressure
I_1, I_2, I_3	principal invariants of G_{ij}
K	kinetic energy

$\hat{n}$, $\hat{n}_o$	unit normal vector in deformed and undeformed body
Q	heat input
q_i	components of heat flux
r	rate of heat supply
S_{oi}	components of surface force per unit undeformed area
$\underset{\sim}{t}$	stress vector
t^{ij}	components of symmetric Piola-Kirchhoff stress tensor
U	internal energy
u_i	displacement components of point on middle surface
v, v_o	deformed and undeformed volume
W	strain energy function
w_i	general displacement components
X^i	material coordinates
x_i	spatial coordinates
γ_{ij}	components of Lagrangian strain tensor
δ_{ij}, δ_β^α	Kronecker delta
ϵ	internal energy per unit mass
$\epsilon^{\alpha\beta}$	two-dimensional permutation symbol
λ	extension ratio of X^3
ρ, ρ_o	deformed and undeformed mass density
τ	time
Ω	mechanical power developed by external forces

Chapter III

A_O	undeformed cross-section area of rod
B, C	material constants
C_O	undeformed reference configuration
c	intrinsic wave speed relative to material
e	internal energy per unit volume
I_1, I_2, I_3	principal invariants of Green's deformation tensor
L_O	undeformed length of rod
$L_O-Y(t)$	all points along the rod except $Y(t)$
q	heat flux
S	surface of discontinuity
t_{CR}	time at which discontinuity forms
u	longitudinal displacement
v	absolute wave speed
v_O	undeformed volume
W	strain energy function
X	material coordinate
X_{CR}	location where discontinuity forms
x	fixed spatial coordinate
$Y(t)$	the particle X reached by wave front at time t
$y(t)$	spatial position of wave
γ	extensional strain

δ	internal dissipation
ϵ	belongs to, is a member of
θ	absolute temperature
λ	longitudinal extension ratio (stretch)
ξ	entropy per unit initial volume
ρ_0	undeformed mass density
σ	stress (first Piola-Kirchhoff)
φ	Helmholtz free energy
$[\![\, f \,]\!]_Y$	jump in $f(X, t)$ across $Y(t)$

Chapter IV

A_0	undeformed cross-section area of rod
c	intrinsic wave speed relative to material
E	total number of finite elements
$\mathscr{E}(0, L_0)$	energy space containing exact variational solution
$\mathscr{H}^1(0, L_0)$	Sobolev Space--the space of functions which, along with their first derivatives with respect to X, are square integrable on $(0, L_0)$
h	mesh length, length of typical element
h-Y	all points along the element except $Y(t)$
L_0	undeformed length of rod
$L_1(0, L_0)$	denotes functions which are integrable on $(0, L_0)$
m	mass of typical element
$m_{\alpha\beta}$	consistent mass matrix

P_N	global generalized force at node N
p_α	local generalized force at node α of the element
p^N	local generalized force on element N
q	stretch rate, $\dot{\lambda}$
S	surface of discontinuity
u	longitudinal displacement
u_N	longitudinal displacement of node N
v	velocity, $\dot{u}$
X	material coordinate
$Y(t)$	the particle X reached by wave front at time t
$\delta_{\alpha\beta}$	Kronecker delta
$\eta_N,\ \varphi_N$	basis functions (global)
λ	longitudinal extension ratio (stretch)
λ_N	longitudinal extension ratio at node N
σ	first Piola-Kirchhoff stress
ψ_α	local interpolation functions
$[\![f]\!]_Y$	jump in f(X, t) across Y(t)

Chapter V

C^i_{max}	maximum wave speed experienced in rod for all X at $t = i\Delta t$
E	total number of finite elements
$E(t)$	total energy of rod

E_n finite-element approximation of total energy

E^i interpolation error at $t = i\Delta t$

$\mathscr{E}^i$ difference between interpolant and finite-element solution at $t = i\Delta t$

$\mathscr{E}(0, L_0)$ energy space containing exact variational solution

e^i actual error in finite-element solution at $t = i\Delta t$

$\mathscr{F}$ finite element subspace of the solution space $\mathscr{E}(0, L_0)$

H internal energy

h minimum finite element length

h_N length of element N

i superscript denoting time increment

$\inf$ infimum, greatest lower bound

K kinetic energy

$\sup$ supremum, least upper bound

T first Piola-Kirchhoff stress : final time

Δt time increment

$U(X, t)$ finite element solution approximating $u(X, t)$

$\tilde{U}(X, t)$ finite element interpolant of $u(X, t)$

$U_N(t)$ nodal displacements of $U(X, t)$

$u(X, t)$ displacement, exact solution to equation of motion

W strain energy function

X material coordinate

Δ_t, ∇_t backward, forward difference operator

δ_t	first order central difference operator
δ_t^2	second order central difference operator
δ_N^M	Kronecker delta
ϵ	belongs to, is an element of
$\notin$	does not belong to
ν_α	constant depending upon mass representation
ψ_N	finite element basis functions
(a, b)	open interval with endpoints a and b
$[a, b]$	closed interval with endpoints a and b
$[a, b), (b, a]$	half-open intervals
$\langle u, v \rangle$	inner product of functions u and v
$\|u\|$	norm of u associated with $\langle u, u \rangle$

Chapter VI

A, A_0	deformed and undeformed area
A_0^*	undeformed middle surface area of element
C, C_0	deformed and undeformed configuration
C_1, C_2	Mooney material constants
$c_{N\alpha}$	node displacement coefficients
d, d_0	deformed and undeformed membrane thickness
d_i	components of rigid-body translation
E	total number of elements
(e)	element label

I_1, I_2, I_3 principal invariants of G_{ij}

m_0 total mass of element e

m_{NM} consistent mass matrix $(N_e \times N_e)$

N_e number of nodes for element e

P_{Ni} components of total generalized force at node N of element e

t^{ij} components of symmetric Kirchhoff stress tensor

u_i displacement components of middle surface in local coordinates

u_i^N node displacement components in local coordinates

v, v_0 deformed and undeformed volume

$X^i, X_{(e)}^i$ global and local material coordinates

$X_{N(e)}^i$ local coordinates of node N of element e

$x_i, x_{i(e)}$ global and local spatial coordinates

γ_{ij} components of Lagrangian strain tensor

$\delta_{\alpha\beta}, \delta^{\alpha\beta}$ Kronecker delta

$\epsilon^{\alpha\beta}$ two-dimensional permutation symbol

λ extension ratio of X^3

μ^N value of λ^2 at node N

ρ_0 undeformed mass density

ψ_N local interpolation functions

Appendix

C_1, C_2 Mooney material constants

c intrinsic wave speed relative to material

u exact solution of displacement equation of motion

$\bar{u}$ perturbed solution

ϵ perturbation about $u(X, t)$

λ longitudinal extension ratio

σ first Piola-Kirchhoff stress

SUMMARY

The purpose of this investigation is to study numerically the
dynamic response of a class of elastic bodies at finite strain. More
specifically, new numerical schemes are developed for the analysis
of shock and acceleration waves and finite-amplitude oscillations of
thin highly elastic membranes of arbitrary shape. Finite-element
models of thin incompressible hyperelastic membranes are developed,
which involve large systems of second-order nonlinear differential
equations in nodal displacements or principal stretches. One-
dimensional versions of these equations are first solved numerically
using a variety of time integration schemes. Qualitative arguments
and studies of various cases confirm that shock waves can develop,
even in cases in which smooth initial data are prescribed. In the
presence of shocks, all of the standard integration schemes break
down, and it is necessary to develop an explicit scheme for shock
propagation studies. A new scheme is proposed which combines
features of the Lax-Wendroff method and finite-elements and which
is used successfully to study the formation, reflection, and propa-
gation of shock and acceleration waves in hyperelastic rods. A
number of representative cases are studied numerically. Motivated
by the absence of any convergence criteria or numerical stability

criteria for finite-element approximations of nonlinear hyperbolic

equations, a study of these questions for the subject class of problems

is then initiated. A rigorous analysis of numerical stability and

convergence of finite-element approximations of nonlinear equations

is given. Precise stability criteria and error estimates are derived.

It is shown that while lumped and consistent mass finite-element

models have the same convergence rate in the natural energy norms,

the lumped mass model is numerically more stable. The investi-

gation then moves to two- and three-dimensional problems. A

number of cases are considered apparently representing the first

solutions of any type to problems of this kind.

CHAPTER I

INTRODUCTION

The foundations of the general theory of elasticity were laid down in the nineteenth century in the works of Cauchy, Green, and St. Venant and, thereafter, the bulk of the work on the subject dealt with the important but restricted theory involving linear constitutive equations for stress and infinitesimal strains. Renewed interest in the general theory began in the early post-World War II years with the works of Rivlin, et al. [1, 2] and Truesdell [3], and others. The former work was motivated by pressing problems of that period in the pneumatic tire industry and involved solutions to static problems of simple shear and extension of cubes and prisms of isotropic, incompressible rubbers.

Over two decades have passed since the modern work on finite elasticity began, and in no other period in history has there been a greater awareness of the need for the general theory in applications affecting our everyday life. Besides the "old" problems related to finite deformations of tires and innertubes, there has been considerable interest in recent years in the use of both inflatable membrane structures and highly flexible pneumatic structures in aerospace and

and civil applications. Some of these structures may undergo finite deformations both before and after acquiring their primary load-carrying capacity. For example, as a fail-safe component, a membrane is first inflated and then expected to sustain large impact loads--sometimes to the point of failure.

Ironically, while the bulk of the phenomena mentioned is dynamic in nature, there are no general solutions to transient dynamic problems in finite elasticity. (In 1971, Shahinpoor and Nowinski [4] did, however, obtain explicit exact solutions for the restricted problem of determining the one-dimensional (radial) displacement field in a thin-walled tube of incompressible Mooney-Rivlin material, subjected to forced finite radial oscillations generated by arbitrary time-dependent pressures.) This unusual state of affairs is due, of course, to the overwhelming complexity of the highly nonlinear equations governing dynamic finite elasticity. For example, when a thin elastic membrane is subjected to a time-dependent lateral pressure, strains very much greater than unity are usually incurred, and the associated finite-amplitude response waves may develop discontinuities, or shocks. Moreover, since the loading surfaces change in area and orientation during deformation, the directions and magnitudes of the applied loads also change, and classical superposition concepts are not valid.

Since the solution of general problems of this type falls well outside the realm of classical methods of mathematical analysis, it is clear that the greatest hope for obtaining quantitative solutions to problems in dynamic finite elasticity rests in the efficient use of modern numerical methods.

1.1 Finite Element Concept and History

Regardless of the concepts employed in formulating the non-linear elasticity problem, if numerical methods are used to get quantative results, the continuum has, in effect, been approximated by a discrete model in the solution process. A logical alternative to this classic approach is to represent the continuum by a consistent discrete model at the onset. This approach is referred to as the finite element method. Based on concepts of piecewise approximations, and specifically designed for computer applications, this method frees the analyst from complications caused by irregular geometries and boundary conditions. Also, the method appeals to our physical intuition: we isolate a small physical element of the continuum, approximate the displacement, temperature, or stress fields over the element uniquely in terms of some generalized coordinates (usually taken as nodal quantities pertaining to the field), and then, using all of the principles of mechanics and thermodynamics at our disposal, describe the behavior of this typical element of the system.

This done, these elements are appropriately fitted together to constitute the discrete model of the continuum.

Although Courant's 1943 analysis [5] was clearly in the spirit of finite elements, the formal application of the finite element method, together with the direct-stiffness approach for assembling elements, was presented in 1956 in the now well-known paper of Turner, Clough, Martin, and Topp [6]. Since then, a preponderance of literature related to the subject has appeared. Extensive references to previous works on applications to linear problems can be found in the books of Zienkiewicz [7, 8], Przemieniecki [9], Martin [10], Przemieniecki, et al. [11], and Berke, et al. [12], and in the survey articles of Argyris [13, 14], Singhal [15], and Felippa and Clough [16]. As would be expected, applications of the finite element method to nonlinear problems have not enjoyed the same frequency of appearance. A detailed list of references on finite element applications in nonlinear problems can be found in the book by Oden [17] and his survey article [18]. Additional references may be found in the books edited by Gallagher, et al. [19] and Oden, et al. [20].

1.2 Dynamic Finite Elasticity--Vibrations

That only recently has there been any interest in the dynamic theory of finite elasticity is evidenced by the first study of steady-state motion in this class of problems appearing in 1960. In this

paper, Knowles [21] considered the problem of arbitrary amplitude free oscillations of a tube of incompressible material. Knowles extended this investigation to include forced oscillations [22], and then, with Jakub [23], examined finite deformations of an infinite elastic medium with a spherical cavity. (Truesdell [24] mentions that Tadjbakhsh and Toupin have pointed out that in [21] the formulation was faulty due to a misuse of convected coordinates; however, the basic differential equation of motion used therein is correct.) Knowles's work served as the basis for several subsequent investigations of both thick- and thin-walled bodies of symmetry [25-28]. In fact, the previously mentioned work of Shahinpoor and Nowinski [4] involved a simplified version of Knowles's governing equation. Apparently, the only other type of finite-amplitude vibration problem to receive attention is that of finite simple shear (e.g., [29-32]).

Using the theory of small elastic deformations superimposed on finite elastic deformations (e.g., [33, 34]), other investigations into dynamic problems of elasticity with constant finite strains have been made (e.g., [35-38]). Douglas [39] studied the effect of initial finite deformation on the subsequent natural small vibrations of some simple elastic structures of incompressible material. An interesting application of this theory was employed by Faulkner [40] wherein the small displacement reflects the small amount of compressibility introduced into the standard incompressible mathematical model.

1.3 Dynamic Finite Elasticity--Nonlinear Wave Motion

In conjunction with the recent developments in the theory of finite amplitude vibrations, there has also been a growing interest in the propagation of finite amplitude waves in elastic materials. Basically, the study of nonlinear wave motion is concerned with systems of hyperbolic partial differential equations, the mathematical foundation of which is well established, e.g., see the books of Courant and Hilbert [41] and Jeffrey and Taniuti [42]. Also, an elementary account of the basic developments in the theory of finite elastic waves is contained in the book by Bland [43].

The early work of Bland [44] and Chu [45] sparked much of the current interest in the propagation of shock and acceleration waves in elastic materials. Solutions of simple boundary and initial value problems for an elastic half-space subjected to a gradually applied surface disturbance were obtained in both [44] and [45]; they also studied the conditions for shock formation and propagation. Similar elastic solid problems were considered by Collins [46] and Achenbach, et al. [47, 48], with a problem of a heterogeneous elastic solid recently investigated by Nair and Nemat-Nasser [49].

Nowinski [50] apparently was the first to qualitatively study the propagation of finite waves in thin perfectly elastic rods of rubber-like materials. The propagation of simple waves which develop into

shocks was initially studied by Reddy and Achenbach [51] for the case of a thin semi-infinite prestressed elastic rod. In recent months, survey articles on shocks have been contributed by Lax [52] and Chen [53]; additional references can be found in these articles.

From the foregoing, it is clear that, while many noteworthy contributions have been made to the general dynamical theory of finite elasticity, actual calculations have invariably involved rather ideal geometries, boundary and initial conditions, and/or material properties. The highly nonlinear character of the momentum equations for the most simple hyperelastic material does not account for all of the computational problems--by definition, the hyperelastic solid possesses no dissipative mechanism to provide smoothing or damping of higher frequencies. Consequently, the computationally convenient features of damping encountered in nonlinear viscoelasticity and thermoviscoelasticity calculations [17, 54, 55] are not present. To complicate matters, it is now generally recognized that shock waves can be easily produced in such materials, even when smooth initial conditions are prescribed. The recent experimental work of Kolsky [56] gives evidence to the possibility of even tensile shock waves developing in certain stretched natural rubbers, a phenomenon already anticipated in the theoretical work of Bland [44] and Chu [45]. In such cases, practically all the popular numerical integration schemes now used in structural dynamics are ineffective.

1.4 Finite Element Approximations

Fortunately, developments in nonlinear theories of material response have been accompanied by significant developments in large-scale digital computers and general methods of numerical analysis. Using these tools, the numerical solution of certain static problems in finite elasticity has been possible during the last five years.

The finite element method was successfully applied to the problem of finite deformation of thin elastic membranes by Oden, et al. [57-60]. These studies were primarily concerned with Mooney-type materials (corresponding to a natural rubber-like material) for computational purposes, but also give specific forms of the nonlinear stiffness relations for general hyperleastic membranes. Since, for incompressible materials (e. g., the Mooney material), the deformation determines the stress only to within an arbitrary hydrostatic pressure, the pressure must be treated as an additional unknown in the general finite element problem formulation. For the membrane formulation, however, this problem is avoided by assuming a state of plane stress in the deformed element so that the hydrostatic pressure for each element is immediately determined from the condition that the transverse normal stress is zero.

In very recent times, there have begun to appear some applications of the finite element method to problems in nonlinear structural dynamics. For example, Stricklin, et al. [61] considered large

rotations but infinitesimal strains of dynamically loaded shells of revolution, while the dynamic response of geometrically and materially nonlinear shells was treated by Marcal [62], Hartzman [63] and Oden, Chung, and Key [64], among others. None of these investigations confronts the nonlinear dynamic problem of finite deformations in which exceedingly large changes in geometry may occur; nor do they account for the possibility of finite strains. Moreover, the few attempts at using finite element models in nonlinear structural dynamics problems seem to either avoid the obvious but difficult questions of convergence of the finite element approximation and stability of the temporal integration schemes, or to make rather vague convergence and stability arguments on the basis of nothing more than numerical experimentation.

1.5 Synopsis

So as to provide a basis for discussion and to establish notation, Chapter II contains a brief review of basic notions of finite elasticity relevant to the study of elastic membranes. Also, specific forms of the strain energy function are given for several highly elastic materials. Attention is then temporarily directed to one-dimensional problems. In Chapter III, we review certain features of the physics of the propagation of shock and acceleration waves in nonlinear hyperelastic materials. Then, in Chapter IV, one-dimensional finite-element

models are developed and solved numerically using a variety of time-integration schemes. Since virtually all of the commonly used explicit time-integration schemes break down in the presence of shocks, a new explicit integration scheme is developed and used successfully in studying the formation, propagation, and reflection of shock waves in hyperelastic thin rods. Motivated by the absence of any convergence and stability criteria for finite element approximations of nonlinear hyperbolic equations, these questions are studied in Chapter V for the subject class of problems. A rigorous analysis of numerical stability and convergence of finite element approximations of nonlinear hyperbolic equations is made wherein precise stability criteria and error estimates are derived. It is shown that while lumped and consistent mass finite-element models have the same convergence rate in the natural energy norms, the lumped mass model is numerically more stable. The investigation returns to two- and three-dimensional problems in Chapter VI where, after a discussion of the general concept of finite elements of membranes, finite element models of thin incompressible hyperelastic membranes are developed. A number of cases are considered, apparently representing the first solutions of any type of problems of this kind. Chapter VII summarizes the work done in this investigation and the conclusions drawn therefrom. Recommendations for future study and investigation are also presented.

CHAPTER II

MECHANICAL PRELIMINARIES

In this chapter, we briefly review certain fundamental principles

of kinematics, mechanics, and thermodynamics necessary to obtain

general constitutive relations and equations of motion pertinent to the

theory of elastic membranes. More complete details can be found in

the books of Green and Zerna [65], Green and Adkins [34], and

Oden [17].

2.1 Kinematics of Elastic Membranes

Consider a continuous elastic body which is in some reference

configuration C_o. To describe the motion of this body relative to C_o,

a rectangular cartesian coordinate system X^i with origin O is

established. At time $\tau = t$ $(0 \leq \tau \leq t)$, the motion of the body has

carried it to a new configuration C, and a representative material

point P_o has moved to P. The point P in C is now referred to a new

fixed rectangular coordinate system $x_i(\tau)$ with origin o, which is taken

coincident with O at $\tau = 0$. Thus, the cartesian coordinates of a

material point at any time τ are $x_i(\tau)$, and at $\tau = 0$ the coordinates

$x_i(\tau)$ and X^i coincide, i.e., $x_i(0) = X^i$. It will be convenient to refer

to the body as undeformed when it occupies the reference configuration C_o and as deformed in other configurations.

Each triple of real numbers X^i may be considered as the intrinsic particle label (or the name) assigned to the corresponding material point in the body. Thus the same numerical values of the X^i which define a material point in C_o define the same point in any subsequent C. (It is assumed that the required functional dependency of the x_i on the X^i and time exists, and vice-versa.) These labels may be considered to be coordinates etched onto the body so that they move continuously with the body as it passes from C_o to any subsequent C. Hence, while coordinates X^i are cartesian in C_o, they are generally curvilinear in C. Moreover, straight lines of material points in C_o become curved lines in C, and coordinate planes in C_o become curved surfaces in C. Such coordinates are called convected or intrinsic coordinates.

Now consider in particular a thin sheet of homogeneous elastic material, bounded by the surfaces $X^3 = \pm d_o/2$, where the initial thickness d_o is, in general, a function of X^1 and X^2. In the undeformed sheet, considered initially flat, an arbitrary material point P_o is located by the position vector

$$\underset{\sim}{r} = \underset{\sim}{r}_o(X^1, X^2) + X^3 \hat{n}_o \tag{2.1}$$

where $\underset{\sim}{r}_0(X^1, X^2)$ is the position vector of a point Q_0 in the X^1, X^2 plane and $\hat{n}_0$ is a unit vector normal to the undeformed middle surface (see Fig. 1).

The sheet is now assumed to undergo a general displacement which carries it from its reference configuration C_0 to another configuration C. (This displacement carries P_0 to P and Q_0 to Q.) The location of P relative to a fixed reference frame in C_0 is given by the position vector

$$\underset{\sim}{R} = \underset{\sim}{R}_0(X^1, X^2, t) + \underset{\sim}{M}(X^1, X^2, X^3, t) \tag{2.2}$$

where $\underset{\sim}{R}_0$ is the position vector of Q on the deformed middle surface and $\underset{\sim}{M}$ is the vector from Q to P. The displacement vector $\underset{\sim}{w}$ of P is

$$\underset{\sim}{w} = \underset{\sim}{R} - \underset{\sim}{r} = \underset{\sim}{u} + \underset{\sim}{M} - X^3\hat{n}_0 \tag{2.3}$$

where $\underset{\sim}{u}$ denotes the displacement of a point on the middle surface

$$\underset{\sim}{u} = \underset{\sim}{u}(X^1, X^2, t) = \underset{\sim}{R}_0(X^1, X^2, t) - \underset{\sim}{r}_0(X^1, X^2) \tag{2.4}$$

With (2.2) we can now calculate the base vectors $\underset{\sim}{G}_i$ tangent to the deformed coordinate lines X^i.
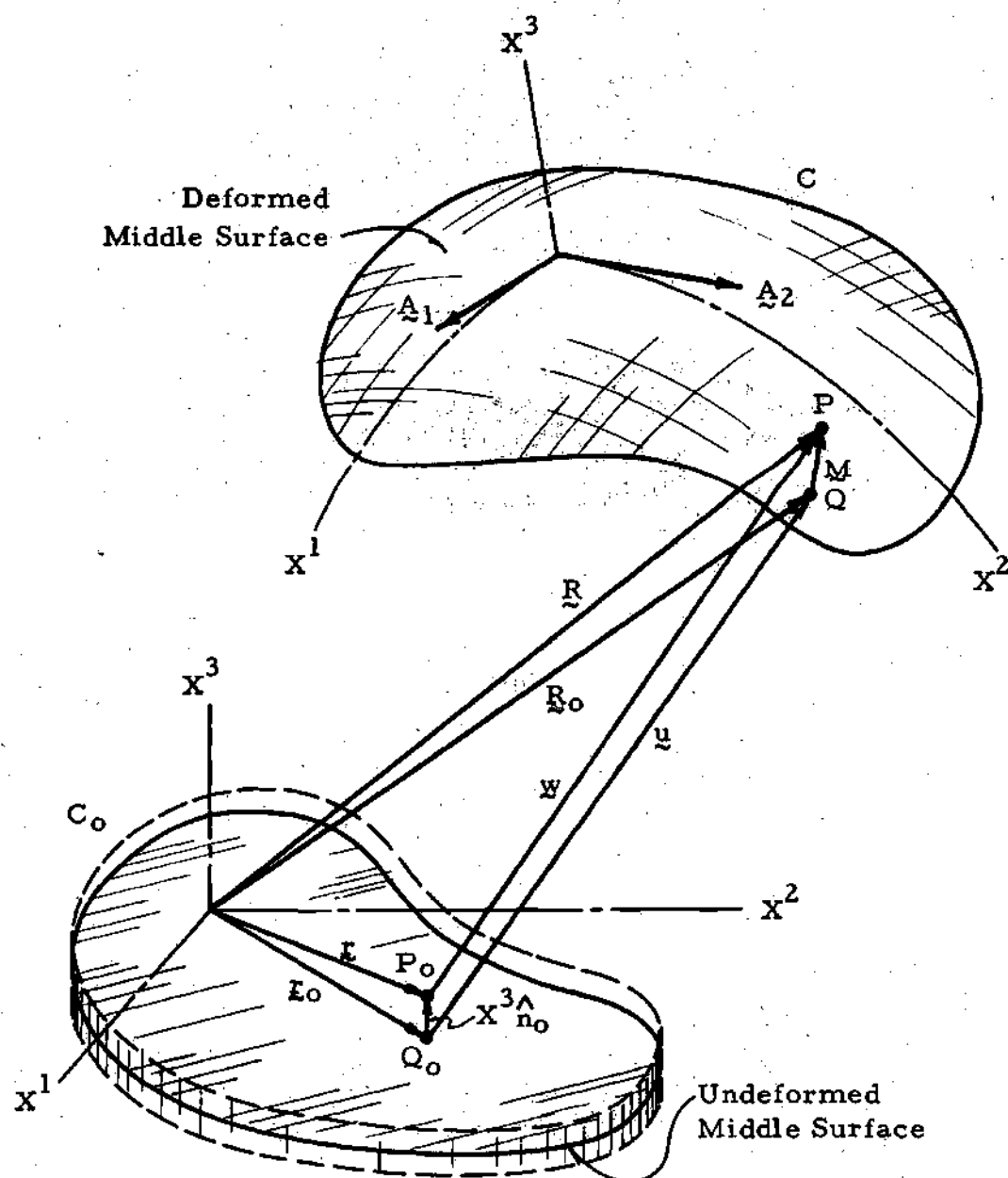
Figure 1.   Geometry of Deformation of a Thin Sheet

$$\underset{\sim}{G}_\alpha = \underset{\sim}{R},_\alpha = \underset{\sim}{R}_o,_\alpha + \underset{\sim}{M},_\alpha = \underset{\sim}{A}_\alpha + \underset{\sim}{M},_\alpha \qquad \alpha = 1, 2$$

$$\text{(2.5)}$$

$$\underset{\sim}{G}_3 = \underset{\sim}{M},_3$$

where the $\underset{\sim}{A}_\alpha$ are the vectors tangent to the deformed middle surface

coordinates X^1 and X^2. Here the comma denotes partial differentiation

with respect to the X^i (e. g. , $M,_i \equiv \partial M / \partial X^i$). Both Greek and Latin

indices are used hereinafter with the understanding that Greek indices

range from 1 to 2 and Latin indices range from 1 to 3.

We now assume that a material line normal to the undeformed

middle surface remains straight and normal to the deformed middle

surface. However, these material lines may undergo finite extensional

strain during the motion. Thus, if λ is the extension ratio of X^3

(i. e. , $\lambda = d/d_o$, the ratio of deformed length to undeformed length),

we choose to write the vector $\underset{\sim}{M}$ of (2.2) in the form

$$\underset{\sim}{M} = \underset{\sim}{M}(X^1, X^2, X^3, t) = \lambda X^3 \hat{n} \qquad \text{(2.6)}$$

where $\hat{n}$ is a unit vector normal to the deformed middle surface. Both

λ and $\hat{n}$ are functions of X^1, X^2, and t. Now, using (2.6), (2.5) becomes

$$G_\alpha = A_\alpha + X^3(\lambda\hat{n})_{,\alpha}$$

$$(2.7)$$

$$G_3 = \lambda\hat{n}$$

Noting that $\hat{n} \cdot A_\alpha = 0$, the components G_{ij} of Green's deformation tensor are

$$G_{\alpha\beta} = G_\alpha \cdot G_\beta = A_{\alpha\beta} - 2\lambda X^3 B_{\alpha\beta} + (X^3\lambda)^2 B_\alpha^\mu B_{\beta\mu} + (X^3)^2 \lambda_{,\beta}\lambda_{,\alpha}$$

$$G_{\alpha 3} = G_\alpha \cdot G_3 = X^3\lambda\lambda_{,\alpha}$$

$$(2.8)$$

$$G_{33} = G_3 \cdot G_3 = \lambda^2$$

Here $A_{\alpha\beta}$ and $B_{\alpha\beta}$ are the covariant components of the first and second fundamental tensors, respectively, of the deformed middle surface and B_β^μ are the mixed components of the second fundamental tensor

$$A_{\alpha\beta} = A_\alpha \cdot A_\beta \quad ; \quad B_{\alpha\beta} = -A_\alpha \cdot \hat{n}_{,\beta} \quad ; \quad B_\alpha^\mu = A^{\mu\beta}B_{\beta\alpha} \qquad (2.9)$$

In this last equation, $A^{\alpha\beta}$ are the contravariant components of the first fundamental tensor of the deformed middle surface (i.e., $A^{\alpha\mu}A_{\mu\beta} = \delta_\beta^\alpha$ or $A^{\alpha\beta} = A^\alpha \cdot A^\beta$, where $A^\alpha \cdot A_\beta = \delta_\beta^\alpha$).

We are interested in a reduced version of (2.8) which corresponds to a theory of thin membranes. Therefore, we restrict our attention to deformations of bodies sufficiently thin that G_{ij} is essentially uniform throughout the thickness. Therefore, instead of (2.8), we have the approximations

$$G_{\alpha\beta} \doteq A_{\alpha\beta} \quad ; \quad G_{\alpha 3} \doteq 0 \quad ; \quad G_{33} \doteq \lambda^2 \tag{2.10}$$

Substituting (2.10) into the general form of the Lagrangian strain tensor, $\gamma_{ij} = \frac{1}{2} (G_{ij} - \delta_{ij})$, where δ_{ij} is the Kronecker delta (e.g., Green and Adkins [35]), yields the strain components for a thin membrane

$$\gamma_{\alpha\beta} = \frac{1}{2} (A_{\alpha\beta} - \delta_{\alpha\beta}) \quad ; \quad \gamma_{\alpha 3} = 0 \quad ; \quad \gamma_{33} = \frac{1}{2} (\lambda^2 - 1) \tag{2.11}$$

In the analysis of deformable membranes, it is convenient to form the principal invariants of Green's deformation tensor, $G_{ij} = 2\gamma_{ij} + \delta_{ij}$ These invariants are:

$$I_1 = \lambda^2 + A_{11} + A_{22} = \lambda^2 + A_{\alpha\alpha}$$

$$I_2 = A + \lambda^2(A_{11} + A_{22}) = \lambda^2 A_{\alpha\alpha} + \frac{1}{2}(A_{\alpha\alpha}A_{\beta\beta} - A_{\alpha\beta}A_{\beta\alpha}) \tag{2.12}$$

$$I_3 = \lambda^2 A = \frac{1}{2}\lambda^2(A_{\alpha\alpha}A_{\beta\beta} - A_{\alpha\beta}A_{\beta\alpha})$$

where

$$A = \det(A_{\alpha\beta}) = A_{11}A_{22} - A_{12}A_{21} = \frac{1}{2}(A_{\alpha\alpha}A_{\beta\beta} - A_{\alpha\beta}A_{\beta\alpha}) \qquad (2.13)$$

Differentiating (2.4) and substituting the result in (2.11) gives the membrane strain-displacement relations

$$\gamma_{\alpha\beta} = \frac{1}{2}(u_{\alpha,\beta} + u_{\beta,\alpha} + u_{k,\alpha}u_{k,\beta})$$

$$\gamma_{\alpha 3} = 0 \qquad (2.14)$$

$$\gamma_{33} = \frac{1}{2}(\lambda^2 - 1)$$

where $\alpha, \beta = 1, 2$, $k = 1, 2, 3$, and the functions $u_i = u_i(X^1, X^2, t)$ are the components of displacement.

2.2 Stress

Let $\underset{\sim}{t}$ denote the stress vector in the deformed body measured per unit area A_o of undeformed material surface area. Then, if $\hat{n}_o = n_{oi}\hat{i}^i = n_o^i\hat{i}_i$ is a unit vector normal to A_o in the undeformed body,

$$\underset{\sim}{t} = t^{ij}n_{oi}G_j \qquad (2.15)$$

where t^{ij} are the contravariant components of the stress tensor measured per unit area A_o referred to the tangent base vectors $\underset{\sim}{G}_j$ in the deformed body, and from the balance of angular momentum, $t^{ij} = t^{ji}$.

2.3 Equations of Motion

The principles of conservation of mass and linear momentum require that at each material point

$$\rho_o = \rho \sqrt{G} \qquad (2.16)$$

$$[t^{ir}(\delta_{jr} + w_{j,r})]_{,i} + \rho_o F_{oj} = \rho_o \ddot{w}_j \qquad (2.17)$$

where ρ_o and ρ are the mass densities of the undeformed and deformed bodies, respectively, $G = \det(G_{ij}) = I_3$, F_{oj} are components of body force per unit mass of undeformed body, and superposed dots mean the time rates-of-change. As will be seen subsequently, to these equations must be added jump conditions when wave phenomena are considered.

2.4 Thermodynamics

The first law of thermodynamics can be written in the form

$$\dot{K} + \dot{U} = \Omega + Q \qquad (2.18)$$

Here K is the kinetic energy, U is the internal energy, Ω is the mechanical power developed by the external forces acting on the body, and Q is the heat input. Equation (2.18) is also referred to as the global form of the first law because it deals with finite volume of material. When no jumps are present,

$$K = \frac{1}{2} \int_{v_o} \rho_o \dot{w}_i \dot{w}_i dv_o \qquad (2.19)$$

$$U = \int_{v_o} \rho_o \epsilon \, dv_o \qquad (2.20)$$

$$\Omega = \int_{v_o} \rho_o F_{oi} \dot{w}_i dv_o + \int_{A_o} S_{oi} \dot{w}_i dA_o \qquad (2.21)$$

$$Q = \int_{v_o} \rho_o r dv_o + \int_{A_o} q_i n_{oi} dA_o \qquad (2.22)$$

In these equations, ρ_o is the mass density, v_o is the volume, A_o is the surface area, $\dot{w}_i$ are velocity components, ϵ is the internal energy per unit mass, F_{oi} are components of body force per unit mass, S_{oi} are components of surface force referred to the X^i and measured per unit area A_o in C_o, r is the rate of heat supply per unit mass, q_i are the components of heat flux with respect to the X^i in C_o, n_{oi} are components of a unit vector normal to A_o, and any quantity subscripted "o" is referred to the undeformed body.

Assuming sufficient conditions of smoothness, the divergence theorem is used to obtain the local form of the first law that represents the energy balance at a point in a continuum

$$\rho_0 \dot{\epsilon} = t^{ij}(\delta_{mj} + w_{m,j})\dot{w}_{m,i} + \rho_0 r + q_{i,i} \qquad (2.23)$$

Corresponding to the theory of thin membranes, (2.23) can be written in the form

$$\rho_0 \dot{\epsilon} = t^{\alpha\beta}(\delta_{i\beta} + w_{i,\beta})\dot{w}_{i,\alpha} + \rho_0 r + q_{i,i} \qquad (2.24)$$

Differentiating the strain tensor $[\gamma_{ij} = \frac{1}{2}(G_{ij} - \delta_{ij})]$ it is easily shown that

$$t^{ij}(\delta_{mj} + w_{m,j})\dot{w}_{m,i} = t^{ij}\dot{\gamma}_{ij} \qquad (2.25)$$

Using (2.25) in (2.23), an alternate local form of the first law is

$$\rho_0 \dot{\epsilon} = t^{ij}\dot{\gamma}_{ij} + \rho_0 r + q_{i,i} \qquad (2.26)$$

Integrating (2.26) and substituting the result into (2.18), the global form of the first law of thermodynamics becomes

$$\dot{K} + \int_{V_0} t^{ij}\dot{\gamma}_{ij}dv_0 = \Omega \qquad (2.27)$$

If the material is hyperelastic, there exists a potential function $W(\gamma_{ij})$ measured per unit volume of the undeformed body, called the strain-energy function, from which the components of the symmetric Kirchhoff stress tensor can be derived by the relation*

$$t^{ij} = \frac{\partial W}{\partial \gamma_{ij}} \qquad (2.28)$$

Hence, using (2.28) in (2.27), we can express the global form of the first law of thermodynamics for hyperelastic materials as

$$\dot{K} + \int_{V_0} \frac{\partial W}{\partial \gamma_{ij}}\dot{\gamma}_{ij}dv_0 = \Omega \qquad (2.29)$$

2.5 Constitutive Equations

Assuming the sheet to be composed of a hyperelastic material with a strain-energy function $W(\gamma_{ij})$ per unit undeformed volume, then

---

*To avoid error, it should be understood that in differentiating W with respect to γ_{ij}, all other components are held constant, including γ_{ij}. Thus (2.28) should actually be written $t^{ij} = \frac{1}{2}[(\partial W/\partial\gamma_{ij}) + (\partial W/\partial\gamma_{ji})]$. We avoid this cumbersome notation with the understanding that, in all equations hereinafter, by $\partial/\partial A_{ij}$ we mean $\frac{1}{2}[(\partial/\partial A_{ij}) + (\partial/\partial A_{ji})]$ for any symmetric tensor A_{ij}.

$$\dot{W}(\gamma_{ij}) = \frac{\partial W}{\partial \gamma_{ij}} \dot{\gamma}_{ij} = t^{ij}\dot{\gamma}_{ij}$$

$$= t^{\alpha\beta}\dot{\gamma}_{\alpha\beta} + t^{33}\dot{\gamma}_{33} \tag{2.30}$$

and the components of the symmetric Kirchhoff stress tensor t^{ij} are determined by

$$t^{\alpha\beta} = \frac{\partial W}{\partial \gamma_{\alpha\beta}} \quad , \quad t^{\alpha 3} = 0 \quad , \quad t^{33} = \frac{\partial W}{\partial \gamma_{33}} \tag{2.31}$$

Assuming further that the sheet is a homogeneous isotropic hyper-elastic material, the strain-energy function W can be expressed as a function of the principal invariants of γ_{ij}, or more conveniently, the principal invariants of G_{ij}: $W = W(I_1, I_2, I_3)$, where I_1, I_2, and I_3 are defined in (2.12) for the membrane. Therefore, we can express the constitutive relations of the membrane in the general form

$$t^{\alpha\beta} = 2\left(\frac{\partial W}{\partial I_1} + \lambda^2\frac{\partial W}{\partial I_2}\right)\delta^{\alpha\beta} + 2\left(\frac{\partial W}{\partial I_2} + \lambda^2\frac{\partial W}{\partial I_3}\right)AA^{\alpha\beta}$$

$$t^{\alpha 3} = 0 \tag{2.32}$$

$$t^{33} = 2\frac{\partial W}{\partial I_1} + 2\frac{\partial W}{\partial I_2}A_{\alpha\alpha} + \frac{\partial W}{\partial I_3}(A_{\alpha\alpha}A_{\beta\beta} - A_{\alpha\beta}A_{\beta\alpha})$$

where

$$AA^{\alpha\beta} = \epsilon^{\alpha\lambda}\epsilon^{\beta\mu}A_{\lambda\mu}$$

(2.33)

and $\epsilon^{\alpha\lambda}$, $\epsilon^{\beta\mu}$ = two-dimensional permutation symbols ($\epsilon^{12} = +1$, $\epsilon^{21} = -1$, $\epsilon^{11} = \epsilon^{22} = 0$).

In general, the normal stress component t^{33} can be determined from the boundary conditions on the deformed middle surface. For very thin membranes, however, since the magnitudes of the membrane stresses $t^{\alpha\beta}$ are usually much greater than t^{33}, it is standard practice to take $t^{33} = 0$ and to reduce the problem to one of determining only a two-dimensional state of stress. This approximation will be incorporated hereinafter.

In the case of incompressible materials, $I_3 = 1$, and W is a function of only I_1 and I_2. Thus, instead of (2.12), we will have

$$I_3 = 1 = \lambda^2 A$$

(2.34)

$$I_1 = \lambda^2 + A_{\alpha\alpha} \quad ; \quad I_2 = \lambda^2 A_{\alpha\alpha} + \frac{1}{\lambda^2}$$

and, as was mentioned previously, since the deformation of incompressible materials only determines the components of the stress tensor to

within a hydrostatic pressure, the constitutive equations for incompressible membranes are:

$$t^{\alpha\beta} = 2\left(\frac{\partial \hat{W}}{\partial I_1} + \lambda^2 \frac{\partial \hat{W}}{\partial I_2}\right)\delta^{\alpha\beta} + 2\left(h + \frac{1}{\lambda^2}\frac{\partial \hat{W}}{\partial I_2}\right)A^{\alpha\beta}$$

$$t^{\alpha 3} = 0 \tag{2.35}$$

$$t^{33} = 2\frac{\partial \hat{W}}{\partial I_1} + 2\frac{1}{\lambda^2}\frac{\partial \hat{W}}{\partial I_2}\delta_{\alpha\beta}A^{\alpha\beta} + \frac{2}{\lambda^2}h$$

where $\hat{W} = \hat{W}(I_1, I_2)$ and h is the hydrostatic pressure. The hydrostatic pressure h, determined by the condition that $t^{33} = 0$, becomes

$$h = -\lambda^2 \frac{\partial \hat{W}}{\partial I_1} - \frac{\partial \hat{W}}{\partial I_2}\delta_{\alpha\beta}A^{\alpha\beta} \tag{2.36}$$

Substituting this into (2.35) gives

$$t^{\alpha\beta} = 2\left(\delta^{\alpha\beta} - \lambda^2 A^{\alpha\beta}\right)\frac{\partial \hat{W}}{\partial I_1} + 2\left[\lambda^2\delta^{\alpha\beta} + A^{\alpha\beta}\left(\frac{1}{\lambda^2} - \delta_{\lambda\mu}A^{\lambda\mu}\right)\right]\frac{\partial \hat{W}}{\partial I_2} \tag{2.37}$$

and $t^{\alpha 3} = t^{33} = 0$.

2.6 Strain Energy Functions

In trying to determine general forms of the strain energy function for compressible materials, it is common to assume that W is an

analytic function of the strains or strain invariants. For example, with the strains

$$W(\gamma_{ij}) = E^{ij}\gamma_{ij} + \frac{1}{2}E^{ijmn}\gamma_{ij}\gamma_{mn} + \frac{1}{3!}E^{ijmnrs}\gamma_{ij}\gamma_{mn}\gamma_{rs} + \dots \qquad (2.38)$$

Here E^{ij}, E^{ijmn},..., are arrays of "elasticities" of order zero, first, second,.... If the body is unstressed in its reference state, $E^{ij} = 0$. Hooke's law is obtained by retaining only quadratic terms.

A standard form for W as a function of the strain invariants is

$$W = \sum_{r=0}^{\infty} \sum_{s=0}^{\infty} \sum_{t=0}^{\infty} C_{rst}(I_1 - 3)^r (I_2 - 3)^s (I_3 - 3)^t \qquad (2.39)$$

with $C_{ooo} = 0$.

Most materials that behave elastically at finite strain are incompressible. For any motion of such materials, $I_3 = 1$, and W determines the stress only to within an arbitrary scalar valued function h called the hydrostatic pressure. Then, in place of (2.28), we have

$$t^{ij} = \frac{\partial W}{\partial \gamma_{ij}} + hG^{ij} \qquad (2.40)$$

where $G^{ij} = (G_{ij})^{-1}$.

A strain energy function for certain isotropic, compressible, elastic solids valid for relatively large strains was proposed by Blatz and Ko [66]:

$$W = \frac{\mu f}{2}[J_1 - 3 + \frac{2}{\alpha}(J_3^{-\alpha} - 1)] + \frac{\mu(1 - f)}{2}[J_2 - 3 + \frac{2}{\alpha}(J_3^{\alpha} - 1)] \qquad (2.41)$$

where μ and f are material constants, ν is Poisson's ratio, $\alpha = 2\nu/(1 - 2\nu)$ and J_1, J_2, and J_3 are the invariants

$$J_1 = I_1 \quad ; \quad J_2 = I_2/I_3 \quad ; \quad J_3 = \sqrt{I_3} \qquad (2.42)$$

In the case of incompressible materials, $W = \widehat{W}(I_1, I_2)$ can sometimes be represented as a power series in I_1 and I_2

$$\widehat{W} = \sum_{r=0}^{\infty} \sum_{s=0}^{\infty} C_{rs}(I_1 - 3)^r (I_2 - 3)^s \quad , \quad C_{oo} = 0 \qquad (2.43)$$

Among materials of this type, the most widely used is the Mooney material [67], which follows from (2.43) by retaining only linear terms in I_1 and I_2

$$\widehat{W} = C_1(I_1 - 3) + C_2(I_2 - 3) \qquad (2.44)$$

where $C_1 = C_{10}$, $C_2 = C_{01}$ are material constants. When $C_2 = 0$, (2.44) reduces to the strain energy function of neo-Hookean material suggested by Treloar [68]

$$\hat{W} = C(I_1 - 3)$$

(2.45)

Extensive experiments with different kinds of rubber led Rivlin and Saunders [69] to suggest a more general form of strain energy function

$$\hat{W} = C_1(I_1 - 3) + F(I_2 - 3)$$

(2.46)

where the form of $F(I_2 - 3)$ may vary from one type of material to another.

Not all proposed forms of W for rubber-like materials have regarded the function $F(I_2 - 3)$ in (2.46) as a polynomial in $(I_2 - 3)$. Using a non-Gaussian molecular theory as a guide, Gent and Thomas [70] assumed that $[\partial F(I_2 - 3)/\partial I_2] = C/I_2$, where C is a material constant. Hart-Smith [71] elaborated on this theory and proposed the exponential-hyperbolic law

$$\hat{W} = C\left(\int \exp[k_1(I_1 - 3)^2]dI_1 + k_2 \ln\left[\frac{I_2}{3}\right]\right)$$

(2.47)

Similarly, Alexander [72] proposed the forms

$$\widehat{W} = C_1(I_1 - 3) + C_2(I_2 - 3) + C_3 \ln\left[\frac{I_2 - 3 + k}{k}\right] \tag{2.48}$$

$$\widehat{W} = C_1 \int \exp\left[k(I_1 - 3)^2\right] dI_1 + C_2(I_2 - 3) + C_3 \ln\left[\frac{I_2 - 3 + k_1}{k_1}\right] \tag{2.49}$$

where C_1, C_2, C_3, k, and k_1 are material constants to be determined experimentally for a given sample of the material. Several other forms for W have been proposed, so that (2.43) to (2.49) are given only to be representative.

CHAPTER III

SHOCK AND ACCELERATION WAVES IN
NONLINEAR ELASTIC MATERIALS

3.1 Justification

In order to gain some insight into general nonlinear behavioral

characteristics of elastic bodies, while still managing not to obscure

the pertinent conceptual and physical details, we temporarily confine

out attention to one-dimensional problems. In particular, we consider

only longitudinal motions of finite homogeneous thin rods of isotropic,

incompressible, hyperelastic materials. We return to the membrane

problem in Chapter VI.

3.2 Physics of Waves in Nonlinear Elastic Materials

We now review certain features of the dynamical and thermo-

dynamical theory of finite elasticity that are essential to our study.

More complete details can be found in the books of Green and Zerna [65],

Green and Adkins [34], and Bland [43]; certain special features are

discussed in the papers of Nowinski [50], Ames [73], and Reddy and

Achenbach [51]. Extensive references can be found in the lengthy

survey article of Chen [53].

Motion of a Thin Rod

We begin by considering longitudinal motions of a thin rod of isotropic, incompressible material. While at rest in a natural reference configuration C_o, the rod has a uniform symmetric cross section of area A_o, a length L_o, and a mass density ρ_o. To describe the motion of the rod relative to its reference configuration, we establish a fixed spatial frame of reference x, with origin o at one end of the bar, which is assumed to be restrained from motion. We denote by X the labels of material particles (material coordinates) of the bar, and we select these labels so as to numerically coincide with the spatial coordinates x when the bar occupies its reference configuration. The function $x = x(X, t)$ then gives the spatial position of the particle X at time t and defines the longitudinal motion of the bar, while $u(X, t) \equiv x(X, t) - X$ defines the displacement of particle X at time t.

The material gradient $\partial x/\partial X$ serves as a convenient measure of the deformation; physically, it represents the longitudinal extension ratio λ (also called the stretch) which is expressible in terms of the displacement gradient u_X according to

$$\lambda = \frac{\partial x}{\partial X} = 1 + \frac{\partial u}{\partial X} = 1 + u_X \qquad (3.1)$$

where for the one-dimensional problems we use the subscript notation $u_X = \partial u/\partial X$ to denote partial differentiation with respect to X. The extensional strain γ is then simply $(\lambda^2 - 1)/2$.

Typically, as Nowinski [50] and Ames [73], we make the following assumptions:

(i)   The original uniform cross-sectional area is sufficiently small so that the radial inertia associated with the lateral contraction may be neglected.

(ii)   In compression and tension zones the rod does not experience material instability.

(iii)   The material is perfectly elastic and incompressible.

(iv)   The rod is subjected to simple unidirectional strain in the sense that the only identically nonvanishing stress component is the longitudinal normal stress component which is uniformly distributed over the cross section which remains plane.

(v)   The effect of strain rate on the constitutive equations is neglected and the static stress-strain relations are extended to the dynamic case.

(vi)   The stress is a continuous monotonically increasing function of the stretch λ, so that $d\sigma/d\lambda > 0$.

Now any disturbance supplied to the rod will travel with finite speed from one particle to another in the form of a surface (curve) of

discontinuity S (a wave) in the X, t plane. If we denote by Y(t) the particle X reached by a wave front at time t, then the set of points $(Y(\tau), \tau)$, τ being a real parameter, defines a curve in the X, t plane across which jump discontinuities in various partial derivatives of u(X, t) can occur. Indeed, acceleration waves involve jumps in the acceleration ü (and the stress gradient $\partial\sigma/\partial X$), and shock waves (shocks) involve the propagation of surfaces across which jump discontinuities in the first derivatives of the displacement (ů and u_X) are experienced. The intrinsic wave speed relative to the material, denoted c, is then simply dY(t)/dt. However, the spatial position y(t) of the wave is clearly

$$y(t) = x(Y(t), t) \qquad (3.2)$$

and the absolute wave speed, as seen by a stationary observer, is

$$v = \frac{dy(t)}{dt} = \frac{dx(Y(t), t)}{dt} \qquad (3.3)$$

The Balance Laws

We assume, of course, that the response of the bar satisfies the basic conservation laws of physics. For the problems at hand, these assume the following global forms:

Linear Momentum

$$A_o \int_{L_o - Y(t)} (\sigma_X - \rho_o \ddot{u}) dX - A_o [\![\sigma + \rho_o \dot{u} c]\!]_Y = 0 \tag{3.4}$$

Energy

$$A_o \int_{L_o - Y(t)} (\rho_o \ddot{u}\dot{u} + \dot{e} - \sigma_X \dot{u} - \sigma \dot{u}_X - q_X) dX \tag{3.5}$$

$$+ A_o [\![\tfrac{1}{2} \rho_o c \dot{u}^2 + c e + \sigma \dot{u} + q]\!]_Y = 0$$

Clausius-Duhem Inequality

$$A_o \int_{L_o - Y(t)} \left[\dot{\xi} - \left(\tfrac{q}{\theta} \right)_X \right] dX + A_o \left[\!\left[c\xi + \tfrac{q}{\theta} \right]\!\right]_Y \geqq 0 \tag{3.6}$$

Here $\sigma(X, t)$ is the first Piola-Kirchhoff stress, e is the internal energy
per unit initial volume, q is the heat flux, ξ is the entropy per unit
initial volume, and θ is the absolute temperature. Quantities in brackets
denote jumps suffered at the surface of discontinuity $(Y(t), t)$; e. g. ,

$$[\![\sigma]\!]_Y = \sigma(Y(t^-), t) - \sigma(Y(t^+), t) \tag{3.7}$$

Mass is conserved in the rod and we have ignored body forces and
internal heat sources for simplicity.

At particles X that do not fall on a surface of discontinuity, (3.4)-(3.6) lead to the local forms of the balance laws

$$\rho_o \ddot{u} - \sigma_X = 0$$

$$\dot{e} - \sigma \dot{\lambda} - q_X = 0 \qquad (3.8)$$

$$\theta \dot{\xi} - q_X + \frac{q\theta_X}{\theta} \geq 0$$

whereas at the surface of discontinuity, we obtain the jump conditions

$$\rho_o c [\![\dot{u}]\!]_Y + [\![\sigma]\!]_Y = 0$$

$$\frac{1}{2} \rho_o c [\![\dot{u}^2]\!]_Y + c [\![e]\!]_Y + [\![\sigma \dot{u}]\!]_Y + [\![q]\!]_Y = 0 \qquad (3.9)$$

$$c [\![\xi]\!]_Y + \left[\!\!\left[\frac{q}{\theta} \right]\!\!\right]_Y \geq 0$$

Equation $(3.9)_2$ is the energy jump condition. We now assume that the momentum jump $(3.9)_1$ is identically satisfied. The wave speed can be expressed as

$$c = \frac{-[\![\sigma]\!]}{\rho_o [\![\dot{u}]\!]} \qquad (3.10)$$

With this, the first term in $(3.9)_2$ takes the form

$$\frac{1}{2} \rho_0 c [\![\dot{u}^2]\!] = -[\![\sigma]\!] \dot{\bar{u}} \tag{3.11}$$

where we have defined the average material velocity $\dot{\bar{u}}$ at the shock by

$$\dot{\bar{u}} \equiv \frac{1}{2}(\dot{u}^+ + \dot{u}^-)$$

and we have denoted $\dot{u}^+ = \dot{u}(Y(t^+), t)$ and $\dot{u}^- = \dot{u}(Y(t^-), t)$. Substituting (3.11) into $(3.9)_2$, expressing the jumps using (3.7) then multiplying and regrouping terms, gives

$$c[\![e]\!] + \bar{\sigma}[\![\dot{u}]\!] + [\![q]\!] = 0 \tag{3.12}$$

where $\bar{\sigma}$ is the average stress at the shock defined by

$$\bar{\sigma} \equiv \frac{1}{2}(\sigma^+ + \sigma^-)$$

Equation (3.12) will be called the local energy jump condition.

It is often convenient to introduce the Helmholtz free energy $\varphi(X, t)$ and the internal dissipation $\delta(X, t)$ defined for $X \neq Y(t)$ by

$$\varphi = e - \xi\theta \quad \text{and} \quad \delta = \theta\xi - q_X \tag{3.13}$$

Then the last member of (3. 8) can be rewritten in the alternate form

$$\delta + \frac{q\theta_X}{\theta} = \sigma\dot{\lambda} - \dot{\varphi} + \xi\dot{\theta} + \frac{q\theta_X}{\theta} \geq 0 \qquad (3.14)$$

Also, we can impose Maxwell's theorem, which asserts that for any function $f(X,t)$ jointly continuous in X and t, but whose first partial derivatives f_X and $\dot{f}$ suffer jump discontinuities at S, the jump across S in the (two-dimensional) gradient of f must be parallel to a vector (-1, c) normal to S. Applying this idea to the motion $x(X,t)$ yields Hadamard's compatibility condition

$$[\![\dot{u}]\!]_Y + c[\![\lambda]\!]_Y = 0 \qquad (3.15)$$

Waves in Hyperelastic Materials

We now aim our analysis toward waves in hyperelastic materials; that is, we wish to consider materials for which there exists a potential W which is a function of the current value of λ, and for which

$$\dot{W} = \sigma\dot{\lambda} \quad \text{and} \quad \sigma = \frac{\partial W}{\partial \lambda} \qquad (3.16)$$

The question arises, however, as to whether or not a theory of hyperelasticity is reconcilable within the thermodynamic framework established

thus far. This is a classic question, and standard arguments can be found in a number of places (e.g., [17, 74]) to the effect that hyperelasticity is indeed possible in a number of physically meaningful situations. The fact that these standard arguments are not valid at surfaces of discontinuity is fundamental to the physics of shock waves.

We mention two cases. First, consider a class of perfect materials (cf., [74], p. 296), the constitution of which is defined by equations for e, σ, θ, and q depicted as functions of the current values of λ and ξ, with q also dependent on $\theta_X(X, t)$. For reversible processes performed on such materials, the dissipation $\delta = \theta \dot{\xi} - q_X = 0$, and (3.8) gives

$$\left(\sigma - \frac{\partial e}{\partial \lambda}\right)\dot{\lambda} + \left(\theta - \frac{\partial e}{\partial \xi}\right)\dot{\xi} + \frac{1}{\theta}q\theta_X \geq 0 \tag{3.17}$$

so long as $X \in (L_o - Y(t))$. Secondly, we consider a class of simple materials (cf., [17], p. 202) whose constitution is defined by equations for φ, σ, ξ, and q in terms of current values of λ and θ, with q also dependent upon $\theta_X(X, t)$. For reversible process ($\delta = 0$), using (3.13) in (3.8) gives us the inequality

$$\left(\sigma - \frac{\partial \varphi}{\partial \lambda}\right)\dot{\lambda} - \left(\xi + \frac{\partial \varphi}{\partial \theta}\right)\dot{\theta} + \frac{1}{\theta}q\theta_X \geq 0 \tag{3.18}$$

for all $X \in (L_o - Y(t))$. If these two inequalities, (3.17) and (3.18),
are to be maintained for arbitrary rates, it necessarily follows (cf.,
[17], p. 214) that in the absence of a shock, a theory of hyperleasticity
is appropriate for reversible isentropic processes ($\delta = 0$, $\dot{\xi} = 0$)
performed on the above class of perfect materials and for reversible
isothermal processes ($\delta = 0$, $\dot{\theta} = 0$) performed on the above class of
simple materials. In the former case, the strain energy is associated
with the internal energy, in the latter case it is associated with the
free energy. However, since a shock is characterized by discontinuities
in the displacement gradient, the necessary derivatives of e in (3.17),
or of φ in (3.18), do not exist for $X = Y(t)$. Therefore, we must have
energy dissipation at $X = Y(t)$, i. e. , $\delta = \theta \dot{\xi} - q_X > 0$, and we lose the
notion of reversibility.

Due to the considerable difficulties involved in solving the nonlinear
thermo-mechanical equations governing irreversible thermodynamic
processes, the only exact solutions available (cf., [44, 46]) are for
shocks with uniform conditions on both sides of the discontinuity. Hence,
for additional solutions, we need to simplify the governing equations so
that they become tractable. One possibility, suggested by the exact
discontinuous solutions themselves, is the well known fact that "weak
shocks" are nearly isentropic (e. g. , [43], [75], or [76] for detailed
discussions). This is, taking the proportional change in magnitude

across the shock of some state parameter, say u_X, as a measure of
shock "strength", the change in entropy across the shock is only of
third order in the shock strength for small changes of u_X. Therefore,
for weak shocks, we can neglect the entropy change and consider ξ as
constant for all X and t, i.e., the deformation takes place isentropically.
It is of special interest to consider this "isentropic approximation" when
the initial, or reference configuration is the natrual stress-free state
where $\lambda(X, 0) = 1$, $\theta(X, 0) = T_0 = $ constant. Then the isentropic approxi-
mation becomes $\xi = 0$ everywhere for all time. Moreover, for this
case, the isentropic approximations render the mechanical equations
independent of the thermal equations, and the mechanical jump conditions
(the first of (3.9) and (3.15)) alone are sufficient to determine the shock
process. (Naturally the energy jump condition remains valid, but here
it would only be used to check the energy balance after solving the
problem.) Also, we can readily define the strain energy function W of
(3.16) in terms of the internal energy $W(\lambda) = e(\lambda, \xi)\big|_{\xi=0}$, so that we
have the constitutive relation for the stress $\sigma = \partial e/\partial \lambda$, in agreement
with (3.16).

We remark that the local balance laws (3.8) suggest another
simplification: the adiabatic approximation, wherein we assume the
heat conduction small enough to take $q = 0$. Outside the shock region,
the adiabatic process is reversible ($\delta = 0$); and then from (3.13) we get

the reversible adiabatic process to be an isentropic process. Hence,
in regions of the rod where $X \neq Y(t)$, a theory of hyperelasticity, in
the sense of (3.17), is possible. At the shock, the adiabatic process
is not reversible: entropy is produced. Then, by integrating the
inequality of (3.8) with $q = 0$, we get $\xi = \xi(X)$. Therefore the entropy
at each material point has a constant value unless a shock passes over
the point, at which time the value of the entropy is changed to a new
constant. Consequently, until the time at which a shock forms, the
adiabatic process is isentropic for every $X \in (0, L_o)$; after this time,
the adiabatic process is, in general, piecewise isentropic, i.e., it is
isentropic for every $X \in \{(0, Y(t^-)], [Y(t^+), L_o)\}$.

Both of these assumptions can, of course, be simultaneously
incorporated if we consider the propagation of weak adiabatic shocks.
In this case, again following (3.17), the material will be everywhere
hyperelastic at all times.

3.3 Evolution and Propagation of Discontinuities

We now look at the physical conditions which are generally required
for the formation and propagation of discontinuities--both shock waves
and acceleration (simple) waves in rubber-like materials. We also
briefly consider methods for determining the time required for dis-
continuities to evolve during the solution process.

Propagation of Shock and Acceleration Waves

In the absence of shocks, we previously obtained the first member
of (3.8) as the local form of the law of conservation of linear momentum.
In view of the constitutive relation (3.16) for hyperelastic materials,
we have $\sigma = \sigma(\lambda)$, so that the local momentum equation for such materials
can be written in the form

$$\ddot{u} - c^2(u_X)u_{XX} = 0 \qquad\qquad (3.19)$$

where the squared intrinsic wave speed, $c^2(u_X)$, is given by

$$c^2(u_X) = \frac{1}{\rho_o}\frac{d\sigma}{d\lambda} \qquad\qquad (3.20)$$

We also note that, since $\lambda = \dot{u}_X$, we can recast the local momentum
equation (3.19) in terms of λ according to

$$\ddot{\lambda} = [c^2(\lambda)\lambda_X]_X \qquad\qquad (3.21)$$

where, clearly, the forms of $c^2(\lambda)$ and $c^2(u_X)$ will be different.

As noted earlier, for hyperelastic solids the stress is derivable
from a potential function W which represents the strain energy per unit
undeformed (reference) volume v_o. For isotropic incompressible

bodies, W is generally defined in terms of the first two principal invariants, I_1 and I_2, of Green's deformation tensor, the third principal invariant being unity. In the present case, $I_1 = 2\lambda^{-1} + \lambda^2$, $I_2 = 2\lambda + \lambda^{-2}$, and elimination of the hydrostatic pressure with the condition that transverse normal stresses are zero, leads to the general constitutive law

$$\sigma = 2(W_1\lambda + W_2)(1 - \lambda^{-3}) \tag{3.22}$$

where $W_\alpha = \partial W/\partial I_\alpha$, $\alpha = 1, 2$. Substituting (3.22) into (3.20), we observe that the square of the wave speed in materials defined by (3.22) is of the form

$$c^2 = \frac{2}{\rho_0}[(1 + 2\lambda^{-3})W_1 + 3\lambda^{-4}W_2 \tag{3.23}$$

$$+ 2(1 - \lambda^{-3})^2(W_{11}\lambda^2 + 2W_{12}\lambda + W_{22})]$$

If we eliminate, on physical grounds, the possibility of complex wave speeds, we, in turn, impose conditions on the form of W and its derivatives W_α, $W_{\alpha\beta}$. In this regard, we assume that the stress σ is a continuous monotonically increasing function of the stretch λ, so that for all $\lambda \in (0,\infty)$, we have $0 < \rho_0 c^2(\lambda) = d\sigma/d\lambda < \infty$. This important

property allows us to interpret qualitatively a number of interesting nonlinear wave phenomena. For example, suppose that a time-dependent surface traction is applied at the free end of the rod. During each infinitesimal increment in time, the corresponding increment in load produces a "wavelet," so that, using Nowinski's terminology [50], the net effect of the loading is to produce an "infinite manifold" of wavelets propagating along the rod. Obviously, each successive wavelet propagates at a speed determined by the instantaneous slope of the σ versus λ curve for the material. Thus if consecutive wavelets are propagated with decreasing speeds, the slope of the wave front will gradually decrease (contrasting markedly with the usual sharp discontinuity at the wave front in materials with linear $\sigma - \lambda$ curves), and the response will be propagated as a simple wave. However, if the distance between successive wavelets decreases during propagation (they are generated with increasing speeds), the wave profile steepens until the discontinuity is transformed into a shock wave.

To be more specific, consider, for example, the following special forms of the strain energy function:

The Neo-Hookean Form

$$W = C(I_1 - 3) \tag{3.24}$$

The Mooney Form

$$W = C_1(I_1 - 3) + C_2(I_2 - 3) \tag{3.25}$$

The Biderman Form

$$W = B_1(I_1 - 3) + B_2(I_1 - 3)^2 + B_3(I_1 - 3)^3 + B_4(I_2 - 3) \tag{3.26}$$

Here C, C_1, C_2, ..., B_4 are material constants. Examples of a variety of other forms of W proposed for real materials were summarized earlier in Section 2.6. Note that for Mooney materials

$$c^2 = \frac{2}{\rho_o}[C_1(1 + 2\lambda^{-3}) + 3C_2\lambda^{-4}] \tag{3.27}$$

whereas in the case of Biderman materials

$$c^2 = \frac{2}{\rho_o}\{[B_1 + 2B_2(2\lambda^{-1} + \lambda^2 - 3) \tag{3.28}$$

$$+ 3B_3(2\lambda^{-1} + \lambda^2 - 3)^2](1 + 2\lambda^{-3}) + 3B_4\lambda^{-4}$$

$$+ [4B_2 + 12B_3(2\lambda^{-1} + \lambda^2 - 3)](\lambda - \lambda^{-2})^2\}$$

The function c^2 for neo-Hookean materials follows from (3.27) by

setting $C_2 = 0$. Equations (3.24)-(3.26) with (3.22) and (3.27) and

(3.28) describe $\sigma - \lambda$ and $c - \lambda$ curves of the type shown in Figs. 2

and 3. Clearly, the type of wave generated by an initial disturbance

depends upon both the initial state (i.e., the initial value of λ) and

whether λ is subsequently increased or decreased. A discontinuity

is propagated as a simple wave if, and only if, the intrinsic wave speed

of the material in front of the discontinuity is greater than that of the

material behind the discontinuity (cf., [75], p. 243). Hence, Fig. 3

suggests that for both the Mooney and neo-Hookean materials, only

compression shock waves can be developed. However, for certain

Biderman-type materials (curve 2 in Fig. 3), it is possible to produce

a tensile shock wave if the material is prestretched sufficiently. The

development of such tensile shocks has, in fact, been observed

experimentally by Kolsky [56]. It is also interesting to consider the

case in which an applied tension load is suddenly removed. From

Fig. 3 we can see that this discontinuity cannot be propagated by a

simple wave since the wave speed is smaller before the load is released

than after. Thus, it follows that the instant the stress at the end of the

rod begins to decrease (after having increased) is also the time at which

the first wavelet emanates from the end with a propagation speed faster

than the preceding wavelets. Therefore, at some time subsequent to
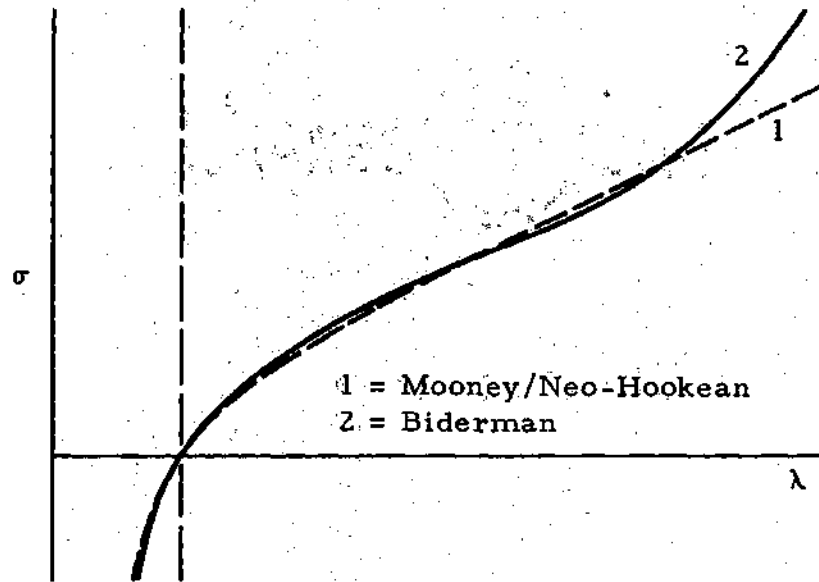
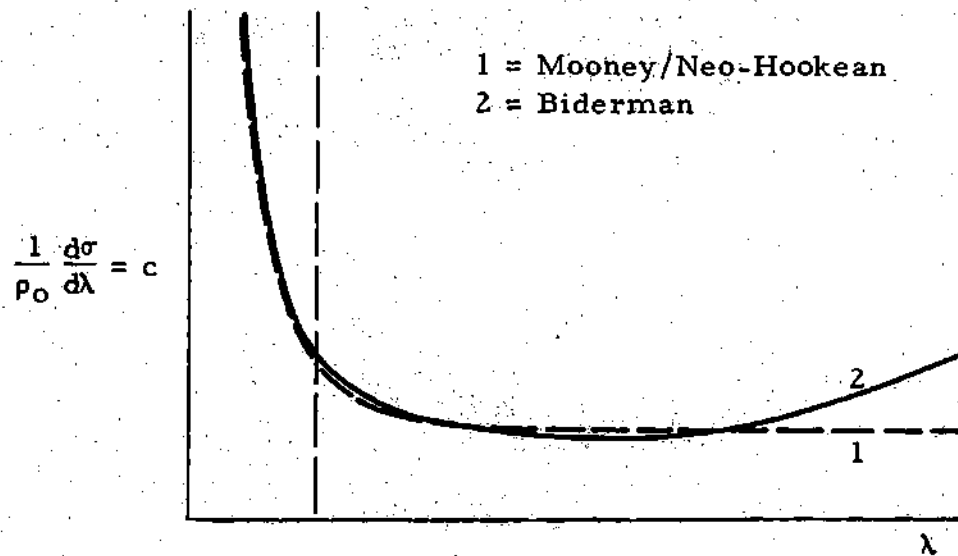Figure 2. Stress versus Stretch for Some Rubber-like Materials

Figure 3. Wave Speed versus Stretch for Some Rubber-like Materials

the moment when the unloading starts, the propagated influence of this

release, or unloading, is expected to develop into a shock wave.

Evolution of Discontinuities

The formation of discontinuities in solutions of nonlinear hyper-

bolic equations has been a topic of interest for many years. The

research on this topic falls into two principal categories: discontinuities

which evolve from Lipschitz continuous initial data and those which

evolve from smooth initial data. In the former case, there is a clearly

defined wave front and a characteristic along which the initial discon-

tinuity (even when starting with analytic initial data, a Lipschitz dis-

continuity can subsequently develop) propagates until it tends to a jump

discontinuity at some critical time, say t_{CR}. This jump discontinuity

then propagates in a completely different manner from the Lipschitz

discontinuity. As this is discussed in detail in [43], [75], and [41], we

will mention only the essential features.

In general, the characteristics of the nonlinear wave equation are

curved lines in the X, t plane. However, if a constant initial state is

prescribed for the rod, the characteristics of positive slope are a

family of straight lines and the corresponding wave is a simple (acceler-

ation) wave. If the excitation at the end of the rod is such that successive

wavelets are generated with decreasing wave speeds, these straight

characteristics diverge in the X, t plane. But, if the wave speed at

the end of the rod increases (e.g., due to compression or, sometimes, tension with an "S-shaped" $\sigma - \lambda$ curve), the characteristics of positive slope will no longer diverge. Instead, they converge and form an "envelope" as shown in Fig. 4. It is on this envelope that the values of velocity and stress, carried by the characteristics, conflict so that the curve C_2 is an approximation of a shock wave propagating with variable speed and carrying a variable stress. The earliest time that such an envelope appears, i.e., when the first two characteristics converge, a cusp is formed at some point X_{CR}. At this point (X_{CR}, t_{CR}) a unique solution of the wave motion, characterized as a simple wave, is mathematically impossible. It is the jump conditions which enable us to continue past (X_{CR}, t_{CR}) with a unique solution for the shock.

The second category; the evolution of discontinuities from smooth initial data, is the topic which seems to be of current interest (e.g., [73], [77], [78], [79]). When applicable, the method presented by Ames [73, 77] is the simpliest and most accurate. This method results from observing that classes of quasi-linear equations can be obtained by differentiation of first-order nonlinear equations. The first order equations are then used to calculate the time t_{CR}.

For the one-dimensional rod considered herein, we find from [73] that the critical time is given by
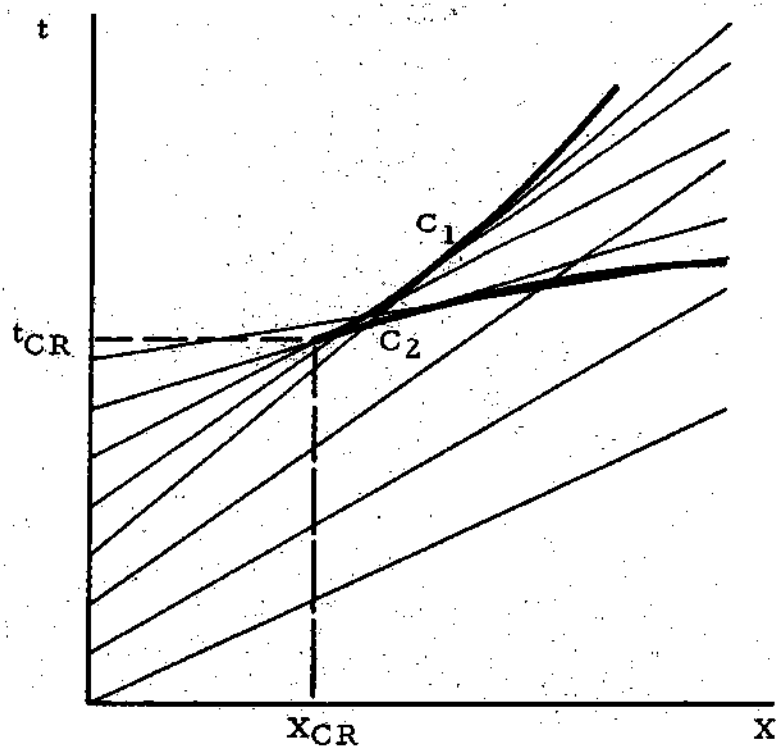
Figure 4. Characteristic Field for Simple Wave with a Shock Formation

$$t_{CR} = \min \frac{1}{h' \phi'} \qquad (3.29)$$

where primes mean differentiation of the quantity with respect to the argument, and the forms of h and ϕ depend upon which form of the wave equation we are considering, (3.19) or (3.21). For the displacement form of the equation of motion, (3.19), we have

$$u_X = h[X + \phi(u_X)t] \qquad (3.30)$$

$$\phi = c(u_X) \qquad (3.31)$$

with $c(u_X)$ being the material shift rate defined in (3.20). If we consider (3.21) on the other hand, we have

$$\lambda = h[X + \phi(\lambda)t] \qquad (3.32)$$

$$\phi = c(\lambda)$$

where the form of $c(\lambda)$ is given in (3.23).

3.4 Mathematical Theory

To complement the preceding physical discussion of shock and acceleration wave propagation, we briefly look at the mathematical side

of the theory. The mathematical theory of hyperbolic systems of conservation laws and the theory of shock waves was recently published by Lax [52]. A brief outline of a portion of this cogent work follows.

It is well known that solutions to initial value problems for some quasi-linear partial differential equation cannot be continued for all time as regular (differentiable) solutions, because they develop discontinuities after a finite time--no matter how smooth the initial data. Since a conservation law is an integral relation, the solutions may be continued, however, by functions which are not differentiable or continuous, but merely measurable and bounded. We refer to these solutions as weak, or generalized solutions. The breakdown of a regular solution may merely mean that although a generalized solution exists for all time, the regular solution ceases to be differentiable after a finite time. All available evidence indicates that this is so. It is possible that more than one generalized solution may satisfy the same initial conditions, and hence these solutions do not possess the important property of uniqueness possessed by regular solutions. However, if our mathematical model describes some aspect of the physical world, then there is indeed a unique generalized solution for the given initial conditions, namely, the one that occurs in nature. Lax presents a class of criteria which ensures uniqueness of the generalized solutions.

Quasi-linear Hyperbolic Equations

A first order system of quasi-linear equations in two independent variables is of the form

$$\dot{\underset{\sim}{u}} + \underset{\sim}{A}\underset{\sim}{u}_X = 0 \tag{3.34}$$

where $\underset{\sim}{u}$ is a vector function of X and t, $\underset{\sim}{A}$ being a matrix function of $\underset{\sim}{u}$ as well as of X and t. Such a system is called strictly hyperbolic if for each X, t, and u the matrix $\underset{\sim}{A} = \underset{\sim}{A}(X, y, \underset{\sim}{u})$ has real and distinct eigenvalues $\tau_j = \tau_j(X, t, \underset{\sim}{u})$, $j = 1, 2, \ldots, n$.

The initial value problem for (3.34) is to find a solution $\underset{\sim}{u}(X, t)$ with prescribed values at t = 0.

$$\underset{\sim}{u}(X, 0) = \underset{\sim}{u}_0(X) \tag{3.35}$$

Conservation Laws

A conservation law asserts that the rate of change of the total amount of substance contained in a fixed domain G is equal to the flux of that substance across the boundary of G. Denoting the density of that substance by u and the flux by f, the global form of the conservation law is

$$\frac{d}{dt} \int_G u \, dv = - \int_{\partial G} f \cdot n \, dS \tag{3.36}$$

where n denotes the outward normal to G and dS is the surface element of ∂G, the boundary of G. Applying the divergence theorem and taking d/dt under the integral sign we obtain, in the limit as G shrinks to a material point where all partial derivatives of u and f are continuous, the differential (local) form of the conservation law

$$\dot{u} + \text{div } f = 0 \tag{3.37}$$

If we have a system of conservation laws, we write

$$\dot{u}^j + \text{div } f^j = 0 \quad , \quad j = 1, 2, \ldots, n \tag{3.38}$$

where each f^j is some nonlinear function of $u^1, \ldots, u^n$. In vector notation, using subscripts to denote partial differentiation, we can write (3.38) as

$$\underset{\sim}{\dot{u}} + \underset{\sim}{f}_X = \underset{\sim}{0} \tag{3.39}$$

Differentiating, we have $\underset{\sim}{f}_X = \underset{\sim}{A}\underset{\sim}{u}_X$, plus possibly a vector valued function $\underset{\sim}{B}$ of $(X, t, \underset{\sim}{u})$; here $A_{ij} = \partial f^i / \partial u^j$. Hence we can write (3.39) as

$$\dot{\underset{\sim}{u}} + \underset{\sim}{A}\underset{\sim}{u}_X + \underset{\sim}{B} = \underset{\sim}{0} \tag{3.40}$$

$\underset{\sim}{u}$ is called a generalized solution of the system of conservation laws (3.39) if it satisfies the integral form of these laws, i. e. , if

$$\int_G \underset{\sim}{u} \, dv \Big|_{t_1}^{t_2} + \int_{t_1}^{t_2} \int_{\partial G} \underset{\sim}{f} \cdot \underset{\sim}{n} \, dS \, dt = 0 \tag{3.41}$$

holds for every smoothly bounded domain and for every time interval (t_1, t_2). This is equivalent to requiring that (3.39) holds in the sense of distribution theory.

Let S(t) be a smooth surface (a curve for one space dimension) moving with t, and $\underset{\sim}{u}$ a continuously differentiable solution of (3.39) on either side of S which is discontinuous across S. The condition which must be satisfied at each point of S if $\underset{\sim}{u}$ is a generalized, or weak, solution across S is

$$a[\![\underset{\sim}{u}]\!] + [\![\underset{\sim}{f}]\!] \cdot \underset{\sim}{n} = 0 \tag{3.42}$$

where $[\![\underset{\sim}{u}]\!]$ and $[\![\underset{\sim}{f}]\!]$ denote the difference between the values of $\underset{\sim}{u}$ and $\underset{\sim}{f}$, respectively in either side of S. $\underset{\sim}{n}$ is the vector normal to S, and a is the speed with which S propagates in the direction of $\underset{\sim}{n}$. Equation (3.42) is called the Rankine-Hugoniot jump condition.

Single Conservation Laws

A single conservation law is an equation of the form

$$\dot{u} + f_X = 0 \tag{3.43}$$

where f is some nonlinear function of u. If we denote $df/du = a(u)$, we can rewrite (3.43) as

$$\dot{u} + a(u)u_X = 0 \tag{3.44}$$

which asserts that u is constant along trajectories $X = X(t)$ which propagate with speed a

$$dX/dt = a \tag{3.45}$$

Hence a is called the signal speed; the trajectories, satisfying (3.45), are called characteristics. Note that if f is a nonlinear function of u, both the signal speed and the characteristics depend on the solution u.

Following this, it is shown, by both analytic and geometric arguments, that if $a(u_0(X))$ is not an increasing function of X, then no function $u(X, t)$ exists for all $t \geq 0$ with initial value u_0 which solves (3.44) in the ordinary sense. Attention is then directed to the study

of distribution solutions, starting with the simpliest kind--those

satisfying (3.43) in the ordinary sense on each side of a smooth curve

$X = Y(t)$ across which u is discontinuous. Integrating the solution

across the discontinuity and envoking the assertion of the conservation

law, the jump condition

$$s[\![\, u \,]\!] = [\![\, f \,]\!] \qquad\qquad (3.46)$$

is then deduced, where $[\![\, u \,]\!] = u_r - u_l$, the difference of the value of u

on the right and left, respectively, of s, and similarly, $[\![\, f \,]\!] = f_r - f_l$,

and $s = dY/dt$ denotes the speed with which the discontinuity propagates.

Using the example when $a(u) = u$ in (3.44), the following criterion

is stated:

The characteristics starting on either side of the discontinuity

curve when continued in the direction of increasing t intersect the line

of discontinuity. This will be the case if

$$a(u_l) > s > a(u_r) \qquad\qquad (3.47)$$

If all discontinuities of a generalized solution satisfy this con-

dition, no characteristic drawn in the direction of decreasing t intersects

a line of discontinuity. This shows that for such solutions every point

can be connected by a backward drawn characteristic to a point on the initial line; therein lies the significance of this condition. When applied to the equations of compressible flow, this generalization amounts to requiring that material which crosses the discontinuity should suffer an increase of entropy. For this reason, condition (3.47) is called the entropy condition.

A discontinuity satisfying the jump relation (3.46) and the entropy condition (3.47) is called a shock.

Lax then goes on to show that every initial value problem for (3.43) has exactly one generalized (weak) solution, for all $t \geq 0$, which has only shocks as discontinuities. Specifically, it is shown that for a function to qualify as a unique solution, four requirements must be met: (1) the function is a solution in a generalized sense; (2) it satifies the initial conditions, (3) it satisfies the jump condition, and (4) it satisfies the entropy condition.

In Chapter IV, rather than attempt to model all four of the required equations mentioned above, we choose an integration scheme which automatically satisfies two of the four requirements. This scheme contains a built-in dissipative mechanism that can increase the entropy across a shock and we obtain solutions of conservation laws as limits of solutions of parabolic equations (they have steep gradients, but no shocks) as the coefficient of the dissipative term goes to zero.

CHAPTER IV

ONE-DIMENSIONAL APPROXIMATIONS

4.1 Finite Element Approximations

We are ready to develop discrete models of the equations govern-
ing nonlinear waves by using the finite-element concept. Toward this
end, we begin by partitioning the rod into a finite number E of segments
connected together at nodal points at their ends. The $E + 1$ nodes are
labeled $0 = X^1 < X^2 < \ldots < X^{E+1} = L_0$, and the mesh length $h_N = X^{N+1}$
$- X^N$ ($N = 1, 2, \ldots, E$) is assumed to be uniform, i.e., $h_N = h$. The
exact solution of the variational problem belongs, for each time t, in
a space we shall term the energy space $\mathscr{E}$, which is suggested naturally
by the variational formulation of the problem. (In the linearized theory,
$\mathscr{E}(0, L_0)$ is the Sobolev space $\mathscr{H}^1(0, L_0)$.) In the finite-element method,
we seek approximate solutions for either the displacement field u, the
solution to (3.19), or the extension ratio (stretch) λ, the solution to
(3.21), in a finite dimensional subspace of $\mathscr{E}(0, L_0)$ containing the exact
variational solution to the problem. We could introduce an approximation
for u of the form

$$u(X, t) \doteq u_N(t)\eta_N(X) \tag{4.1}$$

where $u_N(t)$ are the nodal values of the displacement, $\eta_N(X)$ are basis functions, and the repeated index N is summed from 1 to E + 1. Similarly, we could introduce an approximation for λ of the form

$$\lambda(X, t) \doteq \lambda_N(t)\varphi_N(X) \tag{4.2}$$

where $\lambda_N(t)$ are the nodal values of the extension ratio and $\varphi_N(X)$ are basis functions.

In the finite-element method, it is convenient to first describe the behavior of each element independently in terms of the nodal values; the entire set of elements is then connected together by establishing the nodal connectivity. Hence we now take advantage of this fundamental property of finite-element models and temporarily focus our attention on a typical element from the assemblage representing the continuous rod.

To construct the finite model of an elemental field quantity, say $f(X, t)$, we introduce the approximating functions for each element which are locally of the form

$$f(X, t) \doteq f_\alpha(t)\psi_\alpha(X) \tag{4.3}$$

For simplicity, we consider only first-order representations, so that the repeated index α is a nodal index which ranges from 1 to 2 for the one-dimensional rod element. Here, $f_\alpha(t)$ is the value of $f(X, t)$ at node α of the element at time t, and $\psi_\alpha(X)$ are the usual local (elemental) interpolation functions which have the following properties

$$\psi_\alpha(X^\beta) = \delta_\alpha^\beta \quad , \quad \sum_{\alpha=1}^{2} \psi_\alpha = 1$$

In general, these local interpolation functions contain complete poly-nomials of degree p, where p + 1 is the order of the highest material derivative that appears in the energy equation for the element. In this case, we have p = 1 (cf., [17]). Therefore, the particular elemental field quantity $f(X, t)$ is simply a linear function of the local coordinates of the elements; i. e.,

$$f(X, t) \doteq \psi_\alpha(X)f_\alpha(t) = (a_\alpha + b_\alpha X)f_\alpha(t) \qquad (4.4)$$

where, for any element

$$a_\alpha \sim [a_1, a_2] = [0, 1] \quad , \quad b_\alpha \sim [b_1, b_2] = \frac{1}{h}[-1, 1] \qquad (4.5)$$

Then, from (4.4), we have the well-known linear interpolation expression

$$f(X, t) = (a_1 + b_1 X)f_1(t) + (a_2 + b_2 X)f_2(t)$$

$$(4.6)$$

$$= f_1(t) + (X/h)(f_2(t) - f_1(t))$$

4.2 Galerkin Models for Nonlinear Wave Propagation

Using the local approximation (4.3), we can construct finite

element models for (3.19) and (3.21) using what is sometimes referred

to as the concept of variational solutions. This naturally results

in Galerkin-type models. Initially, consider (3.19). We seek solu-

tions which are weaker than the exact solution of (3.19) by only

requiring that

$$\int_0^h (\ddot{u} - c^2 u_{XX})\beta(X)dX = 0 \qquad (4.7)$$

for any arbitrary function $\beta(X)$ which has a continuous first derivative

and vanishes outside the element. In a similar manner, we can seek

weaker solutions of (3.21) by requiring that

$$\int_0^h (\ddot{\lambda} - (c^2 \lambda_X)_X)\phi(X)dX = 0 \qquad (4.8)$$

where $\phi(X)$ is an arbitrary function which has a continuous first deri-

vative and which vanishes outside the element.

There is an interesting relationship between (4.7) and (4.8). If we integrate (4.8) by parts and let $\beta = -\phi_X$, we have (recall that $\lambda = 1 + u_X$ so that $\dot{\lambda} = \dot{u}_X$)

$$\int_0^h (\ddot{\lambda} - (c^2 \lambda_X)_X)\phi dX = \int_0^h \frac{\partial}{\partial X}(\ddot{u} - c^2 u_{XX})\phi dX$$

$$= -\int_0^h (\ddot{u} - c^2 u_{XX})\phi_X dX \qquad (4.9)$$

$$= \int_0^h (\ddot{u} - c^2 u_{XX})\beta dX$$

This result essentially implies that if λ satisfies (4.8), and if $\beta = -\phi_X$, then u satisfies (4.7). Clearly the converse also holds.

In Section 4.3, we want to examine properties of the finite element models developed from (4.7) and (4.8) using certain fundamental ideas of finite elements concerned with energy. Clearly, under certain conditions, finite element models developed from (4.8) are equivalent to those from (4.7).

Local Form of the Equations of Motion

We now develop finite element models from (4.8) by the following procedure: integrating (4.8) by parts gives

$$\int_0^h \ddot{\lambda}\phi dX + \int_0^h \frac{1}{\rho_o} \sigma_X \phi_X dX = \left[\frac{1}{\rho_o} \sigma_X \phi\right]_0^h \qquad (4.10)$$

where, from (3.20), $\partial\sigma/\partial X = (\partial\sigma/\partial\lambda)\lambda_X = \rho_o c^2 \lambda_X$. If ϕ_X is constant, (4.10) becomes

$$\int_0^h \ddot{\lambda}\phi dX + \frac{1}{\rho_o} \phi_X [\sigma]_0^h = [c^2 \lambda_X \phi]_0^h \qquad (4.11)$$

Taking a piecewise linear approximation (4.3) for λ, we have

$$\lambda(X,t) = \psi_\alpha(X)\lambda_\alpha(t) = (a_\alpha + b_\alpha X)\lambda_\alpha \qquad (4.12)$$

where a_α and b_α are defined in (4.5); hence, with (4.5) in (4.12), we have

$$\lambda_X = \psi_{\alpha,X}\lambda_\alpha = b_\alpha \lambda_\alpha = \frac{1}{h}(\lambda_2 - \lambda_1)$$

$$(4.13)$$

$$\psi_{\alpha,X} = [b_\alpha] = \frac{1}{h}[-1, 1]$$

Taking $\phi(X) = \psi_\alpha(X)$ in (4.11) and incorporating (4.12), we obtain the equation of motion for a typical rod element

$$m_{\beta\alpha}\ddot{\lambda}_\beta + b_\alpha A_o [\sigma]_o^h = p_\alpha \qquad (4.14)$$

where $m_{\beta\alpha}$ is the consistent mass matrix defined by

$$m_{\beta\alpha} = m_{\alpha\beta} = \rho_o A_o \int_o^h \psi_\beta \psi_\alpha dX \qquad (4.15)$$

p_α is the generalized force at node α

$$p_\alpha = \rho_o A_o [\psi_\alpha c^2 \lambda_X]_o^h \qquad (4.16)$$

Equation (4.15) can be integrated to get the usual consistent mass matrix in the form

$$m_{\beta\alpha} = \frac{1}{6} m(1 + \delta_{\beta\alpha}) \qquad (4.17)$$

where $m = \rho_o A_o h$ is the mass of a typical element and $\delta_{\beta\alpha}$ is the Kronecker delta. However, if the mass is considered to be lumped at the nodes, m will be of the diagonal form, $m \delta_{\beta\alpha}/2$. We prefer the lumped mass model in this study, not only for simplicity and increased computational speed, but for concrete theoretical reasons to be mentioned later.

We now turn to the displacement form of the equation of motion (3.19). We develop finite element models from (4.7) using the same procedure used for (4.8); that is, we approximate the local displacement field by

$$u(X, t) = \psi_\alpha(X)u_\alpha(t) = (a_\alpha + b_\alpha X)u_\alpha \qquad (4.18)$$

with a_α and b_α defined in (4.5) and here $u_\alpha = u(X_\alpha, t)$. Accordingly, taking $\beta(X) = \psi_\alpha(X)$ in (4.7), we obtain as the equation of motion for a typical rod element,

$$m_{\beta\alpha}\ddot{u}_\beta + b_\alpha A_o h\sigma = p_\alpha \qquad (4.19)$$

In this case, since $u_X = b_\alpha u_\alpha$, both λ and $\sigma = \sigma(\lambda)$ are constant for each element. The mass matrix is as previously defined, but the generalized nodal force p_α is now

$$p_\alpha = A_o \sigma[\psi_\alpha]_o^h \qquad (4.20)$$

Global Form of the Equations of Motion

To facilitate bookkeeping, we use superscripts as the element index and subscripts as the nodal index. If we define P_N as the net

generalized force applied at node N, so that $P_N = p^{N-1} + p^N$, then the global equation of motion for node N is obtained from (4.15) as

$$P_N = m\ddot{\lambda}_N - \frac{A_o}{h}(\sigma_{N-1} - 2\sigma_N + \sigma_{N+1}) \qquad (4.21)$$

where, from (4.5), $b_N^{N-1} = +h^{-1}$ and $b_N^N = -h^{-1}$, and we have used the lumped mass model. At the ends of the rod, of course, the form of (4.21) changes according to the type of boundary conditions. Equations (4.21) represent the global system of nodal equations of motion for the finite-element model of the rod. Since the solution of these equations will be in terms of the displacement gradients ($\lambda - 1 = \partial u/\partial X$), the nodal displacements, if desired, are obtained by spatial integration.

The displacements can be obtained directly if the global equations of motion are formed as above, but using (4.19) rather than (4.14):

$$P_N = m\ddot{u}_N + A_o(\sigma^{N-1} - \sigma^N) \qquad (4.22)$$

4.3 Justification of the Finite-Element Method for the Analysis of Wave Propagation Problems

In order to justify the finite-element models introduced in Section 4.1, we show that in the neighborhood of surfaces of discontinuity, such as shock waves in hyperelastic bodies, the jump conditions are satisfied in an average sense.

The global energy-balance for a typical element is of the form

$$A_o \int_{h-Y} (\rho_o \dot{u}\ddot{u} - \sigma_X \dot{u})dX + \frac{1}{2}\rho_o A_o c[\![\dot{u}^2]\!]_Y \qquad (4.23)$$

$$+ A_o[\![\sigma\dot{u}]\!]_Y - A_o \bar{\sigma}[\![\dot{u}]\!]_Y = 0$$

where we have used (3.5), assumed the local energy relations $(3.8)_2$ and (3.12) are identically satisfied, and eliminated the internal energy terms. Now, the second term of the integral in (4.23) can be integrated by parts

$$A_o \int_{h-Y} \sigma_X \dot{u}dX = -A_o \int_{h-Y} \sigma \dot{u}_X dX + A_o[\sigma\dot{u}]_o^h + A_o[\![\sigma\dot{u}]\!]_Y \qquad (4.24)$$

so that, with (4.24), (4.23) can be rewritten as

$$A_o \int_{h-Y} (\rho_o \dot{u}\ddot{u} + \sigma\dot{u}_X)dX - A_o[\sigma\dot{u}]_o^h + \frac{1}{2}\rho_o A_o c[\![\dot{u}^2]\!]_Y \qquad (4.25)$$

$$- A_o\bar{\sigma}[\![\dot{u}]\!]_Y = 0$$

Introducing the local finite-element approximation (4.3) for the displacement u and its derivatives in (4.25), we have

$$\left\{ A_o \int_{h-Y} (\rho_o \psi_\alpha \psi_\beta \ddot{u}_\beta + \sigma \psi_{\alpha,X}) dX - A_o [\sigma \psi_\alpha]_o^h \right. \tag{4.26}$$

$$\left. + \frac{1}{2} \rho_o A_o c [\![\psi_\alpha \psi_\beta]\!]_Y \dot{u}_\beta - A_o \bar{\sigma} [\![\psi_\alpha]\!]_Y \right\} \dot{u}_\alpha = 0$$

where, at this point, we need not specify the precise form of the ψ_α; except that here, in general, we intend that the ψ_α be chosen from a very general class of functions. This class is made up of the union of the class of functions $C(0, h)$ which are continuous everywhere in the element and the class of functions $J(0, h)$ which have a finite jump at the surface of discontinuity S but are continuous everywhere else in the element. Of course, if the interpolation functions are continuous everywhere, the jumps in the ψ_α in (4.26) vanish and other means must be used for handling the shocks. But if the ψ_α are discontinuous, a finite-element shock fitting scheme would be obtained. (For reasons discussed in the next section, we choose the former.) Equation (4.26) can be written more compactly as

$$(m_{\alpha\beta} \ddot{u}_\beta + A_o \int_{h-Y} \sigma \psi_{\alpha,X} dX - p_\alpha + R_{\alpha\beta} \dot{u}_\beta - S_\alpha) \dot{u}_\alpha = 0 \tag{4.27}$$

where we have defined

$$m_{\alpha\beta} = \rho_o A_o \int_{h-Y} \psi_\alpha \psi_\beta dX \quad , \quad p_\alpha = A_o [\sigma \psi_\alpha]_o^h$$

$$R_{\alpha\beta} = \frac{1}{2}\rho_o A_o c [\![\psi_\alpha \psi_\beta]\!]_Y \quad , \quad S_\alpha = A_o \bar{\sigma} [\![\psi_\alpha]\!]_Y$$

Since (4.27) must be valid for arbitrary motions of the element, it must also hold for arbitrary values of the nodal velocities $\dot{u}_\alpha$. In particular, if (4.27) is to hold for arbitrary $\dot{u}_\alpha$, the term in the parentheses must vanish for all values of α. Thus,

$$m_{\alpha\beta}\ddot{u}_\beta + A_o \int_{h-Y} \sigma\psi_{\alpha,X} dX - p_\alpha + R_{\alpha\beta}\dot{u}_\beta - S_\alpha = 0 \qquad (4.28)$$

This equation represents the general finite-element equation of motion with shock terms. Thus, as might be expected, a consistent finite-element momentum equation for nonlinear wave propagation problems contains the proper jump conditions at the shock.

Based on the above development, we now examine the finite-element models (4.14) and (4.19) which were developed from (4.8) and (4.7), respectively. We will show that (4.14) and (4.19) can be developed from global balance laws, that using global energy balances and the above modeling procedure insures that the jump conditions (3.9) are satisfied in an average sense, and that this implies that (4.14) and (4.19) satisfy the jump conditions in an average sense.

If the functions $\psi_\alpha(X)$ in (4.28) are assumed to be continuous, then $R_{\alpha\beta} = S_\alpha = 0$ $(\alpha, \beta = 1, 2)$. We examine two cases. First, if the $\psi_\alpha(X)$ are linear over the element, the finite-element scheme (4.19) is

obtained. Thus the finite-element model (4.19) can be derived from the global energy balance (3.5). Secondly, suppose the $\psi_\alpha(X)$ are constant over the element and the $\phi(X)$ introduced in (4.8) are now related to the $\psi_\alpha(X)$ by taking $\phi(X) = \xi_\alpha(X)$ and $\psi_\alpha(X) = \partial\xi_\alpha(X)/\partial X$. Then the $\xi_\alpha(X)$ are linear functions. This implies that models of the form (4.14) can be derived from energy principles. To see this, simply set $\phi = \xi_\alpha(X)$ and $\beta = -\psi_\alpha(X)$ in (4.9). Thus both models of the form (4.14) and (4.19) can be derived from energy balances of the form (3.5).

Satisfaction of Jump Conditions

Now an important question that arises is whether of not the jump conditions (3.9) are satisfied in an average sense in the element when the global energy balances described are used to derive finite-element models. By "an average sense", of course, we mean in a sense at least as weak as $L_1(0, L_o)$. This is certainly true of $(3.9)_2$ since it was obtained from a global energy balance (3.5). Also, in our derivation we assumed that (3.12) was identically satisfied at the shock. Now if (3.12) is satisfied exactly while $(3.9)_2$ is satisfied in an average sense, then $(3.9)_1$ is satisfied in an average sense (see the derivation of (3.12)). Moreover, the Clausius-Duhem inequality $(3.9)_3$ is satisfied because of the constitutive assumptions introduced in the last portion of Section 3.2. Thus, the use of the global energy balance

(3.5) and the procedures introduced above insures that the local jump conditions (3.9) are satisfied in an average sense across the element. To complete the argument, we conclude that because (4.14) and (4.19) can be derived from global energy balances, they satisfy the local jump conditions in an average sense in the element.

4.4 Temporal Approximations

Upon assembling elements and applying boundary conditions, either (4.21) or (4.22) leads to a large system of highly nonlinear second-order ordinary differential equations in the unkown nodal displacements u_N or displacement gradients λ_N. Our only hope for extracting data from such systems is to attempt to solve them numerically. Toward this end, we may choose between the two classes of direct numerical time-integration methods for systems of nonlinear equations: the conditionally stable explicit schemes, and implicit schemes, which are often unconditionally stable for linearized problems. Obviously, the basis for our selection is the optimization of both economy and accuracy.

Here, the principal advantage of implicit schemes (unconditionally stable for large time steps) is overshadowed by the necessity of solving a set of simultaneous nonlinear equations at each time step. Moreover, since we are also interested in nonlinear wave phenomena, the high-frequency response is very important--especially in the region of the

propagated discontinuities. Hence, even if an implicit scheme is used
for this type problem, experience with linear problems suggests that
the associated time step required to retain higher frequencies of the
model is usually just as small as that required for numerical stability
of explicit schemes.

All time integration schemes may involve the inversion of the
mass matrix. If the consistent mass matrix is used, the inverse is a
full matrix which is computationally time consuming. However, if a
diagonal mass matrix is used, obtaining the inverse is trivial, and
the explicit solution process is extremely fast and simple. (Implicit
schemes involve inverting a weighted sum of the mass and stiffness
matrices (cf. ,[80]) so that a diagonal mass matrix affords little advan-
tage in the nonlinear case if implicit schemes are used.) Krieg
and Key [81] have shown that for a number of representative linear
elastodynamic problems the diagonal mass matrix and the explicit
central difference time-integration scheme provide the most practical
means of computing a transient response.

An examination of the order of the derivative of the dependent
variable which suffers a discontinuity during shock formation shows
that any of several well-known explicit schemes might be used effec-
tively if only the evolution of the displacement field in time is desired.
Moreover, certain of these explicit schemes could be used as devices

for determining the points at which the shocks develop in order that

the appropriate jump conditions can be applied. Schemes such as

these are referred to as shock fitting schemes. In the present study,

we shall not consider such schemes for shock analysis since they are

extremely tedious and time consuming in that they require monitoring

the solution process at each time step and applying the jump conditions

at the current location of the shock. Rather, we investigate a number

of simple explicit schemes for predicting the evolution of the displace-

ment field in time, and we develop a new explicit scheme to study the

formation and propagation of shock waves. As will be seen, this new

scheme combines features of the well-known Lax-Wendroff difference

scheme with the finite-element concept.

The following explicit integration schemes were investigated

during the course of this study:

- Runge-Kutta (fourth order) [82]

- Numerov's method [83]

- Standard central differences [82-84]

- Velocity formulated central differences [80]

- Predictor-corrector (fifth order) [84]

- Lax-Wendroff [85-87]

The finite element equations of motion, either (4.21) or (4.22), are of

the form $\ddot{u} = F(u, t)$ where, for time discretization, we denote $t = n\Delta t$,

and typically, $u(t) = u(n\Delta t) = u^n$. These integration schemes are briefly explained below for application to the above form of the equation of motion, unless otherwise noted.

Runge-Kutta (fourth order). First, denoting $n\Delta t = t^n$, we have

$$k_1 = \Delta t \; F(u^n, t^n)$$

$$k_2 = \Delta t \; F\left(u^n + \frac{\Delta t}{2} u^n + \frac{\Delta t}{8} k_1 \, , \; t^n + \frac{\Delta t}{2}\right)$$

$$k_3 = \Delta t \; F\left(u^n + \Delta t u^n + \frac{\Delta t}{2} k_2 \, , \; t^n + \frac{\Delta t}{2}\right)$$

and

$$\Delta u^n = \Delta t \left[\dot{u}^n + \frac{1}{6} (k_1 + 2k_2) \right]$$

$$\Delta \dot{u}^n = \frac{1}{6} (k_1 + 4k_2 + k_3)$$

Then, for the new displacements and velocities, we have

$$u^{n+1} = u^n + \Delta u^n$$

$$\dot{u}^{n+1} = \dot{u}^n + \Delta \dot{u}^n$$

Numerov's method. This method avoids artificially introducing the velocities, $\dot{u}$, into the displacement computation by using the form

$$u^{n+1} = 2u^n - u^{n-1} + \frac{\Delta t^2}{12} (F^{n+1} + 10F^n + F^{n-1})$$

This is a special form of a predictor-corrector scheme, shown below, wherein the predictor and corrector have been combined. It has the error estimate

$$R = -\frac{\Delta t^6}{240} \left(\frac{\partial^6 u}{\partial X^6}\right)$$

Standard central differences. The second time-derivatives are approximated by

$$\ddot{u} \approx \frac{1}{\Delta t^2} (u^{n+1} - 2u^n + u^{n-1})$$

Velocity formulated central differences. We obtain two first order equations from $\ddot{u} = F(u,t)$ by introducing the velocity, $v = \dot{u}$:

$$\ddot{u} = F(u,t) \Rightarrow \begin{cases} \dot{v} = F(u,t) \\ \dot{u} = v \end{cases}$$

These equations are now approximated by the difference equations

$$v^{n+\frac{1}{2}} = v^{n-\frac{1}{2}} + \Delta t\, F(u^n, t^n)$$

$$u^{n+1} = u^n + \Delta t\, v^{n+\frac{1}{2}}$$

These two equations are mathematically equivalent to the standard central differences as can be seen by direct substitution. However, this formulation is, in practice, more accurate due to the finite word lengths of computers (i. e. , a significant degree in round-off error associated with central differences can be realized using this approach).

Predictor-Corrector (fifth order)

For the predictor we used

$$u^{n+1} = 2u^{n-1} - u^{n-3} + \frac{4}{3}\Delta t^2 (F^n + F^{n-1} + F^{n-2})$$

and for the corrector

$$u^{n+1} = 2u^n - u^{n-1} + \frac{\Delta t^2}{12}(F^{n+1} + 10F^n + F^{n-1})$$

Lax-Wendroff

For the equation form

$$\dot{\underset{\sim}{U}} + \underset{\sim}{F}_X(\underset{\sim}{U}) = \underset{\sim}{0}$$

the Lax-Wendroff equations start from a Taylor's series in t:

$$\underset{\sim}{U}^{n+1} = \underset{\sim}{U}^n + \Delta t \dot{\underset{\sim}{U}}^n + \frac{\Delta t^2}{2} \ddot{\underset{\sim}{U}}^n + \ldots$$

The t-derivatives indicated are replaced by X-derivatives by means of the original equation, i. e. ,

$$\frac{\partial^2 \underset{\sim}{U}}{\partial t^2} = -\frac{\partial}{\partial t}\frac{\partial \underset{\sim}{F}}{\partial X} = -\frac{\partial}{\partial X}\frac{\partial \underset{\sim}{F}}{\partial t} = -\frac{\partial}{\partial X}\left(A \frac{\partial \underset{\sim}{U}}{\partial t}\right) = \frac{\partial}{\partial X}\left(A \frac{\partial \underset{\sim}{F}}{\partial X}\right)$$

The X-derivatives are then approximated by difference quotients, to give the Lax-Wendroff system,

$$\underset{\sim}{U}_j^{n+1} = \underset{\sim}{U}_j^n - \frac{1}{2}\frac{\Delta t}{\Delta X}\left(\underset{\sim}{F}_{j+1}^n - \underset{\sim}{F}_{j-1}^n\right) + \frac{1}{2}\left(\frac{\Delta t}{\Delta X}\right)^2 \left[A_{j+\frac{1}{2}}^n\left(\underset{\sim}{F}_{j+1} - \underset{\sim}{F}_j^n\right)\right.$$

$$\left. - A_{j-\frac{1}{2}}^n\left(\underset{\sim}{F}_j^n - \underset{\sim}{F}_{j-1}^n\right)\right]$$

where $A_{j+\frac{1}{2}}^n$ denotes $A\left(\frac{1}{2}\underset{\sim}{U}_{j+\frac{1}{2}}^n + \frac{1}{2}\underset{\sim}{U}_j^n\right)$ and the subscript denotes the spatial discretization, $\underset{\sim}{U}(X) = \underset{\sim}{U}(j\Delta X) = \underset{\sim}{U}_j$.

In order to have a basis for comparing the above integration
schemes, we choose an example wherein the induced extensional strain
is small enough so that the exact solution of the linear theory can be
used for a comparison. In particular, we apply a small force of
constant magnitude at the free end of the rod for a short time and then
removed it. For the linear theory to be applicable, we want $\lambda = 1.05$,
which corresponds to the extensional strain $\gamma = (\lambda^2 - 1)/2 = 0.05125$ in./in.
We choose a thin rod of Mooney material ($C_1 = 24.0$ psi and $C_2 = 1.5$ psi)
with the following undeformed characteristics: length $= 3.0$ in. , cross-
sectional area $= 0.0314$ in^2, and mass density $= 0.0001$ lb-sec^2/in^4.
For the finite element model, we take 60 uniform elements, so that
$h = 0.05$ in. and $E = 60$. Since the applied load, $Q(t)$, can be expressed
as $Q = \sigma A$, we have, using (3.25) in (3.22) with $\lambda = 1.05$, $Q(t) = 0.228$ lb,
and we choose the duration of the loading to be 0.002 seconds. The
typical stress wave response to this loading is shown in Fig. 5 with the
exact linear solution superposed for comparison. The response shown
in Fig. 5 is representative of all the integration schemes mentioned
earlier, except the Lax-Wendroff scheme, since there was no discernable
difference between the responses obtained by each scheme.

A comparison between the velocity-formulated central difference
scheme and the Lax-Wendroff scheme can be seen in Fig. 6 where the
stress wave response to a 2.0 lb applied end load (about 86 percent
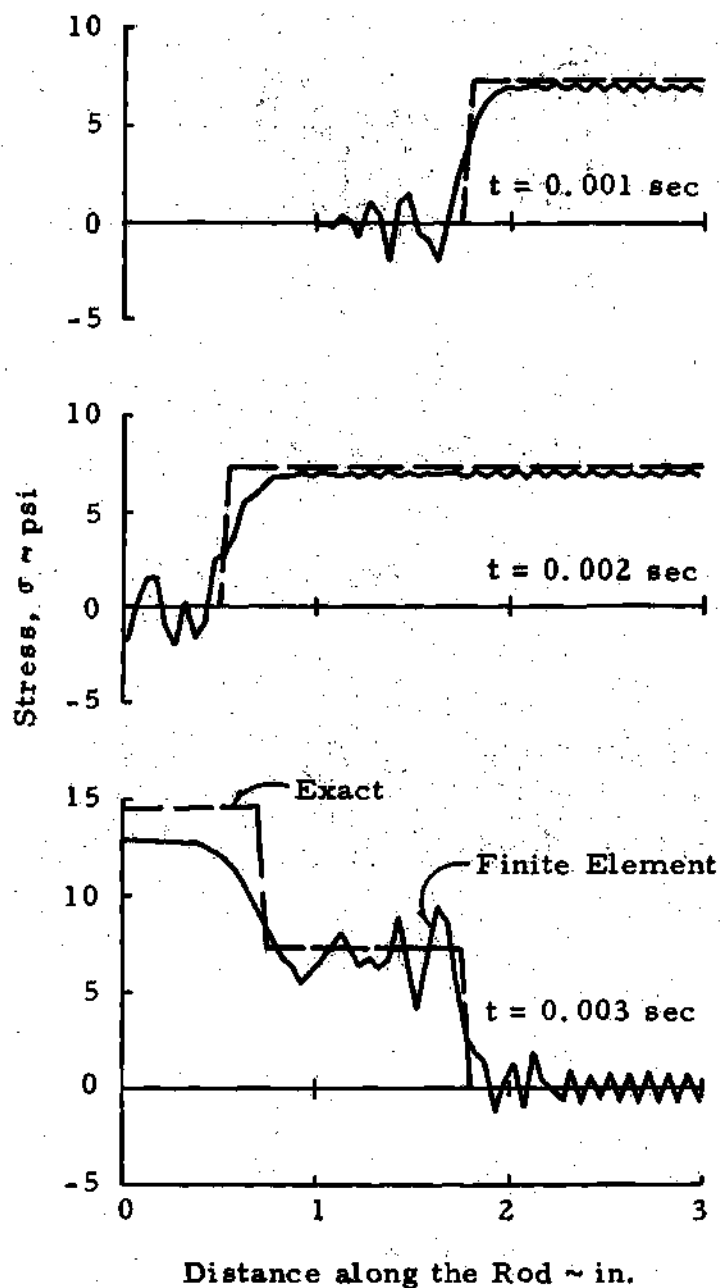
Figure 5.   Time History of Linear Stress Wave for Different
Integration Schemes
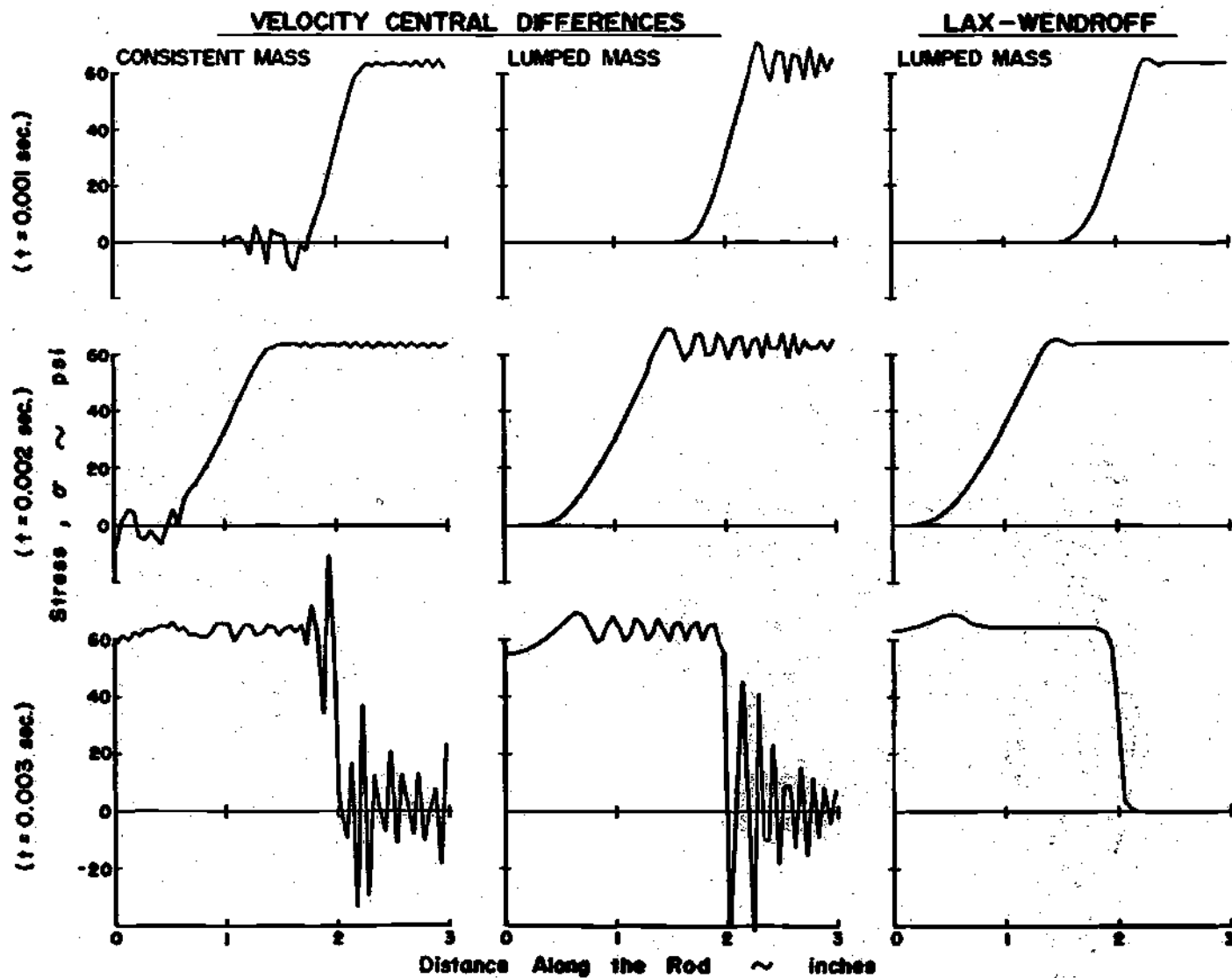
Figure 6. Effects of Mass Distribution and Temporal Operator on Stress Wave Response in a Thin Rod

strain) is shown. Also depicted in Fig. 6 are the differences between the responses of the lumped and consistent mass models. Here it can be seen that the lumped mass model eliminates the spurious oscillations (or "ringing") in front of the stress wave of the consistent mass model. Also, the computational efficiency of the lumped mass model was demonstrated in that only 26 sec were required by the UNIVAC 1108 to compute 3000 integration steps for this model, while 35 sec were required to compute only 2300 integration steps for the consistent mass model.

4.5 Finite Element/Difference Equations

The remaining step in discretizing the nonlinear equations of motion is choosing a time integration scheme to approximate their temporal behavior. Solving the nonlinear equations of motion by stepwise numerical methods can be severely complicated by the presence of shocks. Therefore, we choose an explicit finite difference scheme which can accommodate shock waves, if they occur, without the tedious application of the jump conditions at each time step of the solution process. This method is the well-known Lax-Wendroff difference scheme [85-87], which is generally classified as an artificial dissipative method (cf., [88] where the basic fundamentals of this class of integration schemes was first presented) by virtue of the particular way the equations are differenced. The success of this particular method comes from applying

finite difference approximations to the governing equations expressed as conservation laws. The novel aspect of the following temporal discretization is that, by rewriting (3.19) as (3.21), we obtain the governing equation in the form of a conservation law which, with only a linear finite-element approximation, enables us to develop the desired Lax-Wendroff type integration scheme.

Lax-Wendroff-Finite-Element Scheme

The temporal discretization is accomplished in the spirit of the Lax-Wendroff equations (cf., [87], p. 302): We first denote $\dot{q}_N = \ddot{\lambda}_N$ and expand $q_N(t + \Delta T)$ into a Taylor series up to second order terms

$$q_N(t + \Delta t) = q_N(t) + \Delta t \dot{q}_N + \frac{1}{2}(\Delta t)^2 \ddot{q}_N + O(\Delta t^3) \qquad (4.29)$$

The t-derivatives in (4.29) are now replaced by X-derivatives (except for the nodal force P_i) by means of (4.21) where

$$\dot{q}_N = \frac{A_o}{mh}(\sigma_{N-1} - 2\sigma_N + \sigma_{N+1}) + \frac{1}{m}P_N \qquad (4.30)$$

$$\ddot{q}_N = \frac{\partial}{\partial t}\dot{q}_N = \frac{A_o}{mh}(\dot{\sigma}_{N-1} - 2\dot{\sigma}_N + \dot{\sigma}_{N+1}) + \frac{1}{m}\dot{P}_N \qquad (4.31)$$

Since $\sigma = \sigma(\lambda)$, $\dot{\sigma} = \rho_o c^2 q$, so that (4.31) becomes

$$\ddot{q}_N = \frac{1}{h^2}(c_{N-1}^2 q_{N-1} - 2c_N^2 q_N + c_{N+1}^2 q_{N+1}) + \frac{1}{m}\dot{P}_N \qquad (4.32)$$

Note that since the quantities P_N are prescribed, so also are the $\dot{P}_N$ (e.g., if $P_N = \sin t$, then $\dot{P}_N = \cos t$). Substituting (4.30) and (4.32) into (4.29), we obtain the finite-element/difference equation for the interior nodes of the discrete model:

$$q_N^{n+1} = \left(\frac{\Delta t}{h}\right)^2 \left\{\frac{1}{2}\left(c_{N+1}^n\right)^2 q_{N+1}^n + \left[\left(\frac{h}{\Delta t}\right)^2 - \left(c_N^n\right)^2\right] q_N^n \right. \qquad (4.33)$$

$$\left. + \frac{1}{2}\left(c_{N-1}^n\right)^2 q_{N-1}^n\right\} + \frac{\Delta t A_o}{mh}\left(\sigma_{N-1}^n - 2\sigma_N^n + \sigma_{N+1}^n\right)$$

$$+ \frac{1}{2m}\left[2\Delta t P_N^n + (\Delta t)^2 \dot{P}_N^n\right]$$

where $t = n\Delta t$, and $q(t) = q(n\Delta t) = q^n$, etc. Similarly, the finite-element/difference equations for the end nodes are

$$q_1^{n+1} = \left(\frac{\Delta t}{h}\right)^2 \left\{\left(c_2^n\right)^2 q_2^n + \left[\left(\frac{h}{\Delta t}\right)^2 - \left(c_1^n\right)^2\right] q_1^n\right\} \qquad (4.34)$$

$$+ 2\frac{\Delta t A_o}{mh}\left(\sigma_2^n - \sigma_1^n\right) + \frac{1}{m}\left[2\Delta t P_1^n + (\Delta t)^2 \dot{P}_1^n\right]$$

and

$$q_{E+1}^{n+1} = \left(\frac{\Delta t}{h}\right)^2 \left\{ \left(c_E^n\right)^2 q_E^n + \left[\left(\frac{h}{\Delta t}\right)^2 - \left(c_{E+1}^n\right)^2\right] q_{E+1}^n \right\} \tag{4.35}$$

$$+ 2\frac{\Delta t A_o}{mh}\left(\sigma_E^n - \sigma_{E+1}^n\right) + \frac{1}{m}\left[2\Delta t P_{E+1}^n + (\Delta t)^2 \dot{P}_{E+1}^n\right]$$

To compute the extension ratios, we simply repeat the foregoing procedure. We first expand λ_N^{n+1}:

$$\lambda^{n+1} = \lambda_N^n + \Delta t q_N^n + \left(\frac{\Delta t}{2}\right)^2 \dot{q}_N^n + O(\Delta t^3) \tag{4.36}$$

and so, using (4.30), we get

$$\lambda_n^{n+1} = \lambda_N^n + \Delta t q_N^n + \frac{1}{2\rho_o}\left(\frac{\Delta t}{h}\right)^2 \left(\sigma_{N-1}^n - 2\sigma_N^n + \sigma_{N+1}^n\right) + \frac{(\Delta t)^2}{2m} P_N^n$$

$$\lambda_1^{n+1} = \lambda_1^n + \Delta t q_1^n + \frac{1}{\rho_o}\left(\frac{\Delta t}{h}\right)^2 \left(\sigma_2^n - \sigma_1^n\right) + \frac{(\Delta t)^2}{m} P_1^n \tag{4.37}$$

$$\lambda_{E+1}^{n+1} = \lambda_{E+1}^n + \Delta t q_{E+1}^n + \frac{1}{\rho_o}\left(\frac{\Delta t}{h}\right)^2 \left(\sigma_E^n - \sigma_{E+1}^n\right) + \frac{(\Delta t)^2}{m} P_{E+1}^n$$

where σ_N^n and $(c_N^n)^2$ are determined from (3.22) and (3.20), respectively.

Equations (4.33)-(4.35) and (4.37) are the $2(E + 1)$ finite element/difference equations used herein for the study of shock waves.

Velocity Formulated Central Difference Scheme

To illustrate the effectiveness of the Lax-Wendroff method we will compare the results with the finite-element/difference equations which are obtained using the displacement equations (4.22). The temporal discretization is accomplished for these equations by using the velocity formulated central difference scheme [80], in which the general nodal equation, $\ddot{u}_N(t) = F(t)$, is approximated by introducing the nodal velocity $v_N = \dot{u}_N$ and thereby generating two equivalent first order equations, which are then differenced to obtain

$$v_N^{n+\frac{1}{2}} = v^{n-\frac{1}{2}} + \Delta t\, F_N^n$$

$$(4.36)$$

$$u_N^{n+1} = u_N + \Delta t\, v^{n+\frac{1}{2}}$$

4.6 Numerical Results

In this section, we cite numerical results obtained from application of the preceding theory to representative problems. For our numerical examples, we consider a thin rod of Mooney material ($C_1 = 24.0$ psi, $C_2 = 1.5$ psi) with the following undeformed characteristics: length = 3.0 in., cross-sectional area = 0.0314 in^2, mass density = 10^{-4} lb-sec^2/in^4. For the finite element model, we take 60 evenly spaced elements, so that h = 0.05 in. and E = 60.

Tensile Loading (square wave)

We consider a force of constant magnitude applied at the free end of the rod as a step function at t = 0, then similarly removed at a later time t = t*, i. e., a square wave. For this example, t* = 0. 002 seconds. Figure 6 shows the stress wave response to a 2-lb step loading (this corresponds to 86 percent strain statically) for both mass distributions and both time integration schemes previously discussed. Several important items mentioned earlier can be observed in Fig. 6.

• The lumped mass model does not produce the ringing in front of the wave that the consistent mass model does.

• The acceleration wave front does tend to flatten with time.

• The wave is propagated into the undisturbed portion of the rod as a simple wave. Recall that for a simple wave, $\dot{Y}(t)$ is constant, so that by multiplying Y(0. 001) by 2. 0--the ratio of the elapsed time increments--we obtain Y(0. 002), except, of course, for that portion of the wave affected by the fixed boundary.

• The Lax-Wendroff scheme is clearly superior to the central difference scheme, particularly in the presence of shocks. Not only does it produce no ringing in front of the wave, but the unloading shock wave is depicted without the large oscillations behind the shock. (These oscillations have been interpreted by some as numerical instability of the integration scheme. This is not so: the amplitude

of these oscillations does not grow with increasing time nor with
decreasing Δt. As pointed out in [87], these are lumped mass
oscillations resulting from discretization error, and they represent
the internal energy which must appear in the "shocked" region accord-
ing to the jump conditions. It is conjectured that the Lax-Wendroff
scheme converts this oscillatory energy into true internal energy,
perhaps with the provision that, as may be seen in the investigation
by Hicks and Pelzl [89], the strength of the shock is not too strong.)

Figure 7 shows in some detail the response of the rod to this
2-lb step load. The results confirm the fact that weak shocks propagate
in a manner similar to simple waves--the stress increases at the wall
almost by a factor of two and the stress wave is reflected from the wall
without appreciable change in shape or magnitude.

Sinusoidal Forcing Function

This example dramatically illustrates that the central difference
scheme, without modification, cannot handle shocks. Here, a con-
centrated time-dependent load which varies sinusoidally with an ampli-
tude of 1.7 lb is applied at the free end; a complete loading cycle
occurs in 0.002 seconds. Unlike the response for the tensile step load
where the unloading wave is produced by simply removing the load, the
sinusoidal load actually "pushes" the end of the rod. The instant the
load starts to decrease is the moment when the first wavelet is
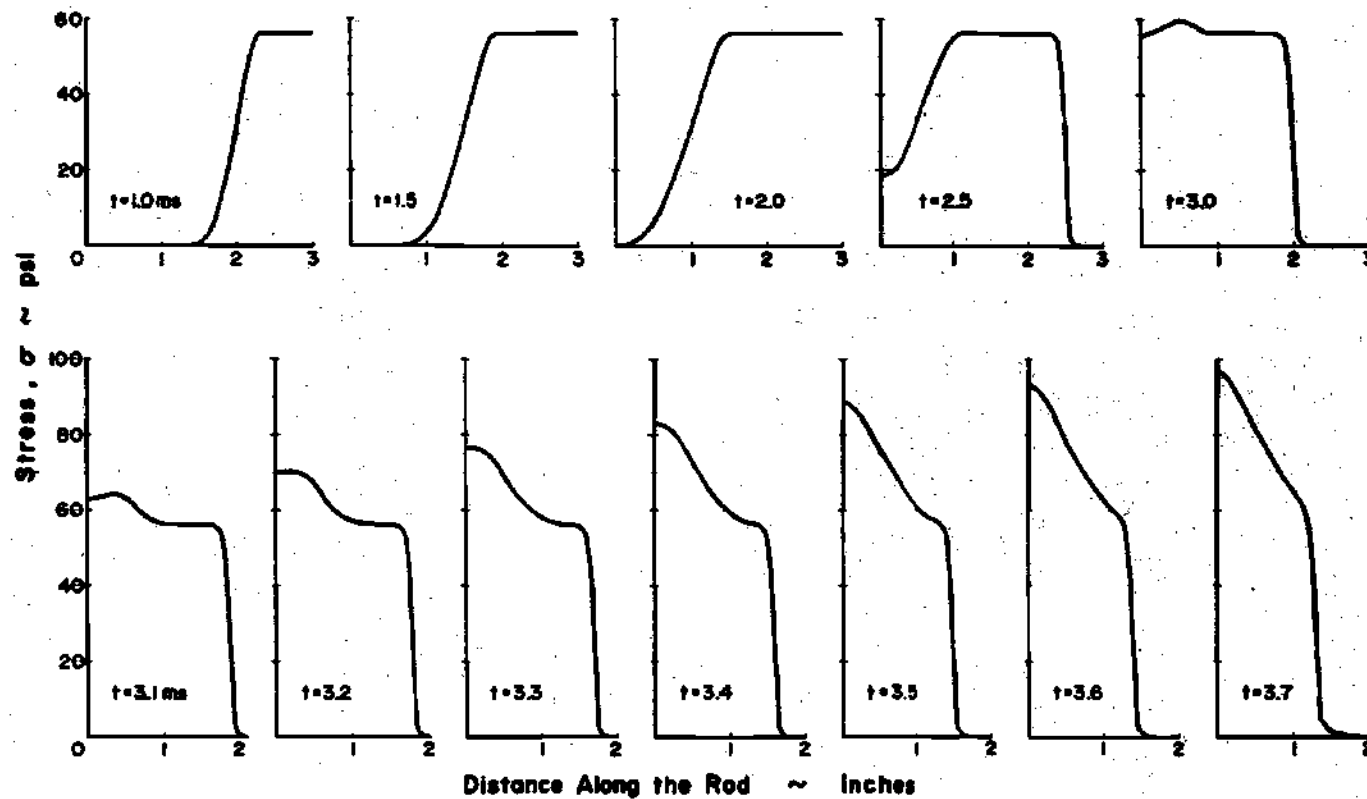
Figure 7.   Time History of Stress Wave Response to Step Load at End of Rod (Sheet 1 of 3)
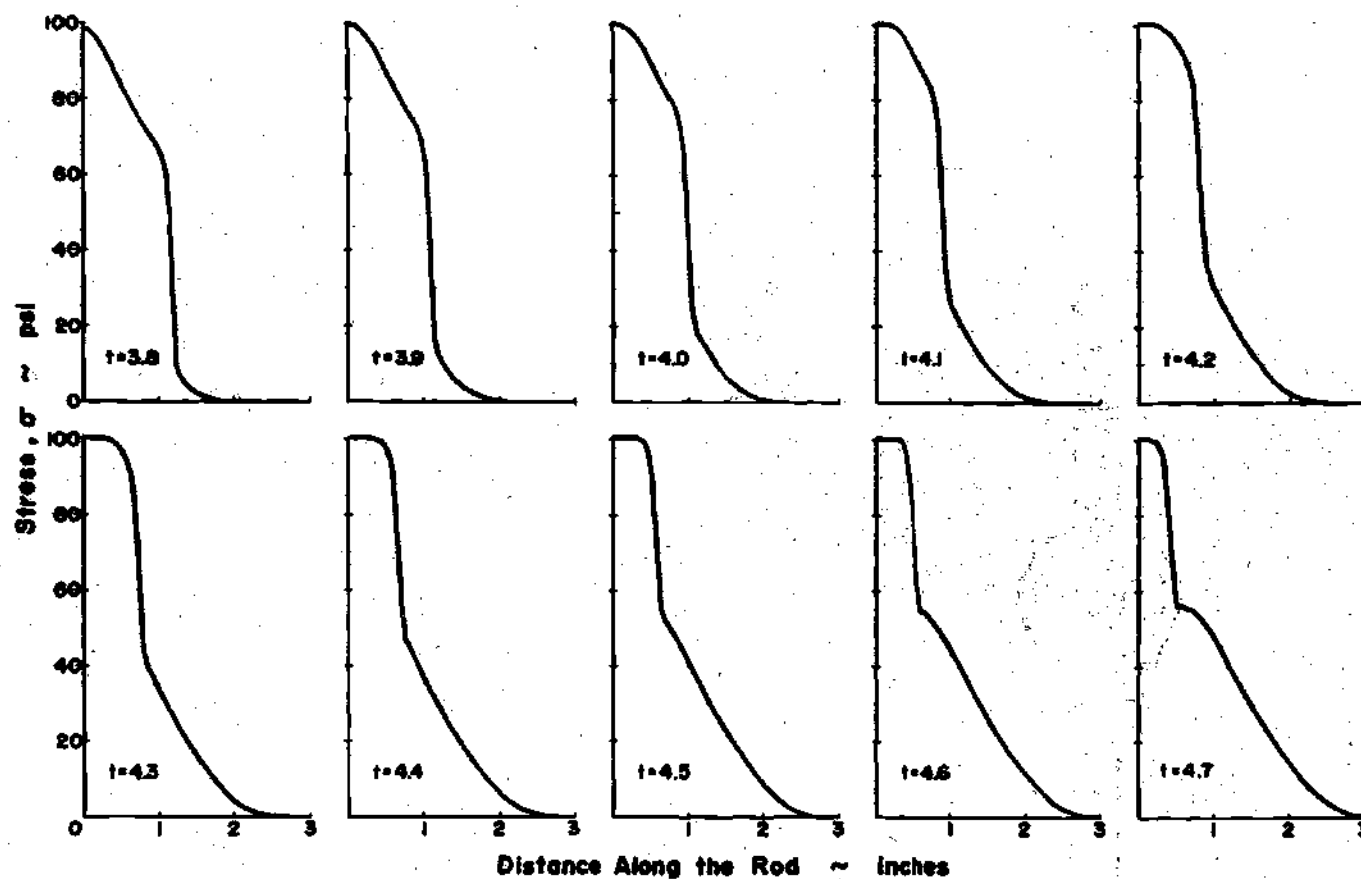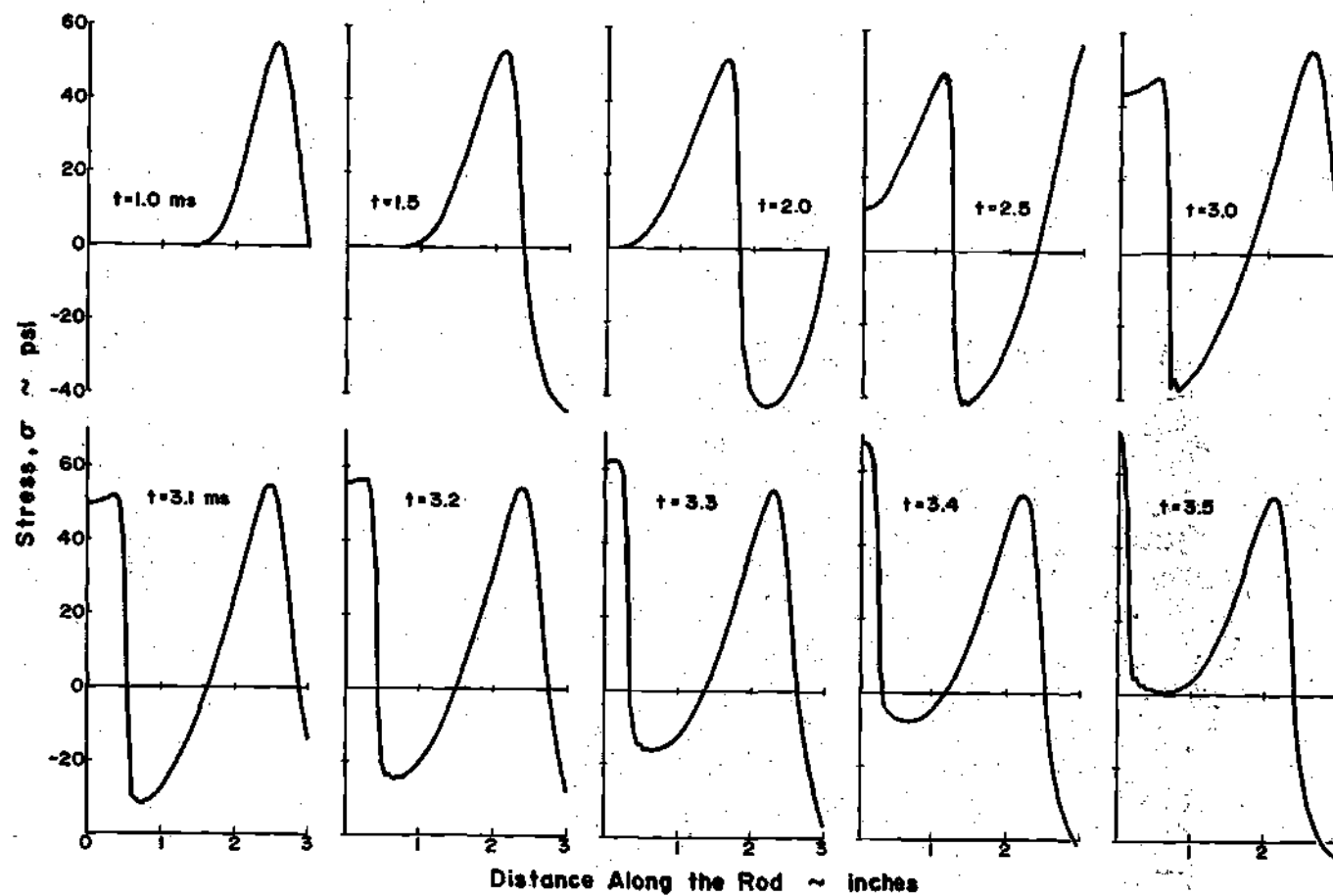
Figure 7.   Time History of Stress Wave Response to Step Load at End of Rod (Sheet 2 of 3)
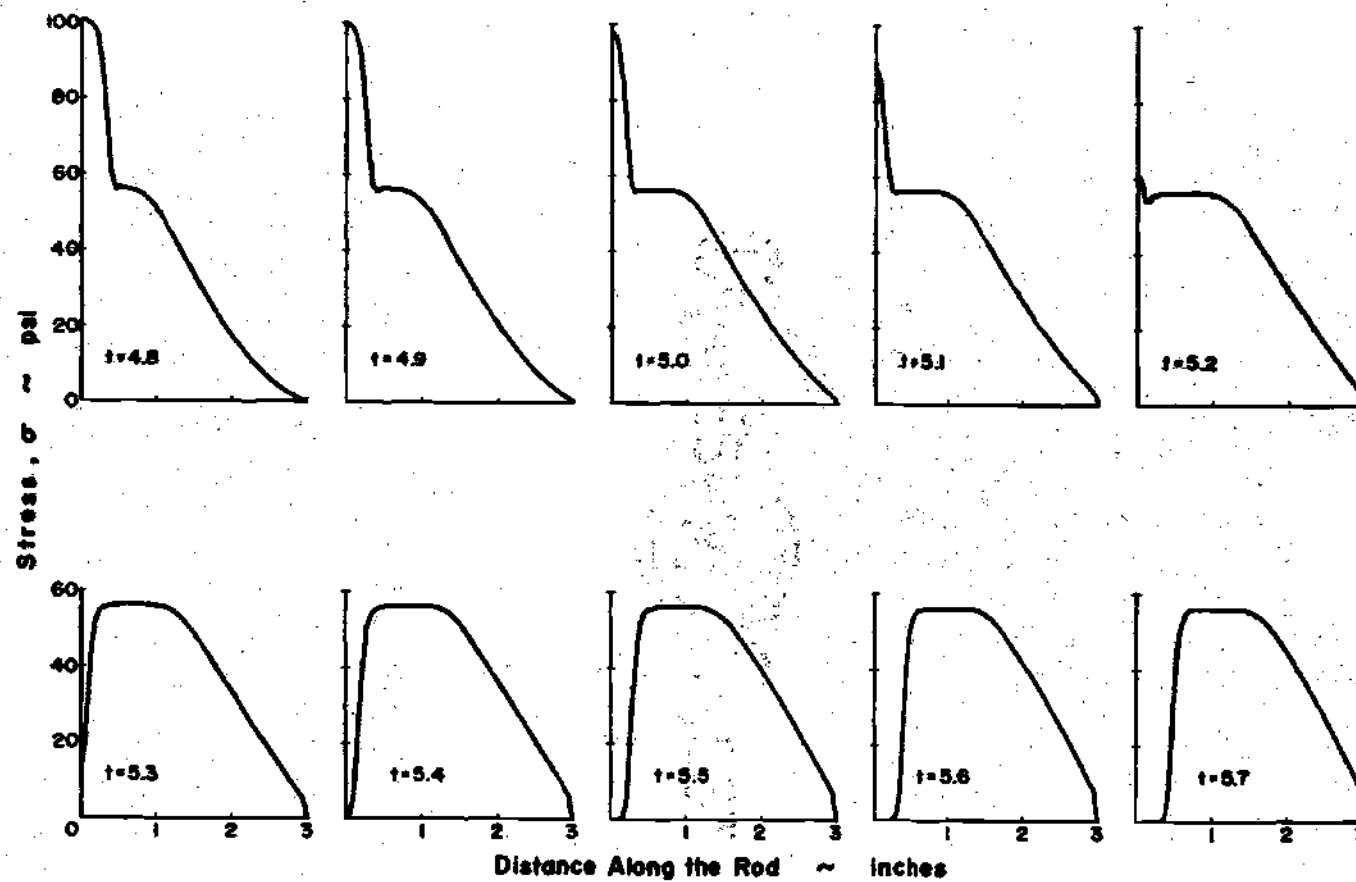
Figure 7. Time History of Stress Wave Response to Step Load at End of Rod (Sheet 3 of 3)

generated which propagates faster than the preceding one. Thus, at some time subsequent to when the compression cycle starts, a compression shock forms in the rod.

A comparison between the two integration schemes is shown in Fig. 8 for the sinusoidal loading. In this case it is clear that the "shocked internal energy" behind the compression shock renders the central difference scheme unacceptable. It is interesting to note, however, that the tension cycle evidently "absorbs" the large oscillations preceding it and again produces a smooth wave front. The detailed response to this loading is shown in Fig. 9. From the response shown, we notice several interesting features of nonlinear wave motion:

● The compressive shock wave is reflected from the wall as a compressive shock wave by almost doubling the compressive stress; but the tension part of the stress wave is reflected with only a small increase in stress.

● At $t = 4.6$ msec, two compression shocks are about to collide. The numerical results shown here indicate that when two shocks collide in a solid material, they penetrate one another with little or no deterioration. This is apparently contrary to the collision of shocks in gases [75].

● By comparing the response at $t = 3$ msec with that at $t = 5$ msec, we note that the response tends to repeat itself (with some variation
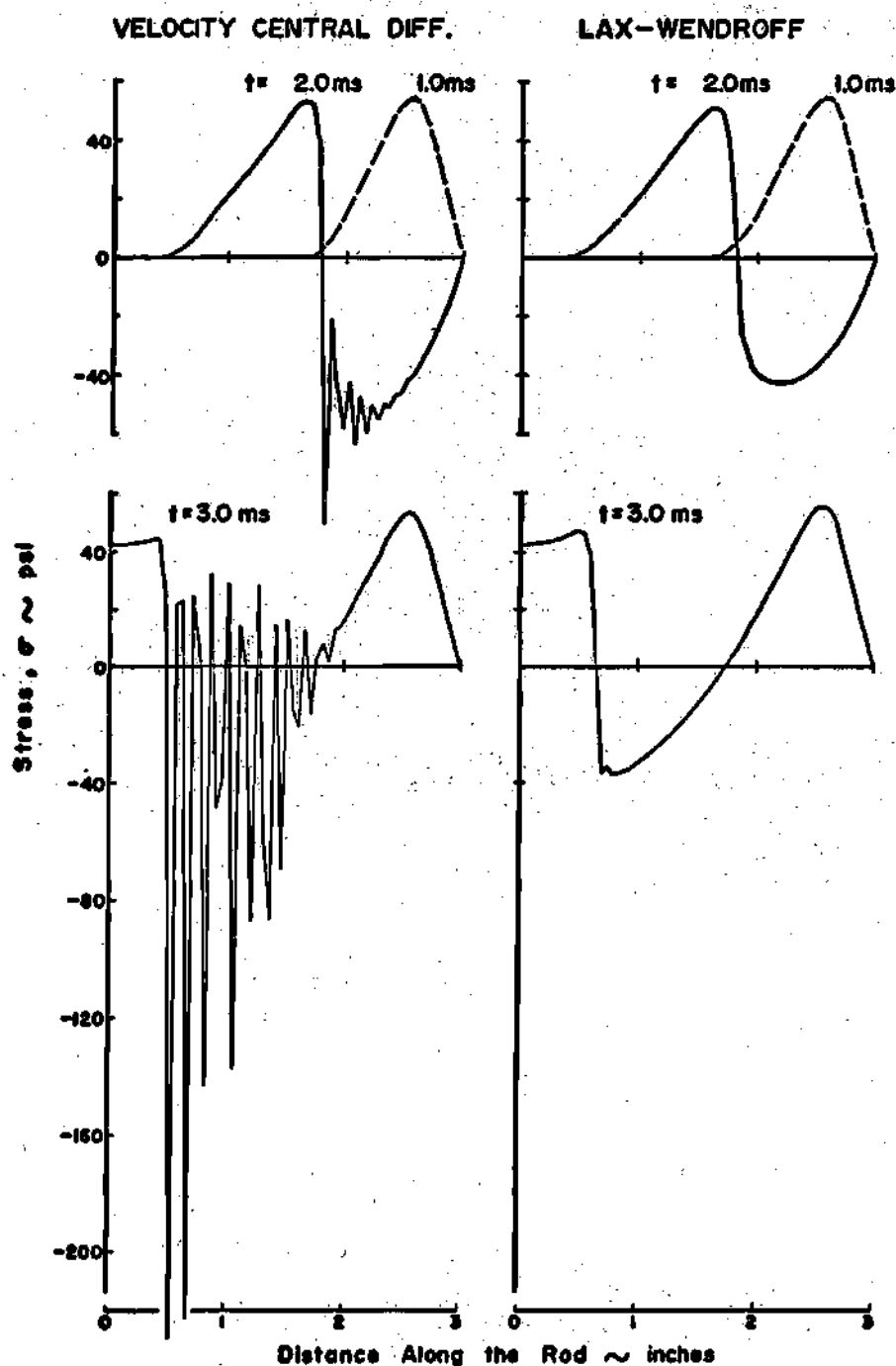
Figure 8. Comparison of Stress Wave Response to Sinusoidal End Load on Rod for Two Integration Schemes

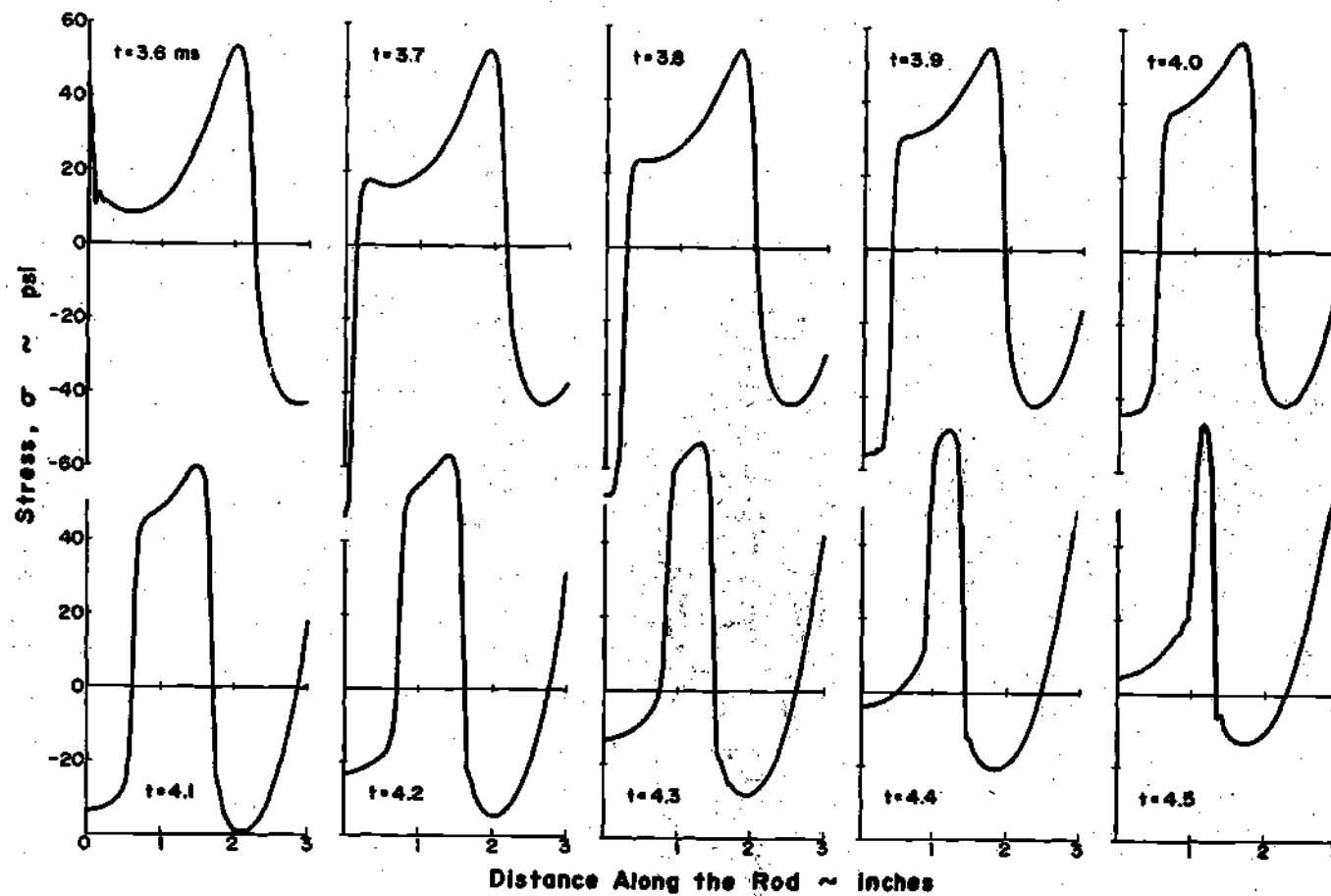Figure 9. Time History of Stress Wave Response to Sinusoidal End Load (Sheet 1 of 3)

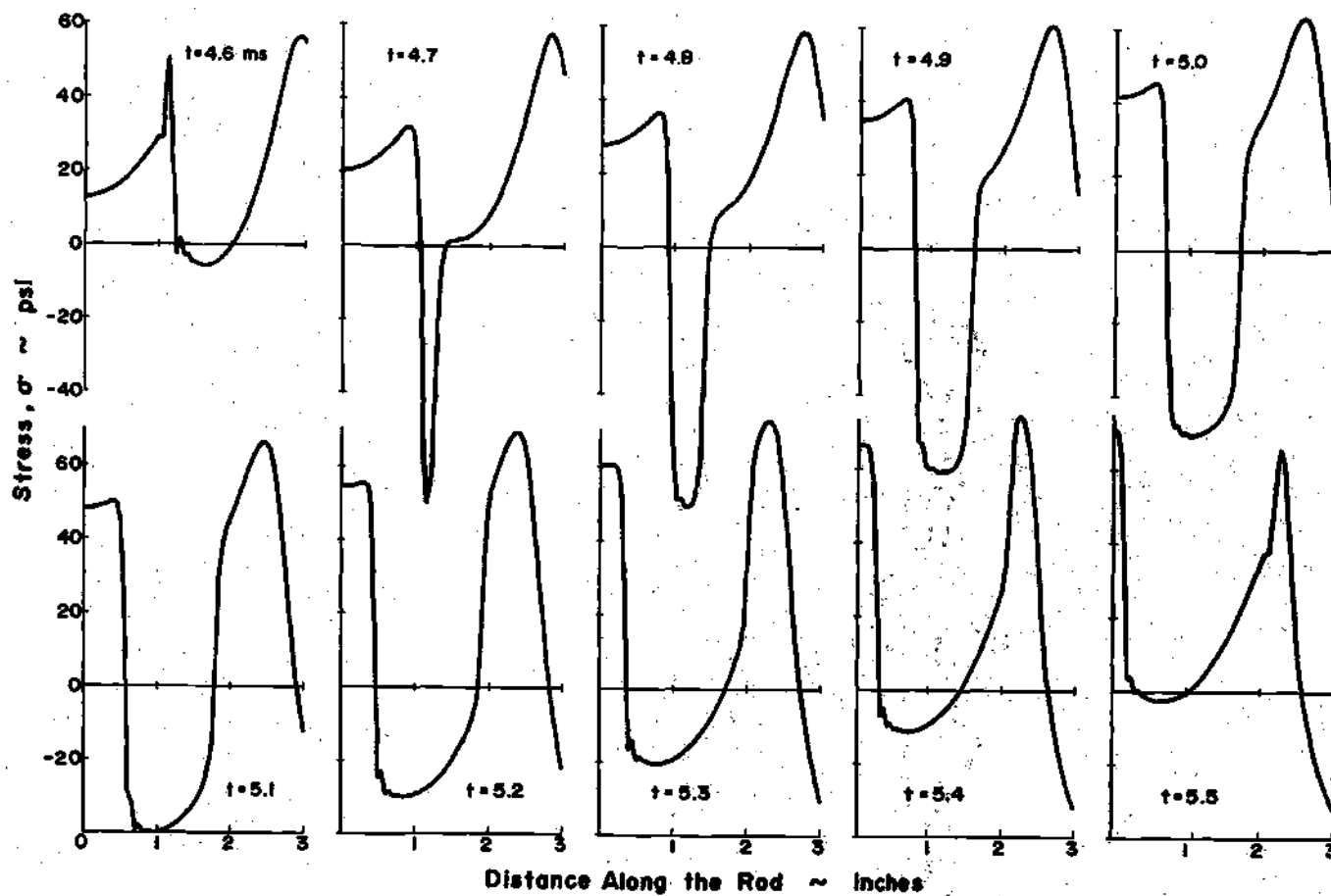Figure 9.   Time History of Stress Wave Response to Sinusoidal End Load (Sheet 2 of 3)

Figure 9. Time History of Stress Wave Response to Sinusoidal End Load (Sheet 3 of 3)

due to the reflection) with essentially the same period as that of the forcing function.

● As in the development of shocks from Lipschitz continuous data (cf., Section 3.3), the shock forms subsequent to initiation of the compressive cycle. Thus we are led to examine the positive slope characteristics in the X-t plane to see if they predict t_{CR} for this type of loading. Figures 10 and 11 show that if we assume straight compression characteristics of positive slope, the cusp of the corresponding envelope in the X-t plane does, in fact, give a good estimate of the t_{CR} observed in the stress-time plots.
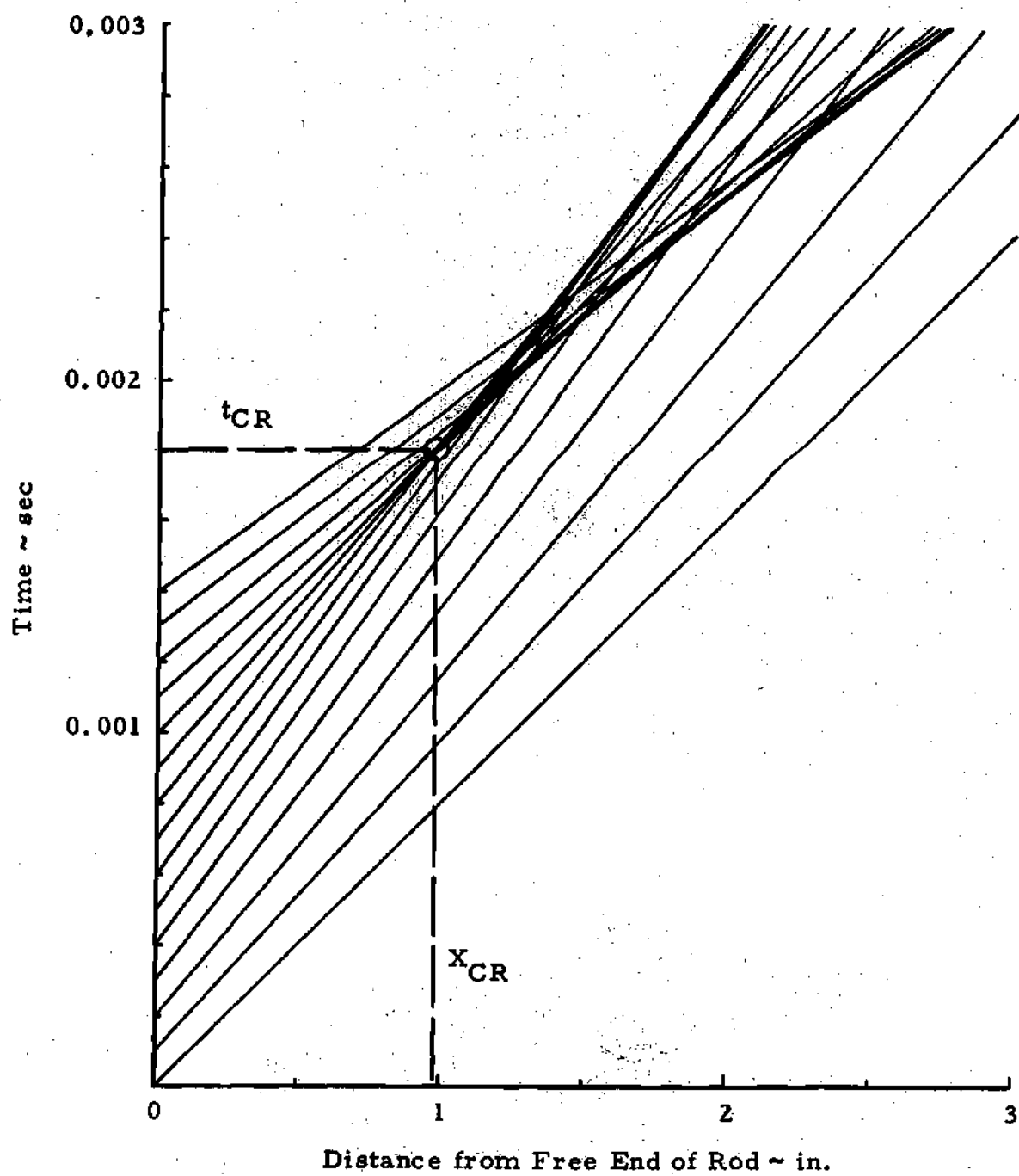
Figure 10. Characteristic Field Computed for Sinusoidal End Load
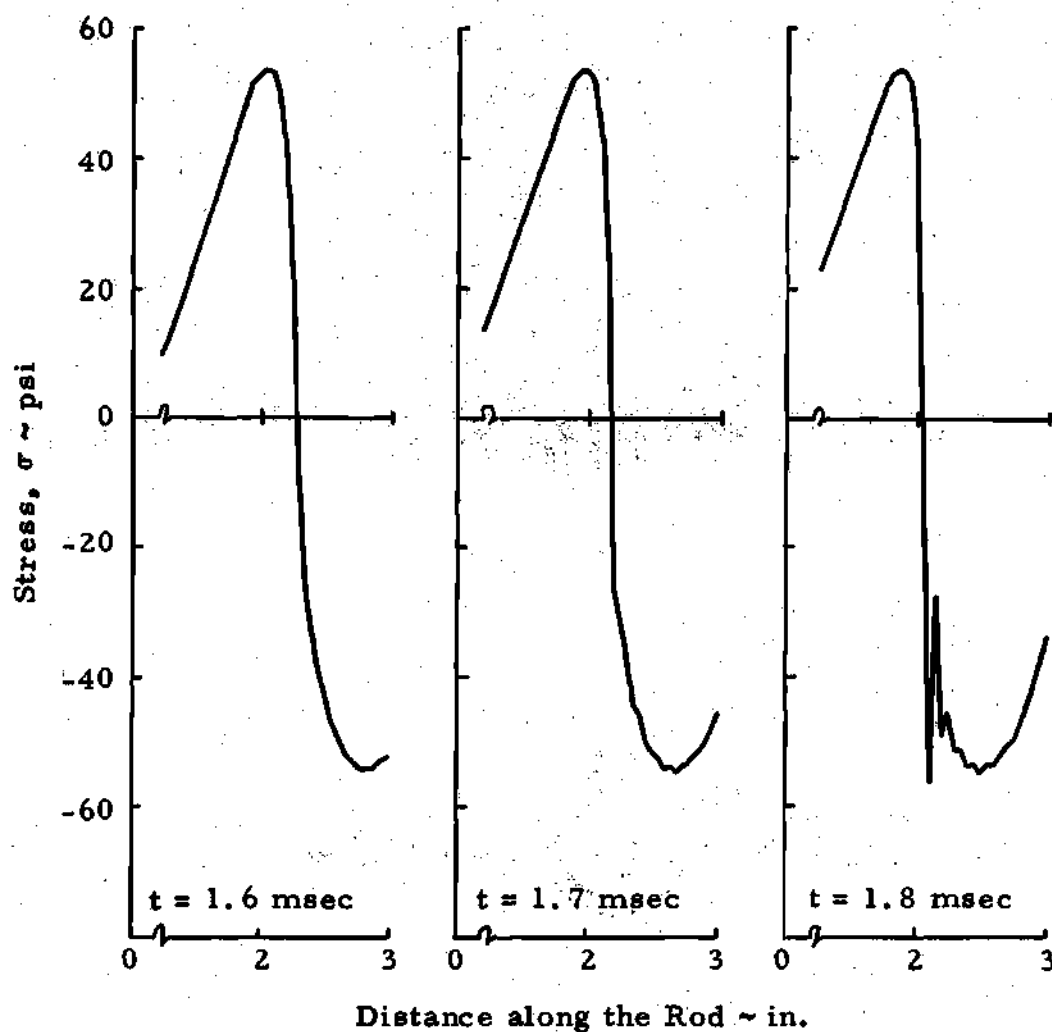
Figure 11. Change in Stress Distribution during Shock Formation

CHAPTER V

STABILITY AND CONVERGENCE

5.1 General Discussion

This chapter, the majority of which is taken virtually intact from

the recent paper by Oden and Fost [90], is concerned with the estimation

of both the rate-of-convergence of finite element approximations and

the stability of time integration schemes for transient solutions of a

rather large class of nonlinear hyperbolic partial differential equations.

The equations of motion of most homogeneous hyperelastic bodies,

including both physically nonlinear materials and finite amplitude motions,

fall within the general class of equations considered; but, for simplicity,

we still limit our attention to one-dimensional bodies. We assume that

the initial data and the solution are smooth enough functions of both X

and t so that we may rule out the possibility of shock discontinuities.

Thus, in the absence of shocks, the results obtained are valid for most

transient nonlinear vibration problems.

Apparently, there are no general methods for the study of stability

and convergence for finite element approximations of nonlinear hyper-

bolic equations. Only within the past year have answers to these

questions been obtained for even the linear case. Fix and Nassif [91]

investigated finite element approximations of linear first-order hyperbolic equations, and Kikuchi and Ando [92] studied properties of finite element approximations of a class of linear and nonlinear initial value problems. Fujii [93] examined both the convergence of finite element approximations and the numerical stability of smooth solutions of linear second-order hyperbolic equations with the Newmark β-method used as the temporal operator. Like Fujii, we also examine the stability in certain natural energy norms and obtain the stability criterion for nonlinear difference schemes. The nonlinear stability criterion reduces to that obtained by Fujii for linear difference approximations. (A perturbation stability analysis of an explicit scheme is presented in the Appendix for comparison.) Also, nonlinear error estimates are obtained which essentially agree with those Fujii obtained for the linear case, but are arrived at by an approach which is necessarily quite different.

5.2 Energy Formulation of the Problem

We prefer to describe the problem in physical terms. Recall the thin homogeneous rod of hyperelastic material described in Chapter III. We wish to study the longitudinal motion of the rod relative to the reference configuration in which the rod is at rest prior to t = 0. Response of the rod is initiated by some prescribed initial velocity $v_0(X)$ or initial displacement $u_0(X)$; for the moment, no body forces or end tractions are prescribed.

The total energy E(t) of the rod at time t is given by

$$E = K + H \tag{5.1}$$

where K is the kinetic energy and H is the internal energy:

$$K = \frac{\rho_o A_o}{2} \int_0^{L_o} \dot{u}^2 dX \quad ; \quad H = A_o \int_0^{L_o} W dX \tag{5.2}$$

Recall $\dot{u} = \partial u/\partial t$ is the particle velocity field and W is the strain energy per unit undeformed volume. The strain energy function W depends upon $\partial u(X,t)/\partial X \equiv u_X$ and is assumed to have the following properties:

(i) $W(u_X)$ has continuous bounded positive second derivatives with respect to the displacement gradients u_X. Indeed, $d^2 W/du_X^2$ is proportional to the square of the natural wave speed of the material, a positive function always $< +\infty$.

(ii) $\dfrac{dW(u_X)}{du_X} \equiv T(u_X) =$ first Piola-Kirchhoff stress $\tag{5.3}$

Property (i) is directly akin to material stability and is a constitutive assumption; property (ii) is merely a definition.

Since the system is conservative and the mechanical power of the external forces is zero, the principle of conservation of energy asserts that for every t

$$\dot{E}(t) = 0 \qquad (5.4)$$

Denoting the inner-product of any two displacement fields $u_1(X, t)$, $u_2(X, t)$ by

$$\langle u_1(\cdot, t), u_2(\cdot, t) \rangle = \int_0^{L_o} u_1 u_2 dX \qquad (5.5)$$

we find, upon introducing (5.2) and (5.3) into (5.4), that

$$\rho_o A_o \langle \ddot{u}, \dot{u} \rangle + A_o \langle T(u_X), \dot{u}_X \rangle = 0 \qquad (5.6)$$

This result is the governing equation for generalized motions of the rod; it is precisely the variational form of the nonlinear hyperbolic momentum equation

$$\rho_o A_o \frac{\partial^2 u}{\partial t^2} - A_o \left(\frac{dT(u_X)}{du_X} \right) \frac{\partial^2 u}{\partial X^2} = 0 \qquad (5.7)$$

Obviously, $\frac{1}{\rho_o} dT/du_X = \frac{1}{\rho_o} d^2 W/du_X^2$ is the square of the natural wave speed of the rod material. We must, of course, add to (5.6) appropriate boundary and initial conditions of the type $\langle u(\cdot, 0) - u_o, v(\cdot, 0) \rangle = 0$, $\langle \dot{u}(\cdot, 0) - v_o, v(\cdot, 0) \rangle = 0$, $T(u_X) \dot{u} \Big|_0^{L_o} = 0$, etc.

5.3 Finite Element/Difference Approximations

To approximate (5.6), we partition the rod as in Chapter IV, but without requiring h_N to be uniform, into a finite number E of connected segments. We assume the exact solution of (5.6) during a time interval $0 \leq t \leq T$ is an element of the space $\mathcal{E}(0, L_o) \times C^3[0, T]$, where $\mathcal{E}(0, L_o)$ is an appropriate energy space associated with the problem and $C^3[0, T]$ is the space of functions whose first three derivatives are continuous on $[0, T]$. In the finite-element method, we seek an approximate solution in a finite dimensional subspace, $\mathcal{F}$, of $\mathcal{E}(0, L_o)$ containing the exact variational solution to the problem. The elements of $\mathcal{F}$ are of the form

$$U(X, t) = U_N(t)\psi_N(X) \tag{5.8}$$

where the repeated nodal index N is summed from 0 to E + 1. Here $U_N(t)$ is the value of $U(X, t)$ at node N at time t and $\psi_N(X)$ are basis functions designed so as to have the usual finite-element properties; i.e.,

$$\psi_N(X^M) = \delta_N^M \quad ; \quad M, N = 1, 2, \dots, E + 1$$

$$\tag{5.9}$$

$$\psi_N(X) = 0 \quad \text{if} \quad X \notin (X^{N-1}, X^{N+1})$$

In general, the functions $\psi_N(X)$ are generated from local (element) basis functions which contain complete polynomials of degree p, where p + 1 is the order of the highest spatial derivative that appears in the functional (5.6) (cf., [17]). In our case, p = 1.

In the present study, we shall also follow the customary procedure and approximate the behavior of $U(X, t)$ in time by finite differences. We divide the time interval $[0, T]$ into R equal time intervals Δt, and describe the variation of $U_N(t)$ in t in terms of its values at times $i\Delta t$, i = 0, 1, ..., R. Thus (5.8) is written

$$U^i = U(X, i\Delta t) = U_N^i \psi_N(X) \qquad (5.10)$$

where $U_N^i = U_N(i\Delta t)$. To represent time-rates, we employ the difference quotients

$$\nabla_t U^i = (U^{i+1} - U^i)/\Delta t \quad ; \quad \Delta_t U^i = (U^i - U^{i-1})/\Delta t$$

$$\delta_t U^i = \frac{1}{2} (\nabla_t U^i + \Delta_t U^i) = (U^{i+1} - U^{i-1})/2\Delta t \qquad (5.11)$$

$$\delta_t^2 U^i = \nabla_t \Delta_t U^i = (U^{i+1} - 2U^i + U^{i-1})/\Delta t^2$$

By direct substitution of (5. 10) and (5. 11) for u and its various time rates in (5. 6), we arrive at the finite-element/difference scheme governing our discrete model:

$$\rho_o A_o \langle \delta_t^2 U^i, \delta_t U^i \rangle + A_o \langle T(U_X^i), \delta_t U_X^i \rangle = 0 \qquad (5.12)$$

Here $U_X^i = \partial U^i / \partial X = U_N^i d\psi_N(X)/dX$ and $\delta_t U_X^i = (\delta_t U_N^i) d\psi_N(X)/dX$.

Physical Interpretation of Equation (5. 12)

It is enlightening to interpret the terms of (5. 12) physically. For instance, consider the first term in (5. 12), and denote by K_+^i and K_-^i the kinetic energy of the discrete model computed using forward and backward difference approximations of the velocities, respectively. Then

$$K_+^i = \frac{1}{2} m_{NM} \nabla_t U_N^i \nabla_t U_M^i$$

$$(5.13)$$

$$K_-^i = \frac{1}{2} m_{NM} \Delta_t U_N^i \Delta_t U_M^i$$

where N, M = 1, 2, ..., E + 1; i = 1, 2, ..., R - 1 and m_{NM} is the consistent mass matrix,

$$m_{NM} = \rho_o A_o \int_0^{L_o} \psi_N \psi_M dX \qquad (5.14)$$

It can now be shown that the first term in (5.12) is, as should be expected, precisely a difference analogue of the time rate-of-change of the kinetic energy of the finite-element model. In fact,

$$\rho_o A_o \langle \delta_t^2 U^i, \delta_t U^i \rangle = \rho_o A_o \langle \psi_N, \psi_M \rangle \delta_t^2 U_N^i \delta_t U_M^i$$

$$= \frac{1}{2 \Delta t} m_{NM} \{ \nabla_t U_N^i \nabla_t U_M^i - \Delta_t U_N^i \Delta_t U_M^i \} \qquad (5.15)$$

$$= (K_+^i - K_-^i) / \Delta t$$

Note also that if $\| u \|$ denotes the norm associated with the inner product (5.5) (i. e., $\| u \|^2 = \langle u, u \rangle$), then (5.13) can also be written

$$K_+^i = \frac{\rho_o A_o}{2} \| \nabla_t U^i \|^2 \qquad ; \qquad K_-^i = \frac{\rho_o A_o}{2} \| \Delta_t U^i \|^2 \qquad (5.16)$$

The second term in (5.12) is clearly analogous to the time rate-of-change of the total internal energy of the model:

$$H = A_o \langle \dot{W}, 1 \rangle = A_o \langle \frac{dW}{du_X}, \dot{u}_X \rangle \approx A_o \langle T(U_X^i), \delta_t U_X^i \rangle \qquad (5.17)$$

This term contains the stiffness relations for the finite-element model. In fact, in the linear theory $T(U_X^i) = \bar{E} U_X^i = U_N^i \bar{E} \psi_{N, X}$, $\bar{E}$ being the

elastic modulus, so that $\dot{H} \approx A_o \bar{E} U_N^i \delta_t U_M^i \langle \psi_{N,X}, \psi_{M,X} \rangle$; the array $K_{NM} = A_o \bar{E} \langle \psi_{N,X}, \psi_{M,X} \rangle$ is the global stiffness matrix for the model. In the present study, of course, the stiffness relations may be highly nonlinear.

Relations (5.15) and (5.17) indicate the manner in which (5.12) approximates (5.6). Equation (5.12) describes a discrete model of the conservation principle (5.4). Since the quantities $\delta_t U_N^i$ $(i = 1, 2, \ldots, R - 1; N = 1, 2, \ldots, E + 1)$ are linearly independent, it is clear that (5.12) also implies the discrete momentum equation,

$$m_{NM} \delta_t^2 U_M^i + A_o \langle T(U_M^i \psi_{M,X}), \psi_{N,X} \rangle = 0 \qquad (5.18)$$

However, we prefer to retain the energy form (5.12) for reasons which will become apparent subsequently.

5.4 Numerical Stability

We now investigate the stability, in an energy setting, of the nonlinear finite-element/difference scheme (5.12). To interpret energy criteria in physical terms, we observe that for the continuous system, (5.4) implies that

$$\int_0^T \dot{E} dt = E(T) - E(0) = 0 \qquad (5.19)$$

While we cannot expect the discrete model to also behave in this ideal fashion owing to round-off errors inherent in our method, we can expect that errors in the energy do not become unbounded during the time interval $[0, T]$. In other words, if $E_h(t)$ is our finite element approximation of the total energy at time t, we shall consider our numerical scheme to be stable in energy, if there exists a constant $C > 0$ such that

$$E_h(i\Delta t) \leq CE_h(0) \quad , \quad \text{for } i = 1, 2, \ldots, R$$

Equivalently, stability in energy is assured if

$$E_h(i\Delta t) \leq C^i E_h((i - 1)\Delta t) \tag{5.20}$$

for all $i = 0, 1, 2, \ldots, R$.

Out stability analysis is based on the following assumptions:

● $W(u_X)$ has property (i) of (5.3).

● The finite-element interpolation functions $\psi_N(X)$ satisfy the usual convergence and completeness criteria for linear elliptic problems; i.e., the family of functions $U_N \psi_N(X)$ contains complete polynomials of degree $p = 1$, and the finite element approximation $U_N \psi_N(X)$ is continuous across interelement boundaries. In particular, $\psi_N(X)$ may

be taken to be the common piecewise linear pyramid functions

$$\psi_N(X) = \begin{cases} 0 & X \notin [X^{N-1}, X^{N+1}] \\ [h_N + (X - X^N)]/h_N & , \quad X \in [X^{N-1}, X^N] \\ (X^{N+1} - X)/h_{N+1} & X \in [X^N, X^{N+1}] \end{cases} \quad (5.21)$$

We next cite the following lemmas:

Lemma 1.   Let (5.21) hold, and denote by h the minimum element length

$$h = \min_{N=1, E} h_N \quad (5.22)$$

Then, for every finite element approximation $U = U_N \psi_N$,

$$\left\| \frac{\partial U}{\partial X} \right\| \leq \frac{\nu_1}{h} \| U \| \quad (5.23)$$

where $\| U \|^2 = \langle U, U \rangle$ and ν_1 is the constant $2\sqrt{3}$.

Inequality (5.23) is a fairly well known result and can be found elsewhere (e.g. [93, 94]). It can be proved directly by merely substituting (5.21) into (5.23) and carrying out the integration. We omit the details here.

Lemma 2. Let the strain energy function $W(u_X)$ satisfy property (5.3). Then

$$A_o \langle T(U_X^i), \delta_t U_X^i \rangle = \frac{H^{i+1} - H^{i-1}}{2\Delta t} - \frac{A_o}{4\Delta t} \langle T'(\bar{U}_X^i), (U_X^{i+1} - U_X^i)^2 \rangle \qquad (5.24)$$

$$+ \frac{A_o}{4\Delta t} \langle T'(\hat{U}_X^i), (U_X^i - U^{i-1})^2 \rangle$$

where

$$\bar{U}_X^i = U_X^i + \bar{\theta}(U_X^{i+1} - U_X^i) \quad , \qquad 0 \le \bar{\theta} \le 1$$

$$\qquad (5.25)$$

$$\hat{U}_X^i = U_X^i - \hat{\theta}(U_X^i - U_X^{i-1}) \quad , \qquad 0 \le \hat{\theta} \le 1$$

Proof: If (5.3) holds, we may expand the strain energy function in a finite Taylor series about $W^i = W(U_X^i)$ (this is an implicit expansion in time):

$$W^{i+1} = W^i + T(U_X^i)(U_X^{i+1} - U_X^i) + \frac{1}{2} T'(\bar{U}_X^i)(U_X^{i+1} - U_X^i)^2 \qquad (5.26)$$

$$W^{i-1} = W^i - T(U_X^i)(U_X^i - U_X^{i-1}) + \frac{1}{2} T'(\hat{U}_X^i)(U_X^i - U_X^{i-1})^2 \qquad (5.27)$$

where $T(u_X) = dW/du_X$ and $T'(u_X) = d^2W/du_X^2 = dT/du_X$. Subtracting (5.27) from (5.26), multiplying the result by $A_0/2\Delta t$, and integrating over the length of the bar gives the desired relation.

Our numerical stability criterion is given in

__Theorem 1.__ Let Lemmas 1 and 2 hold. Then a sufficient condition for the finite-element/difference scheme defined by (5.12) to be stable in energy in the sense of (5.20) is that

$$\frac{h}{\Delta t} > \frac{\nu_1}{\sqrt{2}} C_{max}^i \qquad (5.28)$$

where $\nu_1 = 2\sqrt{3}$ and C_{max}^i is the maximum wave speed experienced in the rod for all X at time $t = i\Delta t$:

$$C_{max}^i = \max_X [T'(U_X)/\rho_0]^{\frac{1}{2}} \qquad (5.29)$$

Proof: According to (5.15) and (5.24), we have

$$\Delta t \dot{E}_h^i = K_+^i - K_-^i + H_+^i - H_-^i - \frac{A_0}{4}\langle T'(\bar{U}_X^i), (U_X^{i+1} - U_X^i)^2 \rangle \qquad (5.30)$$

$$+ \frac{A_0}{4}\langle T'(\hat{U}_X^i), (U_X^i - U_X^{i-1})^2 \rangle$$

where $H_+^i - H_-^i = \frac{1}{2}[(H^{i+1} + H^i) - (H^i + H^{i-1})] = \frac{1}{2}(H^{i+1} - H^{i-1})$.

Observing that $T'(u_X)$ is always positive, that $\|U_X^{i+1} - U_X^i\|^2$ $\leq \Delta t^2 v_1^2 \|\nabla_t U^i\|^2/h^2$, and using (5.16), we find, after rearranging terms, that

$$K_+^i \left(1 - \frac{\Delta t^2 v_1^2}{2h^2} C_{max}^{i\,2}\right) + H_+^i \leq K_-^i + H_-^i \qquad (5.31)$$

Now $K_-^i + H_-^i = K_+^{i-1} + H_+^{i-1}$. Moreover, if there exists a positive constant α such that $0 < \alpha \leq 1$ and such that

$$\left(1 - \frac{\Delta t^2 v_1^2}{2h^2} C_{max}^{i\,2}\right) \geq \alpha > 0 \qquad (5.32)$$

then obviously $\alpha(K_+^i + H_+^i) \leq K_+^i(1 - \Delta t^2 v_1^2 C_{max}^{i\,2}/2h^2) + H_+^i \leq K_+^{i-1} + H_+^{i-1}$. Our stability criterion comes from the fact that (5.32) is satisfied if

$$\frac{\Delta t^2 v_1^2}{2h^2} C_{max}^i \leq 1 - \alpha < 1 \qquad (5.33)$$

which leads directly to the desired result, (5.28).

This stability estimate, as should be expected, is consistent with the well-known von Neumann linear stability criteria [95] which requires the discrete system to propagate information at a rate greater than or equal to the speed of propagation of the actual system. The

stability criterion (5. 28) for the nonlinear system (5. 12) simply requires

the approximate wave speed to exceed the actual wave speed times a

constant, $(\nu/\sqrt{2}) \geq 1$, for all $X \in (0, L)$. The constant $\nu/\sqrt{2}$ depends

upon properties of the discrete model: by Lemma 1, $(\nu_1/\sqrt{2}) = \sqrt{6}$

a consistent mass approximation, and, as discussed in the following

remarks $(\nu/\sqrt{2}) = \sqrt{2}$ for the lumped mass approximation.

Remark 1: If a lumped-mass finite-element formulation is used

rather than a consistent-mass formulation (i. e. , if m_{NM} is diagonal),

then the constant ν_1 in (5. 23) must be replaced by $\nu_2 = 2$. All other

steps in the analysis are the same. Consequently, instead of (5. 28),

we obtain stability for the lumped mass model if

$$\frac{h}{\Delta t} > \frac{\nu_2}{\sqrt{2}} C^i_{max} = \sqrt{2} \, C^i_{max} \qquad (5.34)$$

Remark 2: Our stability criterion (5. 28) is not altered if we

consider, instead of (5. 6), the nonhomogeneous wave equation,

$\rho_0 A_0 \langle \ddot{u}, v \rangle + A_0 \langle T(u_X), v_X \rangle = A_0 \langle f, v \rangle$, provided $\| f(\cdot, t) \| < \infty$ for all t.

The inclusion of such a nonhomogeneous term merely adds to (5. 19)

a term on the right side of the form $c \int_0^T \| f(\cdot, t) \|^2 dt$.

Remark 3: The stability criterion is easily adapted to variable

step time integration schemes, since it holds "step-wise"; i. e. , it is

developed for a typical time step Δt. Thus, a possibly more useful

criterion is obtained by replacing Δt in (5.28) by $(\Delta t)^i$.

5.5 Error Estimates and Convergence

Our error estimate and consequently our convergence proof

depend strongly on the smoothness properties that $u(X, t)$ and $W(u_X)$

are assumed to have. The strain energy function $W(u_X)$ is assumed to

have the bounded positive character reflected in (5.3). Indeed, we

noted earlier that $d^2W/du_X{}^2 = T'(u_X)$ is a constant times the squared

speed of propagation of simple waves for the material. It is customary

to assume, for real wave speeds, that this function is always positive

and, barring such exceptional cases as perfectly constrained incom-

pressible materials, is also finite. If $T(u_X) = dW/du_X$ is continuous

in u_X, then, for any two displacement gradients u_X and w_X, $T(u_X)$

$= T(w_X) \pm T'(w_X + \theta_\alpha(u_X - w_X))(u_X - w_X)$, $\theta_\alpha = \theta_1, \theta_2$, $0 \leq \theta_1, \theta_2 \leq 1$.

Hence

$$c_o \langle u_X - w_X, v_X \rangle \leq \langle T(u_X) - T(w_X), v_X \rangle \leq c_1 \langle u_X - w_X, v_X \rangle \qquad (5.35)$$

$$c_o = \inf |T'(u_X)| \quad ; \quad c_1 = \sup |T'(u_X)| \qquad (5.36)$$

Moreover, at points (X, t) which do not lie on the surfaces of discon-

tinuity corresponding to acceleration waves, the exact solution $u(X, t)$

can be assumed to have third derivatives with respect to time.
Therefore,

$$\delta_t^2 u(X, i\Delta t) = \frac{\partial^2 u(X, i\Delta t)}{\partial t^2} + \omega^i(X, t)\Delta t \qquad (5.37)$$

where $\omega^i(X, t) = [\bar{u}(X, i(1 + \theta)\Delta t) - \ddot{u}(X, i(1 - \bar\theta)\Delta t)]/3!$, with $0 \leq \theta$,
$\bar\theta \leq 1$ and $\|\omega^i\| < \infty$. These observations and assumptions set the
stage for our convergence study.

We consider now the nonhomogeneous form of (5.12); i.e., if
$u(X, t)$ is the exact (generalized) solution and $U^i = U(X, i\Delta t)$ is the
finite-element solution approximating $u(X, t)$, then

$$\rho_o \langle \delta_t^2 u^i, V \rangle + \langle T(u_X^i), V_X \rangle = \langle f, V \rangle + \rho_o \langle \omega^i \Delta t, V \rangle \qquad (5.38)$$

and

$$\rho_o \langle \delta_t^2 U^i, V \rangle + \langle T(U_X), V_X \rangle = \langle f, V \rangle \qquad (5.39)$$

Here $\|f\| < \infty$ and $V = V_N \psi_N$ is an arbitrary element of the finite-element
subspace $\mathcal{F}$. Moreover, if $\hat{U}^i = \hat{U}(X, i\Delta t) = \hat{U}_N^i \psi_N(X)$ is another arbitrary
function in $\mathcal{F}$, a little algebra leads to the relation

$$\rho_0 \langle \delta_t^2 (\hat{U}^i - U_X^i), V \rangle + \langle T(\hat{U}_X^i) - T(U_X^i), V_X \rangle \tag{5.40}$$

$$= \rho_0 \langle \delta_t^2 (\hat{U}^i - u^i), V \rangle + \langle T(\hat{U}_X^i) - T(u_X^i), V_X \rangle + \rho_0 \langle \omega^i \Delta t, V \rangle$$

Now, as is customary in convergence studies of linear elliptic problems, we shall identify $\hat{U}^i$ in (5.40) as the finite-element interpolant $\tilde{U}^i$ of the exact solution u^i. That is, if $u(X,t)$ is given, $\tilde{U}(X,t)$ is that element of the finite-element subspace $\mathcal{F}$ that coincides with $u(X,t)$ at each nodal point X^N for every $i\Delta t$, $i = 0, \ldots, R$. It is well known (e.g., [17], pp. 111-116) that if $\tilde{U}$ is a linear combination of the functions $\psi_N(X)$ of (5.21), then

$$\| E^i \| \leq \mu_0 h^2 \quad \text{and} \quad \| E_X^i \| \leq \mu_1 h \tag{5.41}$$

Here μ_0 and μ_1 are positive constants, $E^i \equiv \tilde{U}^i - u^i$, and $E_X^i \equiv \frac{\partial}{\partial X}(\tilde{U}^i - u^i)$. The quantity E^i is the interpolation error at $t = i\Delta t$, whereas the actual error inherent in the finite-element solution is

$$e^i = U^i - u^i = E^i - \mathscr{E}^i \tag{5.42}$$

where

$$\mathcal{E}^i = \tilde{U}^i - U^i \qquad (5.43)$$

The stage is now set for the following lemma.

<u>Lemma 3.</u> Let (5.35) - (5.40) hold. Then

$$\rho_o \langle \delta_t^2 \mathcal{E}^i, \mathcal{E}^i \rangle + \alpha_o \| \mathcal{E}^i_X \|^2 \leq \rho_o \langle \delta_t^2 E^i, \mathcal{E}^i \rangle + \alpha_1 h^2 + \alpha_2 (\Delta t)^2 \qquad (5.44)$$

and

$$\rho_o \langle \delta_t^2 e^i, \mathcal{E}^i \rangle \leq \beta_o \| E^i_X \|^2 + \beta_1 \| \mathcal{E}^i_X \|^2 + \beta_2 (\Delta t)^2 \qquad (5.45)$$

where α_r, β_r, $r = 0, 1, 2$, are positive constants.

Proof: While somewhat lengthy, the proof is straightforward. We shall only outline the essential steps. Out proof makes use of the inequality

$$\langle u, v \rangle \leq \frac{1}{4\epsilon} \| u \|^2 + \epsilon \| v \|^2 \quad , \quad \epsilon > 0 \qquad (5.46)$$

which follows from the Schwarz inequality and the elementary inequality

$|ab| \leq (1/4\epsilon)a^2 + \epsilon b^2$, and the fact that there exists a constant $k > 0$ such that

$$\|u\| \leq k\|u_X\| \qquad (5.47)$$

Inequality (5.47) is the well-known Friedrichs inequality and its validity is proved in a number of texts (e. g., [96], p. 290). To obtain (5.44), set $V = \mathcal{E}^i$ in (5.40), replace the second term on the left side by $C_1\|\mathcal{E}_X^i\|^2$ using (5.35), and apply (5.46) and (5.35) simultaneously to the second and third terms on the right side. Then making use of (5.41) and (5.47) and collecting terms gives the desired result. Equation (5.45) is obtained by subtracting (5.38) from (5.39), using (5.35), applying inequalities (5.46) and (5.47), and then using the identity (5.42). This completes the proof. We now have

Theorem 2. Let (5.35) through (5.40) hold. Then, as h and $\Delta t \to 0$, e^i in the finite-element approximation satisfies

$$\|e_X^i\| \leq M_o h + M_1 \Delta t \qquad (5.48)$$

where M_o and M_1 are constants independent of h and Δt.

Proof: We know from the triangle inequality that

$$\| e_X^i \| = \| E_X^i - \mathcal{E}_X^i \| \le \| E_X^i \| + \| \mathcal{E}_X^i \| \tag{5.49}$$

The term $\| E_X^i \|$ is $O(h)$ in accordance with (5.41). To estimate $\| \mathcal{E}_X^i \|$, we observe that (5.44) implies that

$$\alpha_o \| \mathcal{E}_X^i \|^2 \le \rho_o \langle \delta_t^2 (E^i - \mathcal{E}^i), \mathcal{E}^i \rangle + \alpha_1 h^2 + \alpha_2 (\Delta t)^2$$

Since $E^i - \mathcal{E}^i = e^i$, we may introduce (5.45) to obtain

$$\| \mathcal{E}_X^i \|^2 \le \gamma_o \| E_X^i \|^2 + \gamma_1 h^2 + \gamma_2 (\Delta t)^2$$

where γ_o, γ_1, and γ_2 are constants. Substituting this result along with (5.41) into (5.49) gives (5.48).

Equation (5.48) proves that the finite-element approximation U_X^i converges in the mean to the gradient of the exact solution u_X^i for each i. We assume, of course, that in taking the limit h, $\Delta t \to 0$, the stability criterion (5.28) is satisfied. Since $\| e^i \| \le C \| e_X^i \|$, convergence of U^i to u^i is also assured, but we do not attempt to assess its rate of convergence here. Since the Sobolev inequality $\sup | e^i |$ $\le C \left(\| e^i \| + \| e_X^i \| \right)$ holds, we observe as did Fujii [93], that U^i

converges uniformly to u^i. We also remark that the use of lumped or

consistent masses has no bearing on the final error estimate, other

than possibly altering the constants M_0 and M_1 in (5.48): the lumped

mass and consistent mass approximations have the same rate-of-

convergence.

CHAPTER VI

DYNAMICS OF ELASTIC MEMBRANES

We now return to the problem of elastic membranes. Having reviewed the fundamental principles necessary to obtain general constitutive relations and equations of motion pertinent to the theory of elastic membranes in Chapter II, we are ready for the spatiotemporal discretization of the continuous system.

6.1 Finite Elements of Elastic Membranes

Kinematics of a Finite Element

Consider again the membrane which, in the reference configuration C_o, occupies a region R_o in three-dimensional euclidean space. To describe the motion of the membrane, we established intrinsic global coordinates X^i which, for simplicity, are taken to be rectangular cartesian in C_o. The rectangular cartesian coordinates of a particle P in a subsequent configuration C at some time $t > 0$, which was initially at P_o located at the point $\underset{\sim}{X} = \underset{\sim}{X}(X^i)$ in C_o are denoted x_i, and the functions

$$x_i = x_i(\underset{\sim}{X}, t) \qquad (6.1)$$

are said to define the motion of the body.

In order to reduce the continuous system to a discrete one, the membrane is approximated by a discrete model which consists of a finite number E of flat finite elements connected appropriately at their nodes. Within each finite element e of the membrane, intrinsic local coordinates $X^i_{(e)}$ are established which, for simplicity, are taken to be rectangular cartesian in the reference configuration $C_{o(e)}$ of element e. The rectangular cartesian coordinates of a particle P in an arbitrary configuration $C_{(e)}$ of element e at some time t > 0, which was initially at the point $X_{(e)} = X_{(e)}(X^i_{(e)})$ in $C_{o(e)}$, are denoted $x_{i(e)}$, and the functions

$$x_{i(e)} = x_{i(e)}(X_{(e)}, t) \tag{6.2}$$

are said to define the motion of the element e.

In the finite element method, it is convenient to first describe the behavior of each element independently in terms of the displacements of its nodes; the entire set of elements is then connected together by establishing the nodal connectivity. For further simplicity, it is assumed that the middle surface of each element lies in the $X^1_{(e)}, X^2_{(e)}$ plane of its local coordinate system. Also, it is assumed that the reference configuration C_o is such that the local coordinates $X^i_{(e)}$ for each element

can be taken parallel to the corresponding global coordinates X^i. (If C_o will not allow this coordinate alignment, it is a simple matter to determine the direction cosines which will perform the desired orthogonal transformation of coordinates.)

We now take advantage of the fundamental property of finite element models: the elements can be considered disjoint and disconnected for the purpose of describing local approximations over each element. Hence attention can be placed on a typical element e of the assemblage representing the continuous membrane. In considering e to be isolated from the system, the element label (e) can be neglected for simplicity and convenience--except in cases where its omission may lead to confusion. For simplicity, only first-order approximations are considered and thus the local displacement field of the middle surface of the membrane is represented in terms of the nodal displacements by

$$u_i(\underset{\sim}{X}, t) = \psi_N(X^1, X^2)u_i^N(t) \tag{6.3}$$

Here ψ_N are the local interpolation functions for the element and, as before, have the following properties:

$$\psi_N(X^M) = \delta_N^M \quad , \quad \sum_{N=1}^{N_e} \psi_N = 1$$

the u_i are the components of displacement of a material point (X^1, X^2) on the middle surface, u_i^N are components of displacement at node N, $N = 1, 2, \ldots, N_e$, N_e represents the number of nodes, and $i = 1, 2, 3$. Then according to (2.14) the strain components are

$$2\gamma_{\alpha\beta} = \psi_{N,\alpha} u_\beta^N + \psi_{N,\beta} u_\alpha^N + \psi_{N,\alpha} \psi_{M,\beta} u_k^N u_k^M$$

$$2\gamma_{\alpha 3} = 0 \qquad\qquad\qquad (6.4)$$

$$2\gamma_{33} = \lambda^2 - 1$$

For compressible materials, λ^2 can be approximated over the element by

$$\lambda^2 = \psi_N(X^1, X^2)\mu^N \qquad\qquad (6.5)$$

where $\mu^N = (\lambda^2)^N$ is the value of λ^2 at node N. For incompressible materials, by introducing (2.11)$_1$ into (2.34)$_1$, λ^2 is obtained in terms of the membrane strains

$$\lambda^2 = [1 + 2\gamma_{\alpha\alpha} + 2\epsilon^{\alpha\beta}\epsilon^{\lambda\mu}\gamma_{\alpha\lambda}\gamma_{\beta\mu}]^{-1}$$

(6.6)

$$= [1 + 2\gamma_{\alpha\alpha} + 2(\gamma_{\alpha\alpha}\gamma_{\beta\beta} - \gamma_{\alpha\beta}\gamma_{\beta\alpha})]^{-1}$$

With (6.4) in (6.6), λ^2 is expressed in terms of the nodal displacement by

$$\lambda^2 = [1 + \psi_{N,\alpha}u_k^N(2\delta_{\alpha k} + \psi_{M,\alpha}u_k^M)$$

(6.7)

$$+ \frac{1}{2}\epsilon^{\alpha\lambda}\epsilon^{\beta\mu}(\psi_{N,\alpha}u_\beta^N + \psi_{N,\beta}u_\alpha^N + \psi_{N,\alpha}\psi_{M,\beta}u_k^N u_k^M)(\psi_{R,\lambda}u_\mu^R$$

$$+ \psi_{R,\mu}u_\lambda^R + \psi_{R,\lambda}\psi_{P,\mu}u_j^R u_j^P)]^{-1}$$

Here $i, j, k = 1, 2, 3$; $\alpha, \beta, \lambda, \mu = 1, 2$; $N, M, P, R = 1, 2, \ldots, N_e$.

Equations of Motion of a Membrane Element

According to (6.3), the displacement, velocity, and acceleration fields for the middle surface of this typical element are of the form

$$u_i = \psi_N(\underset{\sim}{X})u_i^N(t)$$

$$\dot{u}_i = \psi_N(\underset{\sim}{X})\dot{u}_i^N(t)$$

(6.8)

$$\ddot{u}_i = \psi_N(\underset{\sim}{X})\ddot{u}_i^N(t)$$

Then all of the kinematic relations for the element can be computed in terms of the nodal displacement components and their time derivatives. Note that all of the previously mentioned thermodynamic concepts for any representative material point P with displacement w, will, in particular, hold for material points on the middle surface of the membrane Q with displacement u.

Introducing (6. 4) and (6. 8) into (2. 27) and simplifying, we obtain the general energy balance for a typical membrane finite element in the form

$$[m_{NM}\ddot{u}^M_i + \int_{v_o} t^{\alpha\beta}\psi_{N,\alpha}(\delta_{i\beta} + \psi_{M,\beta}u^M_i)dv_o - p_{Ni}]\dot{u}^N_i = 0 \qquad (6.9)$$

where m_{NM} is the symmetric $N_e \times N_e$ consistent mass matrix, defined here by

$$m_{NM} = \int_{v_{o(e)}} \rho_o(\underset{\sim}{X})\psi_N(\underset{\sim}{X})\psi_M(\underset{\sim}{X})dv_o \qquad (6.10)$$

and p_{Ni} are the components of the total generalized force at node N

$$p_{Ni} = \int_{v_{o(e)}} \rho_o F_{oi}\psi_N dv_o + \int_{A_{o(e)}} S_{oi}\psi_N dA_o \qquad (6.11)$$

It is important to note that the actual surface forces $\underset{\sim}{S}_o(X)$ are available to us only in the deformed element. Thus, the forces $\underset{\sim}{S}_o(X)$ are, in general, dependent on the deformation and, consequently, are functions of the nodal displacements $\underset{\sim}{u}^N$; that is to say, the nodal forces p_{Ni} are generally nonconservative.

Since (6.9) must be valid for arbitrary motions of the element, it must also hold for arbitrary values of the nodal velocities, $\dot{u}_i^N$. This being the case, the expression inside the brackets of (6.9) must vanish for all values of N and i. Thus we have

$$p_{Ni} = m_{NM}\ddot{u}_i^M + \int_{v_{o(e)}} t^{\alpha\beta}\psi_{N,\alpha}(\delta_{\beta i} + \psi_{M,\beta}u_i^M)dv_o \qquad (6.12)$$

Equation (6.12) represents the general equations of motion of a finite element of a membrane. Note that no restrictions have been placed on the order of magnitude of the strains or displacements. To apply these results to specific materials, constitutive equations must be introduced so that the stress tensor can be eliminated from the equations of motion of the discrete model.

Assuming that the initial thickness d_o is constant over the undeformed element and denoting the undeformed middle surface area by A_o^*, (6.12) becomes

$$p_{Ni} = m_{NM}\ddot{u}_i^M + d_o \int_{A_{o(e)}^*} t^{\alpha\beta}\psi_{N,\alpha}(\delta_{\beta i} + \psi_{M,\beta}u_i^M)dA_o^* \qquad (6.13)$$

where now

$$m_{NM} = d_o \int_{A_{o(e)}^*} \rho_o\psi_N\psi_M dA_o^* \qquad (6.14)$$

Specific forms of the equations of motion for membrane elements of isotropic compressible materials are obtained by introducing (2.32) and (6.5) into (6.13)

$$p_{Ni} = m_{NM}\ddot{u}_i^M + 2d_o \int_{A_{o(e)}^*} \left[\left(\frac{\partial W}{\partial I_1} + \psi_R\mu^R\frac{\partial W}{\partial I_2}\right)\delta^{\alpha\beta}\right. \qquad (6.15)$$

$$\left. + \left(\frac{\partial W}{\partial I_2} + \psi_R\mu^R\frac{\partial W}{\partial I_3}\right)f^{\alpha\beta}\right]\psi_{N,\alpha}(\delta_{\beta i} + \psi_{M,\beta}u_i^M)dA_o^*$$

where, using (6.4),

$$f^{\alpha\beta} = AA^{\alpha\beta} = \epsilon^{\alpha\lambda}\epsilon^{\beta\mu}A_{\lambda\mu} = \delta^{\alpha\beta} \qquad (6.16)$$

$$+ \epsilon^{\alpha\lambda}\epsilon^{\beta\mu}(\psi_{N,\lambda}u_\mu^N + \psi_{N,\mu}u_\lambda^N + \psi_{N,\lambda}\psi_{M,\mu}u_k^N u_k^M)$$

The N_e values $\mu^R = (\lambda^2)^R$ are determined from requiring t^{33} to vanish

in an average sense over the element. So, from (2.32), at each node N we have

$$0 = \int_{A^*_{o(e)}} \left(\frac{\partial W}{\partial I_1} + \frac{\partial W}{\partial I_2} \delta_{\alpha\beta} f^{\alpha\beta} + \frac{\partial W}{\partial I_3} A \right) \psi_N dA^*_o \qquad (6.17)$$

The $3N_e$ equations (6.15) with the N_e equations (6.17) constitute $4N_e$ equations in the $4N_e$ unknowns u_i^N and μ^N.

In the case of isotropic incompressible materials, by using (2.37) in (6.13), the equations of motion for membrane elements are of the form

$$P_{Ni} = m_{NM} \ddot{u}_i^M + 2d_o \int_{A^*_{o(e)}} \left[(\delta^{\alpha\beta} - \lambda^4 f^{\alpha\beta}) \frac{\partial W}{\partial I_1} + \left[\lambda^2 \delta^{\alpha\beta} \right. \right. \qquad (6.18)$$

$$\left. \left. + f^{\alpha\beta}(1 - 2\lambda^4 - 2\lambda^4 \gamma_{\mu\mu}) \right] \frac{\partial W}{\partial I_2} \right] \psi_{N,\alpha} (\delta_{\beta i} + \psi_{M,\beta} u_i^M) dA^*_o$$

where $f^{\alpha\beta}$ is defined in (6.16) and λ^2 is given by (6.7).

The Simplex Finite Element

When dealing with finite deformations of membranes with general material properties, numerical integration of the equations of motion can involve inordinate complications. Seeking to facilitate this process, it is natural to consider the incorporation of the simplest finite element approximation available. The simplest of all finite elements are the

so-called simplex elements--ones in which the local fields can be described linearly in terms of the nodal values of the local field and nodal coordinates. For the case of a thin membrane, the simplex model is a triangular shaped element with nodes at the three vertices.

It has been shown for the static nonlinear analysis of membranes (e.g., [57-60]) that this model is adequate in obtaining quite accurate results. That this should be so is easily seen from the physical problem: if concentrated forces (or point loads) are applied to a thin membrane, the material surfaces between these loads physically tend to take on the appearance of the finite element description. Moreover, the simplex model affords us the convenience of constant strain fields over the element, thereby eliminating the lengthy and tedious integrations incurred for varying strain fields. Also, if desired, various composite elements can be obtained from the appropriate grouping of the triangular elements.

In addition to the above, for the simplex element, the completeness and continuity requirements for convergence are satisfied. A linear function is uniquely determined by any two of its values. Since the local functions $u(\underline{X})$ are linear along each boundary of the element, fitting two of these elements together amounts to prescribing the same nodal values of adjacent local approximations at the two nodes on their interelement

boundary. Thus the local fields coincide at all interelement boundary points in the connected model, and the finite element model is everywhere continuous.

Triangular (Simplex) Membrane Element

A general motion of the membrane which carries the system from its initial, or reference, configuration C_0 to a deformed configuration C is again considered. In general, straight lines in C_0 will become curved lines in C. However, if node points in C_0 are chosen sufficiently close, node lines in C may be adequately approximated by straight line segments, and plane elements before deformation will remain plane after deformation. This is equivalent to assuming the elemental displacement fields to be linear functions of the local coordinates of the elements

$$u_i = d_i + a_{i\alpha} X^{\alpha} \tag{6.19}$$

where u_i are displacement components, d_i are components of rigid-body translations of the element, $a_{i\alpha}$ are undetermined constants, $i = 1, 2, 3,$ $\alpha = 1, 2,$ and again the element label (e) has been discarded for convenience. Also, the dependence of $\underset{\sim}{u}$, $\underset{\sim}{d}$, and $a_{i\alpha}$ on time is understood.

Evaluating (6.19) at each node point, noting that each component of rigid-body displacement is the same for all nodes (i.e., $d_{Ni} = d_i$), gives

$$u_i^N = d_i + a_{i\alpha} X_N^\alpha \qquad (6.20)$$

Here u_i^N (N = 1, 2, 3) are displacement components of node N, and X_N^α are local coordinates of node N. Again, it is understood that indices N = 1, 2, 3 are to be associated with the three nodes of element e. Now, (6.20) represents nine simultaneous linear equations for the three components d_i and the six parameters $a_{i\alpha}$. If (6.20) is expanded by first letting the index i take on values 1, 2, 3 and then expanding on N, the resulting form of the coefficient matrix is particularly easy to invert. The solutions are found to be

$$d_i = k_N u_i^N \qquad (6.21)$$

and

$$a_{i\alpha} = c_{N\alpha} u_i^N \qquad (6.22)$$

where

$$k_1 = (X_2^1 X_3^2 - X_3^1 X_2^2)/2A_o$$

$$k_2 = (X_1^2 X_3^1 - X_1^1 X_3^2)/2A_o \qquad (6.23)$$

$$k_3 = (X_1^1 X_2^2 - X_1^2 X_2^1)/2A_o$$

and

$$c_{\alpha N} = \frac{1}{2A_o} \begin{bmatrix} (X_2^2 - X_3^2) & (X_3^2 - X_1^2) & (X_1^2 - X_2^2) \\ (X_3^1 - X_2^1) & (X_1^1 - X_3^1) & (X_2^1 - X_1^1) \end{bmatrix} \qquad (6.24)$$

Here A_o is the area of the undeformed triangle. The quantities $c_{\alpha N}$ are called the displacement coefficients. Note that they are independent of the deformation of the membrane and are computed directly from the geometry of the undeformed element. Also, $c_{N\alpha} = (c_{\alpha N})^T$.

With (6.21) and (6.22), (6.19) becomes

$$u_i = k_N u_i^N + c_{N\alpha} u_i^N X^\alpha = (k_N + c_{N\alpha} X^\alpha) u_i^N \qquad (6.25)$$

Thus, with (6.25), the derivatives of the displacement components are

$$u_{i,\alpha} = c_{N\alpha} u_i^N \qquad (6.26)$$

Comparing (6.25) and (6.3) we see that, for the simplex triangular element, the local interpolation functions here are

$$\psi_N(X^1, X^2) = k_N + c_{N\alpha} X^\alpha \qquad (6.27)$$

And so,

$$\psi_{N,\alpha} = c_{N\alpha} \qquad (6.28)$$

With (6.28), the strain components of (6.4) will become

$$2\gamma_{\alpha\beta} = c_{N\alpha} u_\beta^N + c_{N\beta} u_\alpha^N + c_{N\alpha} c_{M\beta} u_k^N u_k^M$$

$$2\gamma_{\alpha3} = 0 \qquad (6.29)$$

$$2\gamma_{33} = \lambda^2 - 1$$

Also, (6.16) and (6.7) are now expressed in the form

$$f^{\alpha\beta} = \delta^{\alpha\beta} + \epsilon^{\alpha\lambda} \epsilon^{\beta\mu} (c_{N\lambda} u_\mu^N + c_{N\mu} u_\lambda^N + c_{N\lambda} c_{M\mu} u_k^N u_k^M) \qquad (6.30)$$

$$\lambda^2 = \left[1 + c_{N\alpha} u_k^N \left(2\delta_{\alpha k} + c_{M\alpha} u_k^M \right) + \frac{1}{2} \epsilon^{\alpha\lambda} \epsilon^{\beta\mu} \left(c_{N\alpha} u_\beta^N + c_{N\beta} u_\alpha^N \right. \right. \tag{6.31}$$

$$\left. \left. + c_{N\alpha} c_{M\beta} u_k^N u_k^M \right) \left(c_{R\lambda} u_\mu^R + c_{R\mu} u_\lambda^R + c_{R\lambda} c_{P\mu} u_j^R u_j^P \right) \right]^{-1}$$

wherein $i, j, k = 1, 2, 3$; $\alpha, \beta, \lambda, \mu = 1, 2$; $N, M, P, R = 1, 2, 3$.

It should be noted that, since (6.29) gives the strains in terms of a specified displacement field, the compatibility equations are automatically satisfied within each finite element.

To obtain the appropriate form of the consistent mass matrix, (6.27) is introduced into (6.14) where, if ρ_0 is assumed to be constant in the undeformed element, it can be shown (e. g. , [7], p. 173) that

$$m_{NM} = \frac{1}{12} m_0 (1 + \delta_{NM}) \tag{6.32}$$

where $m_0 = \rho_0 d_0 A_0^*$ is the total mass of element e.

For compressible materials

$$\lambda^2 = (k_N + c_{N\alpha} X^\alpha) \mu^N \tag{6.33}$$

Introducing (6.32), (6.33), and (6.27) into (6.15) and simplifying, the equations of motion for a simplex membrane element of isotropic compressible material are

$$P_{Ni} = \frac{1}{12} m_o (1 + \delta_{NM}) \ddot{u}_i^M + 2v_o \left\{ \left[\frac{\partial W}{\partial I_1} \right. \right. \tag{6.34}$$

$$+ \left(k_R + c_{R\alpha} \overline{X}^\alpha \right) \mu^R \frac{\partial W}{\partial I_2} \right] \delta^{\alpha\beta} + \left[\frac{\partial W}{\partial I_2} + \left(k_R \right. \right.$$

$$\left. + c_{R\alpha} \overline{X}^\alpha \right) \mu^R \frac{\partial W}{\partial I_3} \right] f^{\alpha\beta} \Bigg\} c_{N\alpha} (\delta_{\beta i} + c_{M\beta} u_i^M)$$

where

$$\overline{X}^\alpha = \frac{1}{A_o^*} \int_{A_{o(e)}^*} X^\alpha dA_o^* \tag{6.35}$$

$$= \text{the centroidal coordinates of } A_o^* \text{ with}$$

$$\text{respect to the local } X_{(e)}^\alpha \text{ axes.}$$

and $f^{\alpha\beta}$ is given by (6.30), and $v_o = d_o A_o^*$.

Finally, introducing (6.28), (6.29), and (6.32) into (6.18) yields the nonlinear equations of motion for the simplex membrane element of isotropic incompressible material

$$P_{Ni} = \frac{1}{12} m_o (1 + \delta_{NM}) \ddot{u}_i^M + 2v_o \left(\left(\delta^{\alpha\beta} - \lambda^4 f^{\alpha\beta} \right) \frac{\partial \hat{W}}{\partial I_1} + \left\{ \lambda^2 \delta^{\alpha\beta} + f^{\alpha\beta} \right| 1 \tag{6.36}$$

$$- 2\lambda^4 - 2\lambda^4 c_{R\mu} \left(\delta_{\mu k} + \frac{1}{2} c_{P\mu} u_k^P \right) u_k^R \right] \right\} \frac{\partial \hat{W}}{\partial I_2} \right) c_{N\alpha} \left(\delta_{\beta i} + c_{M\beta} u_i^M \right)$$

and $f^{\alpha\beta}$ and λ^2 are given in terms of the nodal displacements in (6.30) and (6.31); or by using (6.4), in the condensed form

$$f^{\alpha\beta} = \delta^{\alpha\beta} + 2\epsilon^{\alpha\lambda}\epsilon^{\beta\mu}\gamma_{\lambda\mu}$$

(6.37)

$$\lambda^2 = \left[1 + 2c_{N\alpha}(\delta_{\alpha\beta} + c_{M\alpha}u_\beta^M)u_\beta^N + 2\epsilon^{\alpha\lambda}\epsilon^{\beta\mu}\gamma_{\alpha\lambda}\gamma_{\beta\mu}\right]^{-1}$$

Also, for simplicity, and for the sound theoretical reasons mentioned earlier, we want to use the lumped mass approximation. Hence, in (6.10), we take $\psi_N(\underset{\sim}{X}) = \delta(\underset{\sim}{X}^N - \underset{\sim}{X})$, $\delta(\underset{\sim}{X})$ being the Dirac delta function, and obtain the lumped mass matrix

$$m_{MN} = \frac{1}{3}\rho_o v_{o(e)}\delta_{MN}$$

(6.38)

With (6.38), the first term on the right-hand-side of (6.36) becomes

$$m_{MN}\ddot{u}_i^M = \frac{1}{3}\rho_o v_{o(e)}\delta_{MN}\ddot{u}_i^M$$

(6.39)

6.2 Temporal Approximations

Upon assembling elements and applying the boundary conditions, (6.37) leads to a large system of highly nonlinear second-order ordinary differential equations in the unknown nodal displacements u_i^N. The

arguments presented in Section 4.4 are still applicable here. Therefore, as for the one-dimensional case, the velocity formulated central difference scheme is used (remembering, of course, its inadequacy in the presence of shocks), together with a lumped mass representation for the numerical examples presented at the end of this chapter. Here, the general second-order nodal equations of motion being of the form

$$\ddot{u}_i^N(t) = F_i^N(u_j^M(t)) \tag{6.40}$$

result in difference equations of the form

$$v_i^{N(n+\frac{1}{2})} = v_i^{N(n-\frac{1}{2})} + \Delta t\, F_i^N(u_j^{M(n)})$$

$$\tag{6.41}$$

$$u_i^{N(n+1)} = u_i^{N(n)} + \Delta t\, v_i^{N(n+\frac{1}{2})}$$

where we have denoted the time discretization by $u^N(t) = u^N(n\Delta t) = u_i^{N(n)}$.

6.3 Stability and Convergence

Although at the present time we do not have any stability criteria for the two-dimensional nonlinear wave equation, we conjecture that our work in Chapter V on one-dimensional nonlinear problems furnishes some insight into at least the order of magnitude expected of the

two-dimensional estimates. The plausibility of this conjecture can be argued by noting that, for the linear case, the time step associated with stability estimates of Richtmyer and Morton [87] (pp. 304, 361) decreases by only thirty percent in going from one to two dimensions. Also, the two-dimensional stability estimates of Fujii [93] seem to require a time step twice as small as that needed for one-dimensional stability.

The one-dimensional error estimates and convergence rates derived in Chapter V have recently been generalized by Oden [97] to include three-dimensional dynamic finite elasticity problems. Therein, he proves the general convergence theorem:

For each $i = 1, 2, \ldots, n$, the finite-element approximation error $e_m^{(i)}$, $m = 1, 2, 3$, is such that

$$\| e_m^{(i)} \|_{W_2^1(B)} \leqq \gamma_0 \Delta t^r + \gamma_1 \| E_m^{(i)} \|_{W_2^1(B)} \tag{6.42}$$

where γ_0 and γ_1 are positive constants, $E_m^{(i)}$ is the interpolation error, $r \geqq 1$, and $W_2^1(B)$ denotes the Sobolev space of functions $u(X, t)$ which, along with their first derivatives with respect to X^i, are square integrable.

6.4 Numerical Results

In this section, we present numerical results obtained by applying the procedures described earlier to the problem of a beam with a central load, a square sheet with a transverse load applied suddenly at the center and then removed, and the dynamic inflation of a thin rubber membrane.

Highly Elastic (Rubber-like) Beam with Central Load

As the first example, a beam with fixed ends is subjected to a central impulse load and allowed to deform as a function of time. The undeformed beam is 18 in. long, 0.4 in. deep and 0.05 in. thick, and is constructed of an isotropic, incompressible material of the Mooney type (i.e., $W = C_1(I_1 - 3) + C_2(I_2 - 3)$) with material constants of $C_1 = 24$ psi, $C_2 = 1.5$ psi. The mass density of the material is 0.0001 lb-sec^2/in^4.

Since the loading is symmetric, a finite element model was generated for only one-half of the beam. The model consisted of 20 bays along the length and 4 bays through the depth of the beam, as shown in Fig. 12a. This resulted in a model with 105 nodes and 160 triangular elements. Upon applying boundary conditions and restricting 15 degrees of freedom, the number of unknown displacements reduced to 195. Impulse loads of 1.0, 0.9, and 0.25 lbs were applied for 0.001 sec to the node representing the center, the node 0.25 in. from the center and 0.6 in. from the center,

Note: Not to scale.

(a) The Beam

18 in.

20 in.

20 in.
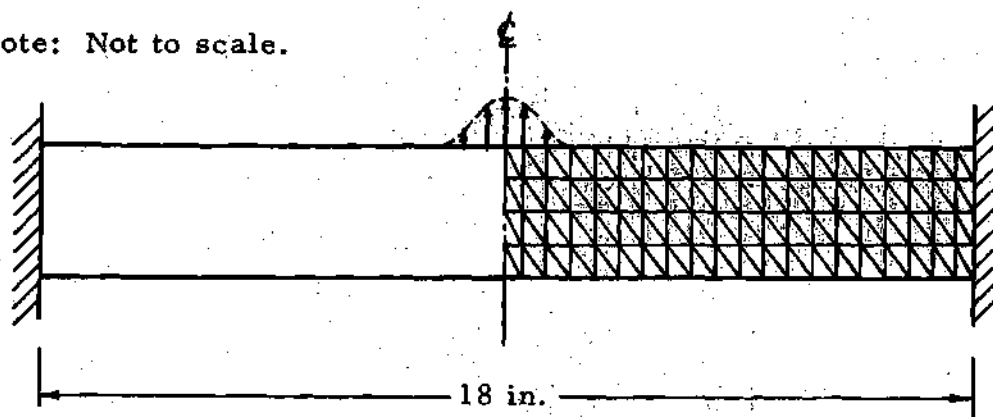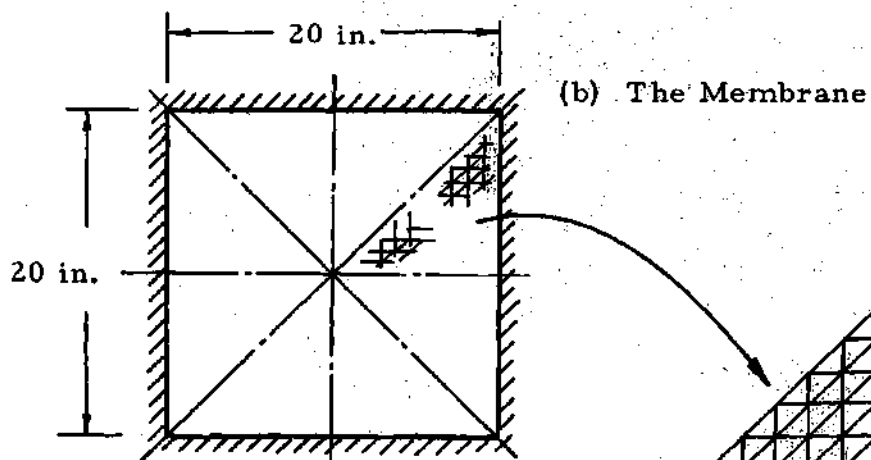
(b) The Membrane

Loaded Nodes
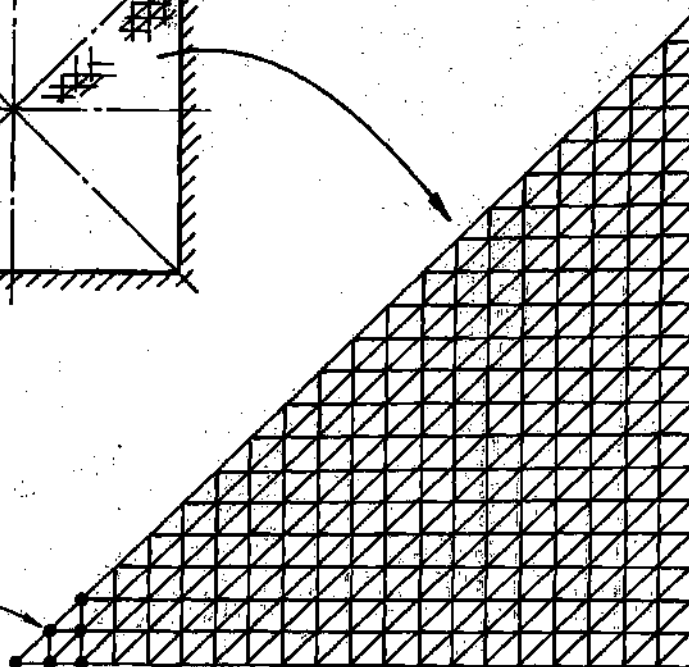
Figure 12. Finite-element Models of a Highly Elastic Beam and a Square Membrane

respectively, to avoid stress singularities at the center. Figure 13 shows

the deformed shape of half the beam computed at various times.

It is emphasized that the deformation is plotted to scale. Hence,

very large-amplitude motions are clearly developed. Figure 13a shows

the undeformed beam, Figure 13b shows the beam just prior to termina-

tion of the impulse load, and Figs. 13c and 13d show the propagation of

the wave toward the fixed edge. At this point in time there are two

significant motions, one is a general vertical (flexural) motion of the

whole beam and the other is a longitudinal wave traveling along the

deformed axis of the beam. In Fig. 13e, the wave traveling along the

beam is reflected off the boundary and starts moving toward the center.

In Fig. 13f, the vertical motion is resisted by bending at the fixed edge,

and the wave traveling along the beam is reflected from the center. The

remaining frames of the figure show the interaction of the slow bending

wave and the faster moving wave along the beam at various times. The

12 frames presented here were selected from a 16mm movie film con-

taining approximately 1200 frames. It was evident from the movie that

longitudinal waves (i. e. , waves along the deformed X^1-axis) resulted

in very fast oscillations ahead of the much slower flexural type motions.

Approximately 12, 000 integration steps were required to solve

this problem. This was achieved on the UNIVAC 1108 in 35 minutes.

It is interesting to note that an additional 40 min of computer time
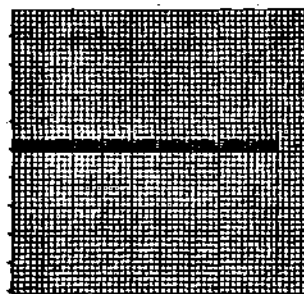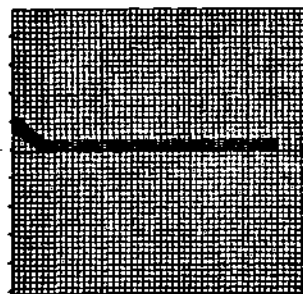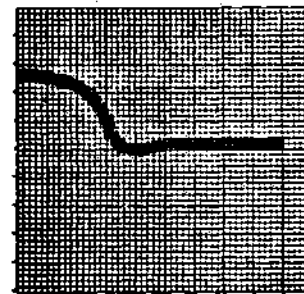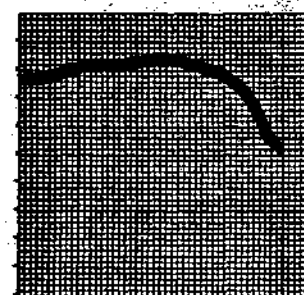
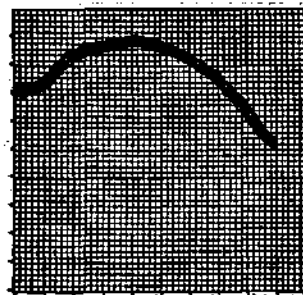(a) t = 0.0   (b) t = 0.00098   (c) t = 0.00791
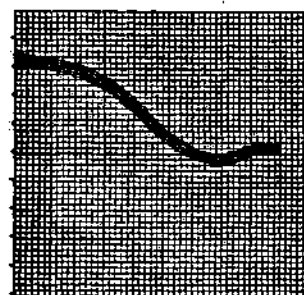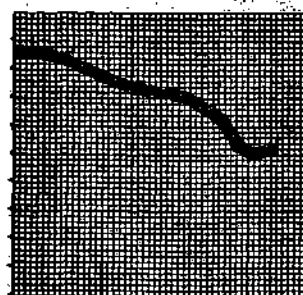
(d) t = 0.01286   (e) t = 0.01682   (f) t = 0.02177
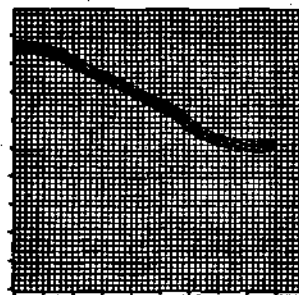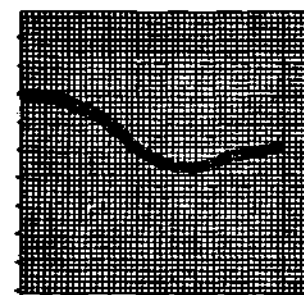
Figure 13.   Deformed Shapes of Centrally Loaded Beam (Sheet 1 of 2)
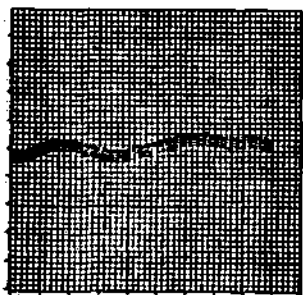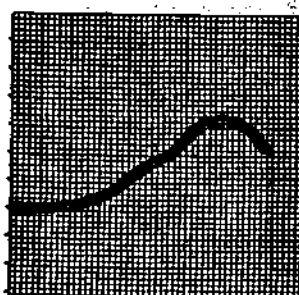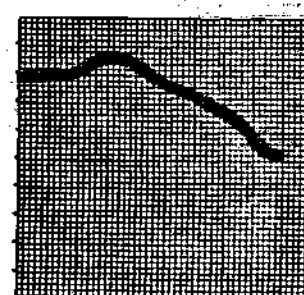
(g) t = 0.02573

(h) t = 0.03266

(i) t = 0.04058

(j) t = 0.04553

(k) t = 0.05048

(l) t = 0.11857

Figure 13.   Deformed Shapes of Centrally Loaded Beam (Sheet 2 of 2)

was required to generate the 16mm film containing 1200 frames which can be shown in 40 seconds.

Square Sheet with Normal Load

As a second example, the square sheet with clamped edges shown in Fig. 12b is subjected to a central impulse load, normal to the plane of sheet, and allowed to deform as a function of time. The membrane is a 20 in. square with a thickness of 0.05 in., and the material properties are the same as the first example. Here it was necessary to model only one-eighth of the membrane since symmetry was assumed. The finite element model of the membrane contains 400 elements and 231 nodes. The supported model resulted in 590 unknown displacements. A uniformly distributed impulse load of 3 pounds per element was applied to the four elements closest to the node representing the center of the sheet. The duration of the impulse load was 0.001 seconds.

Figure 14a shows the initial finite element model of the sheet; Fig. 14b shows the sheet just after the removal of the load. The energy imparted to the membrane continues the vertical movement of the center in Fig. 14c. In Fig. 14d the internal forces overcome the inertia effects, and the center of the sheet collapses and forms a standing wave which propagates toward the fixed edge in Figs. 14e through 14i. The wave which travels with a circular front strikes the nearest edge and starts to rebound, while the wave is still traveling toward the extreme edge

(a) t = 0.0   (b) t = 0.001   (c) t = 0.002

(d) t = 0.003   (e) t = 0.009   (f) t = 0.016

(g) t = 0.019   (h) t = 0.022   (i) t = 0.027

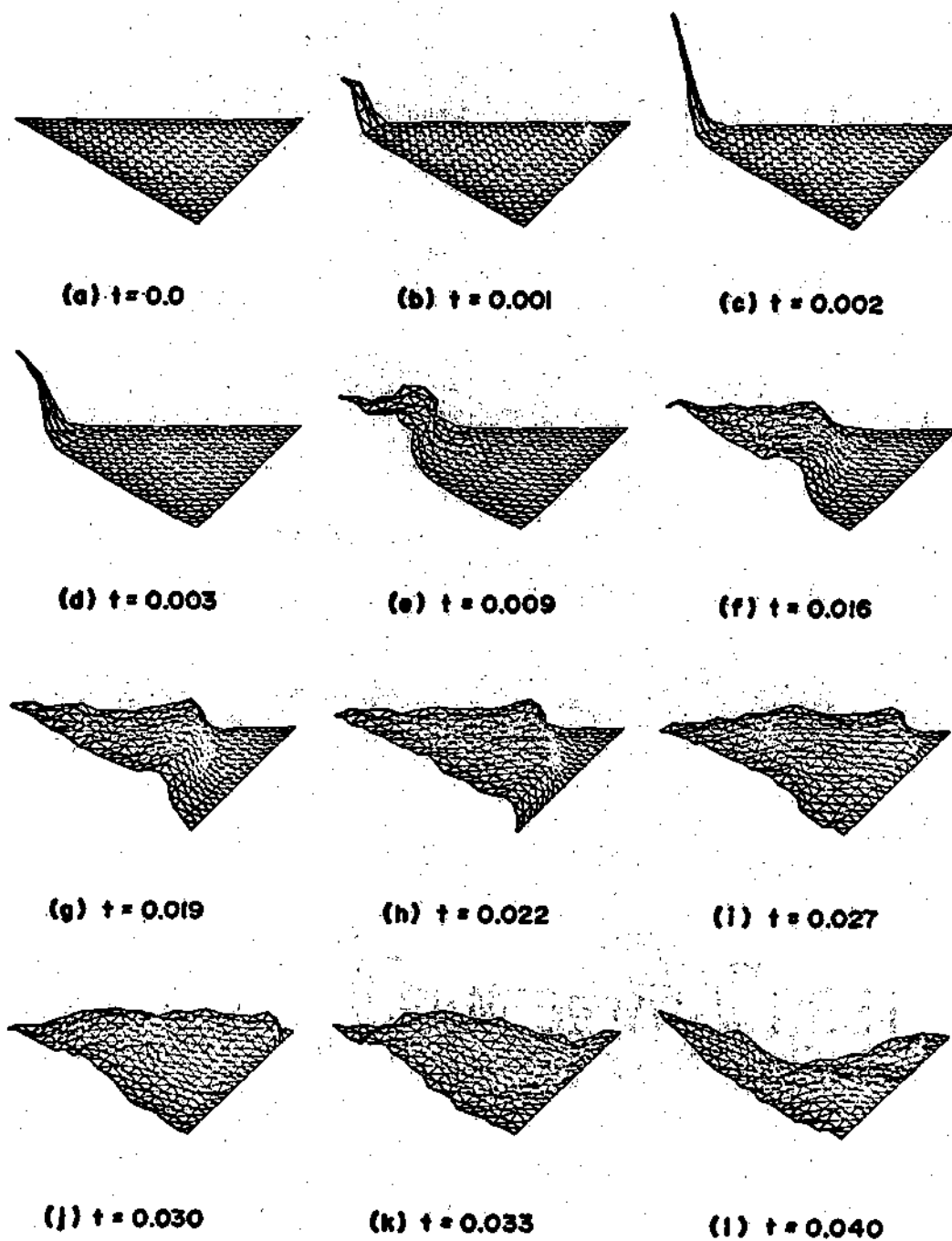(j) t = 0.030   (k) t = 0.033   (l) t = 0.040

Figure 14. Deformed Shapes of Centrally Loaded Sheet

in Fig. 14i. The rebound wave continues to propagate in Figs. 14j through 14l. Again, a closer examination of the response indicated that "membrane" waves propagating along the deformed sheet are developed which traveled much faster than the "ripple" obvious in the figures.

Thirty minutes on the UNIVAC 1108 were required to complete 4200 integration steps. A 16mm film containing 1300 frames were made and the 12 frames presented here were selected from the film.

Dynamic Inflation of a Membrane

In this final example, we present some results of the finite-element analysis of an interesting class of problems: the dynamic inflation of thin rubber membranes. We consider a thin, initially flat circular membrane of Mooney material (C_1 = 24.0 psi, C_2 = 1.5 psi) with an undeformed radius of 4.0 in. and an initial thickness of 0.05 inches. Here, as in the previous example, it was only necessary to model an octant of the circular membrane due to the symmetry of the problem. The finite element model of the membrane, shown in Fig. 15, has 400 elements and 231 nodes. Applying the boundary conditions and restricting the symmetric degrees of freedom reduces the number of unknown displacements to 590. The membrane was subjected to a uniform transverse pressure p(t) applied as indicated below.
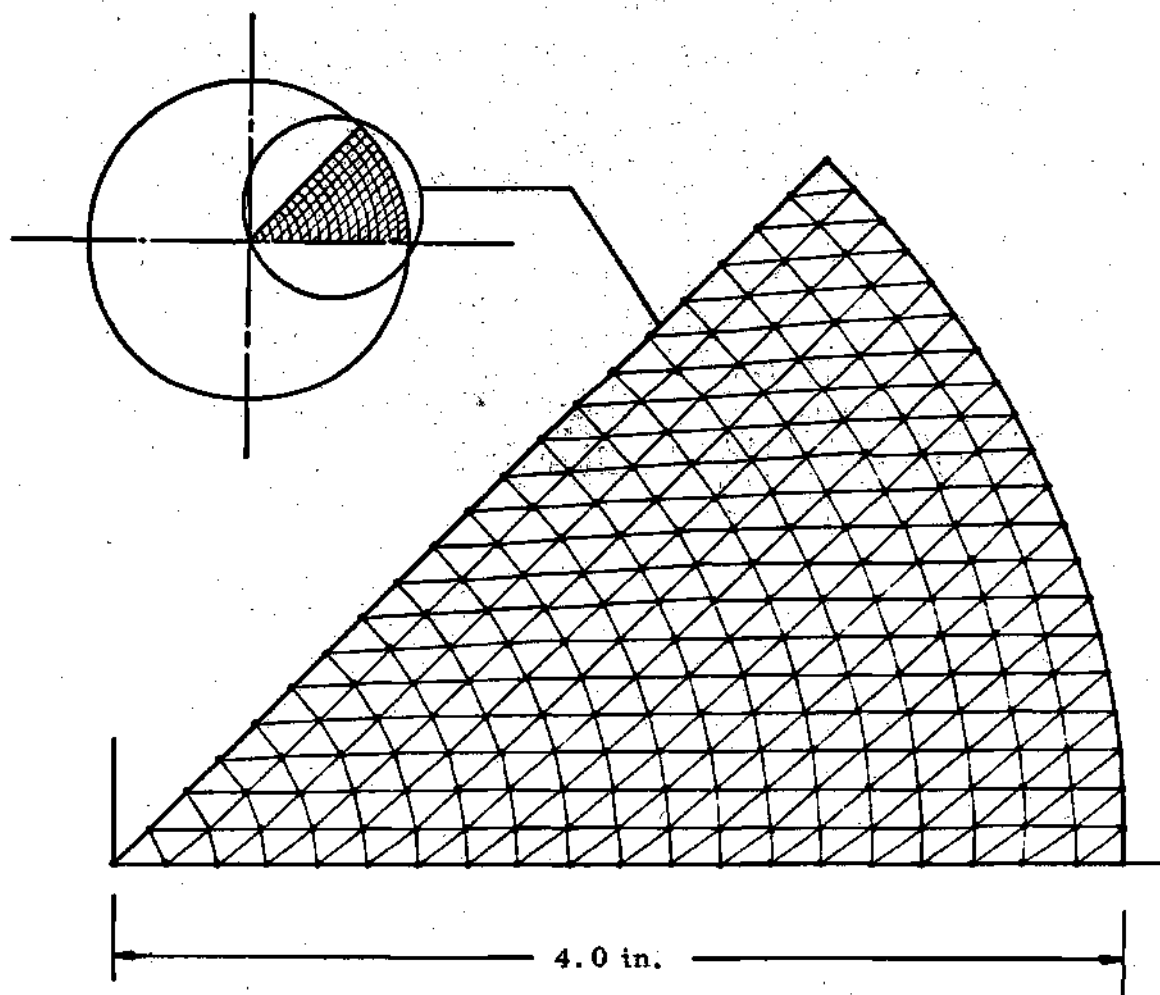
Figure 15. Finite-element Model of a Circular Membrane

Case 1: $p(t) =$
$$\begin{cases} 825t \text{ psi} & 0 \leq t \leq 0.002 \text{ sec} \\ 1.65 \text{ psi} & 0.002 \leq t \leq 0.006 \text{ sec} \\ 0 & t \geq 0.006 \text{ sec} \end{cases}$$

Case 2: $p(t) =$
$$\begin{cases} 825t \text{ psi} & 0 \leq t \leq 0.002 \text{ sec} \\ 1.65 \text{ psi} & t \geq 0.002 \text{ sec} \end{cases}$$

Case 3: $p(t) =$
$$\begin{cases} 825t \text{ psi} & 0 \leq t \leq 0.002 \text{ sec} \\ 1.65 \text{ psi} & 0.002 \leq t \leq 0.004 \text{ sec} \\ 1.65 + Q\sin \omega t & t \geq 0.004 \text{ sec} \end{cases}$$

where $Q = 1.0$ psi and $\omega = 1000\pi$ rad/sec.

Rather than try to cope with the nonconservative nature of the generalized nodal forces, p_{Ni}, as defined in (6.11), we turn to the simplified method, which is fully explained in [17], p. 245, for approximating these forces. The essence of this method is calculating the instantaneous configuration of each element, applying the current pressure to the deformed area, so that the associated generalized nodal forces are obtained by simply distributing the resulting applied force equally at each node.

Case 1. Profiles of the membrane, calculated at various times, are shown in Fig. 16. Here we notice that the central portion of the membrane initially tends to remain flat due to the central elements responding primarily in rigid body vertical translation (with some in-plane stretching) until the effect of the fixed boundary reaches them.
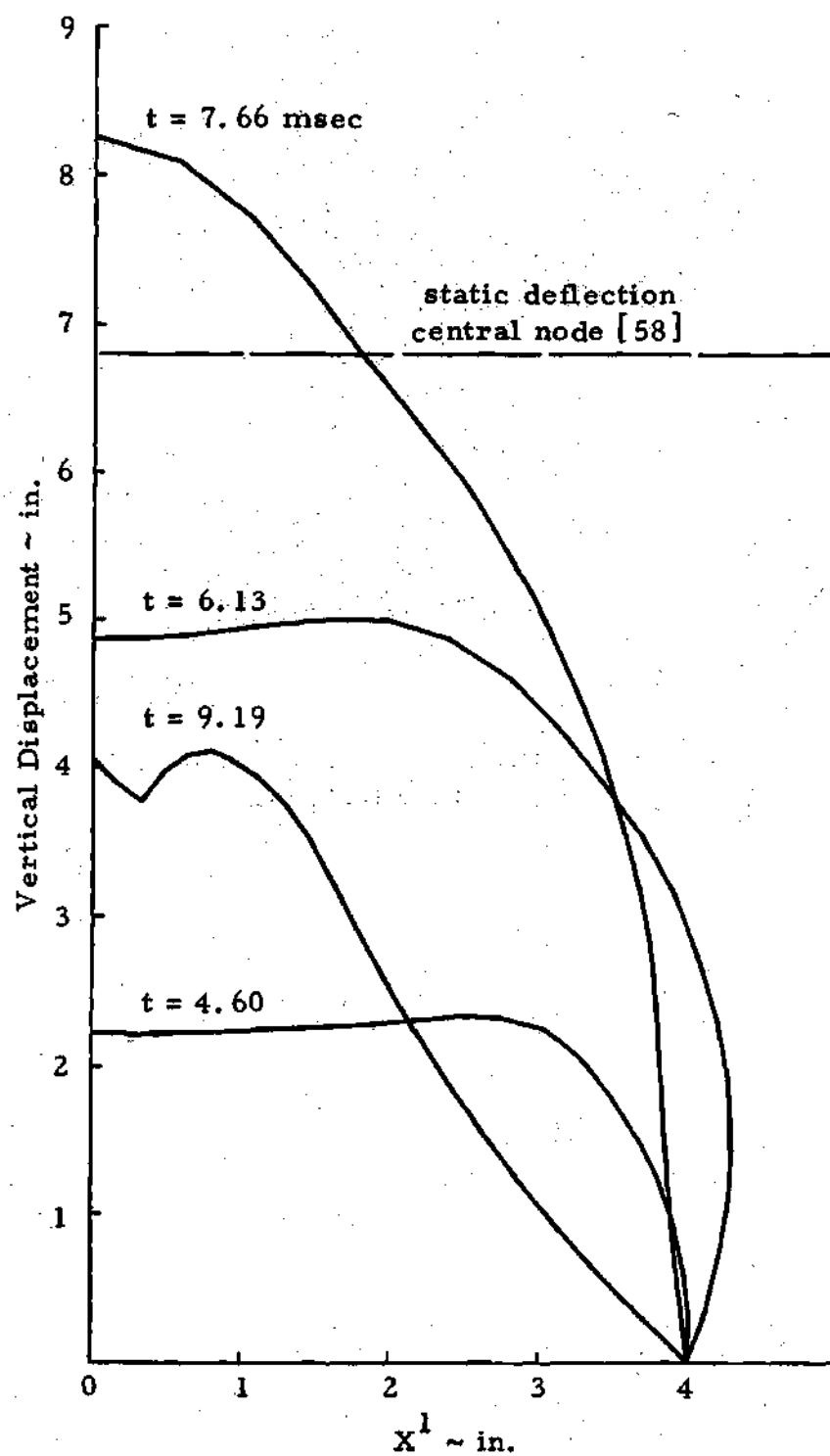
Figure 16. Deformed Profiles of Circular Membrane. Case 1

Then, even though the pressure is removed at t = 0.006 sec, the membrane continues to expand until t = 7.66 msec, and then rebounds until it wrinkles as shown in Fig. 16. Figure 17 shows perspective views of the deformed finite-element mesh calculated at about every millisecond.

Since the static vertical displacement of the center of the membrane was found in [57] to be 6.8 in. due to a uniform transverse pressure of 1.65 psi, we can define a dynamic magnification factor of sorts for this problem.

$$\mu = \frac{u_3^1 \text{ (dynamic)}}{u_3^1 \text{ (static)}} = \frac{u_3^1 \text{ (dynamic)}}{6.8} \qquad (6.43)$$

where u_3^1 is the vertical displacement of node 1, the center node. For this case then, we have $\mu = 1.21$.

Case 2. The membrane profile at various times is shown in Figs. 18 and 19. As before, the membrane initially expands with a flat central part, but in this case, the central portion "snaps" past the peaked configuration shown at t = 7.66 msec into a round balloon-like shape shown at t = 8.17 millisecond. This "snap-through" motion is also indicated in Fig. 20 where the vertical deflection time history of
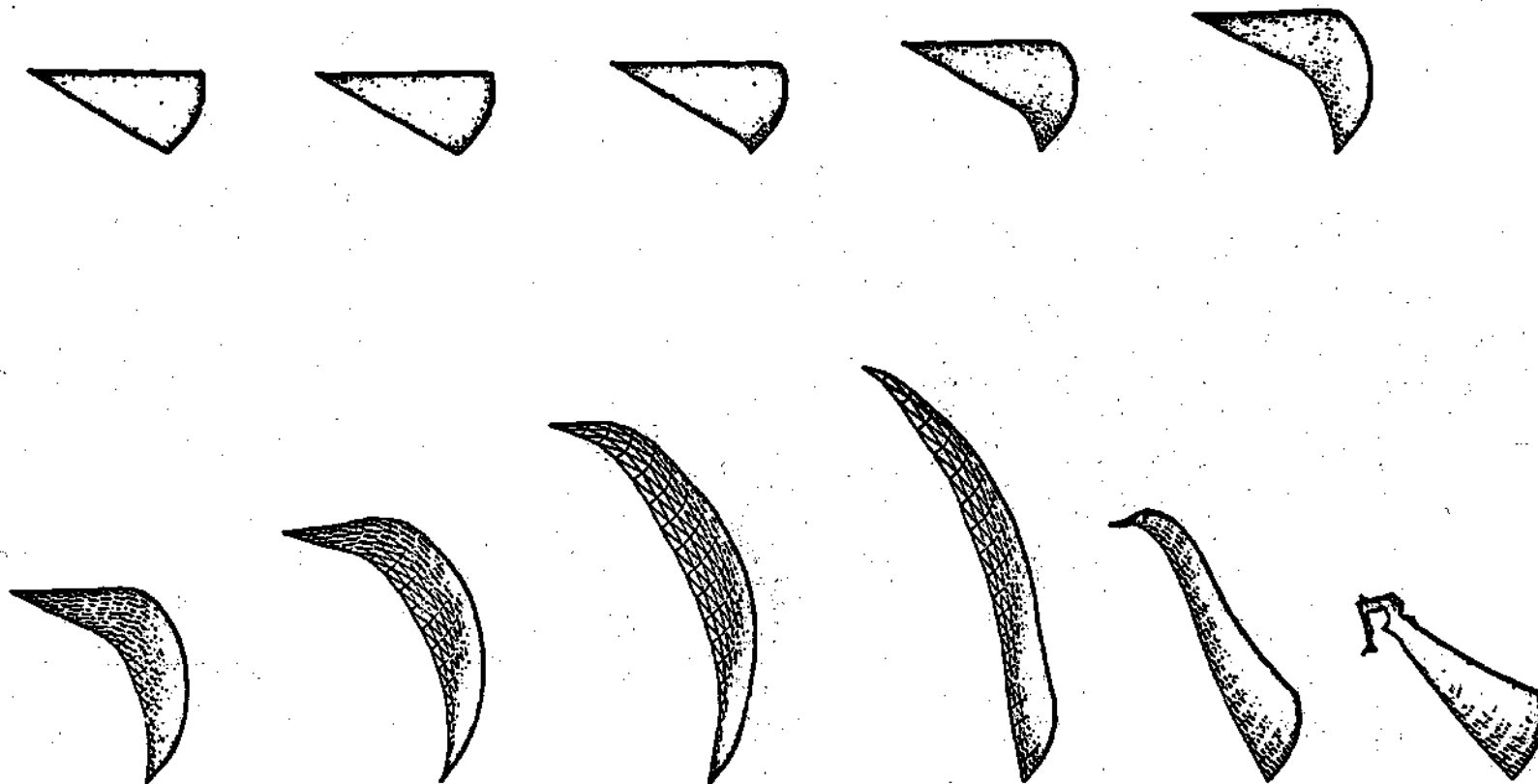
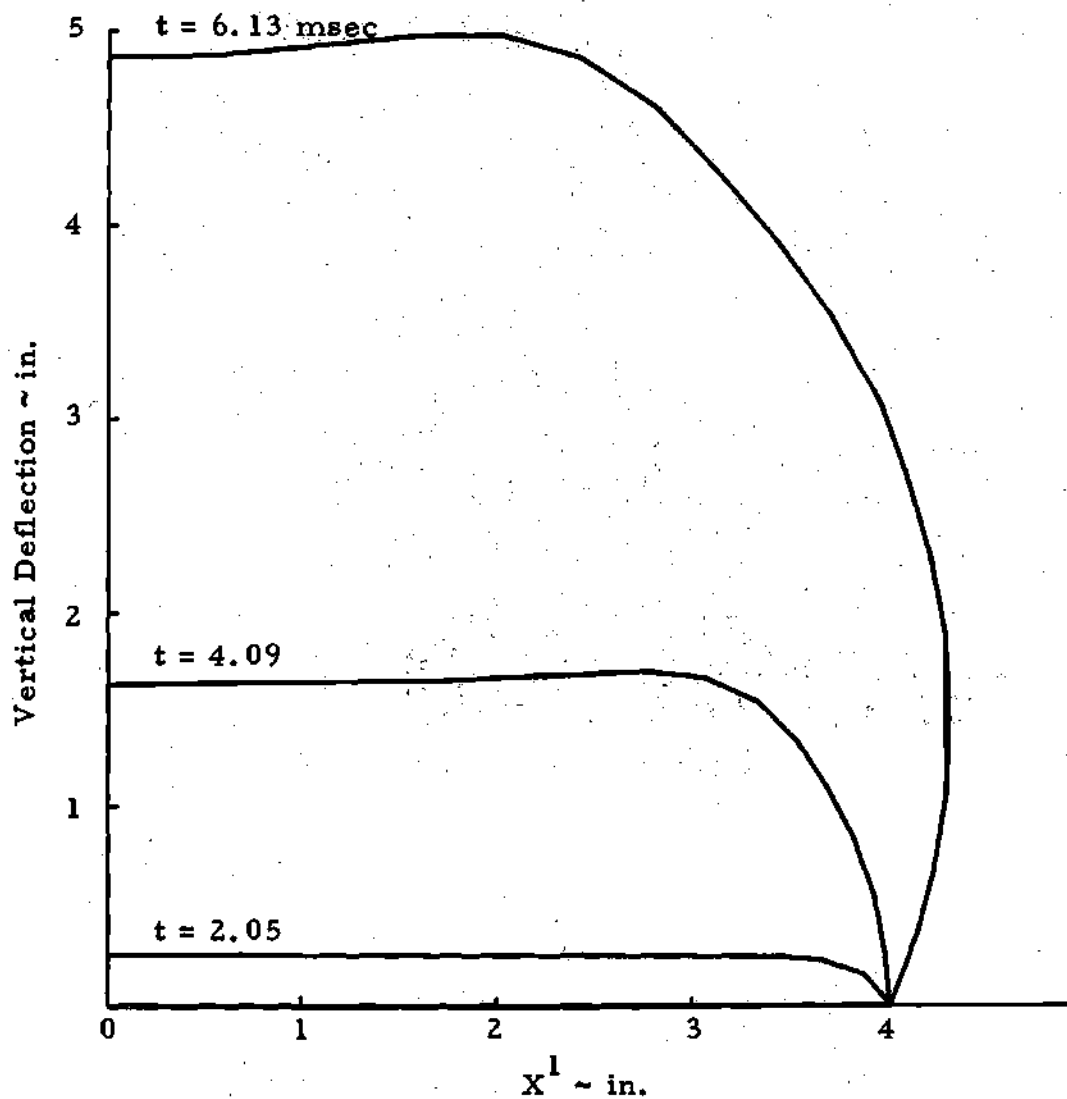Figure 17. Perspective Views of Deformed Finite-element Mesh. Case 1

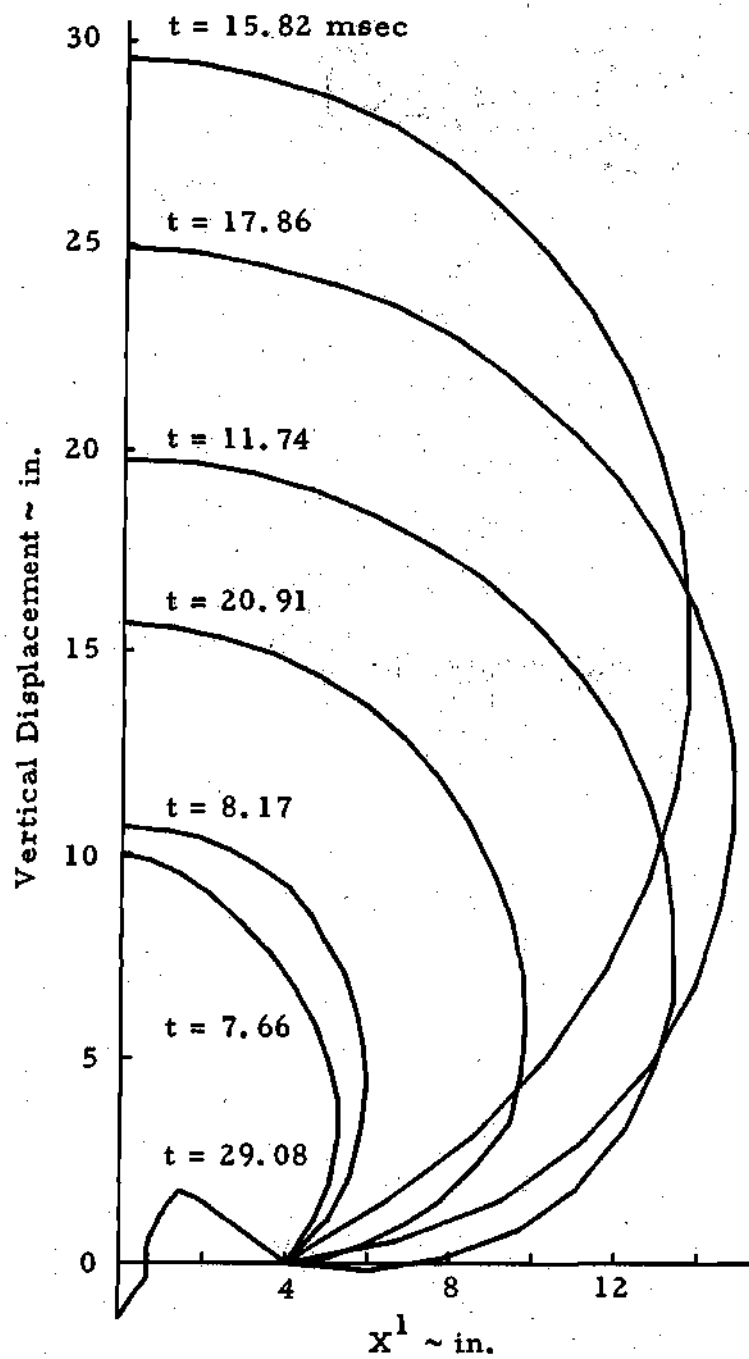Figure 18. Deformed Profiles of Circular Membrane. Case 2

Figure 19. Deformed Profiles of Circular Membrane. Case 2
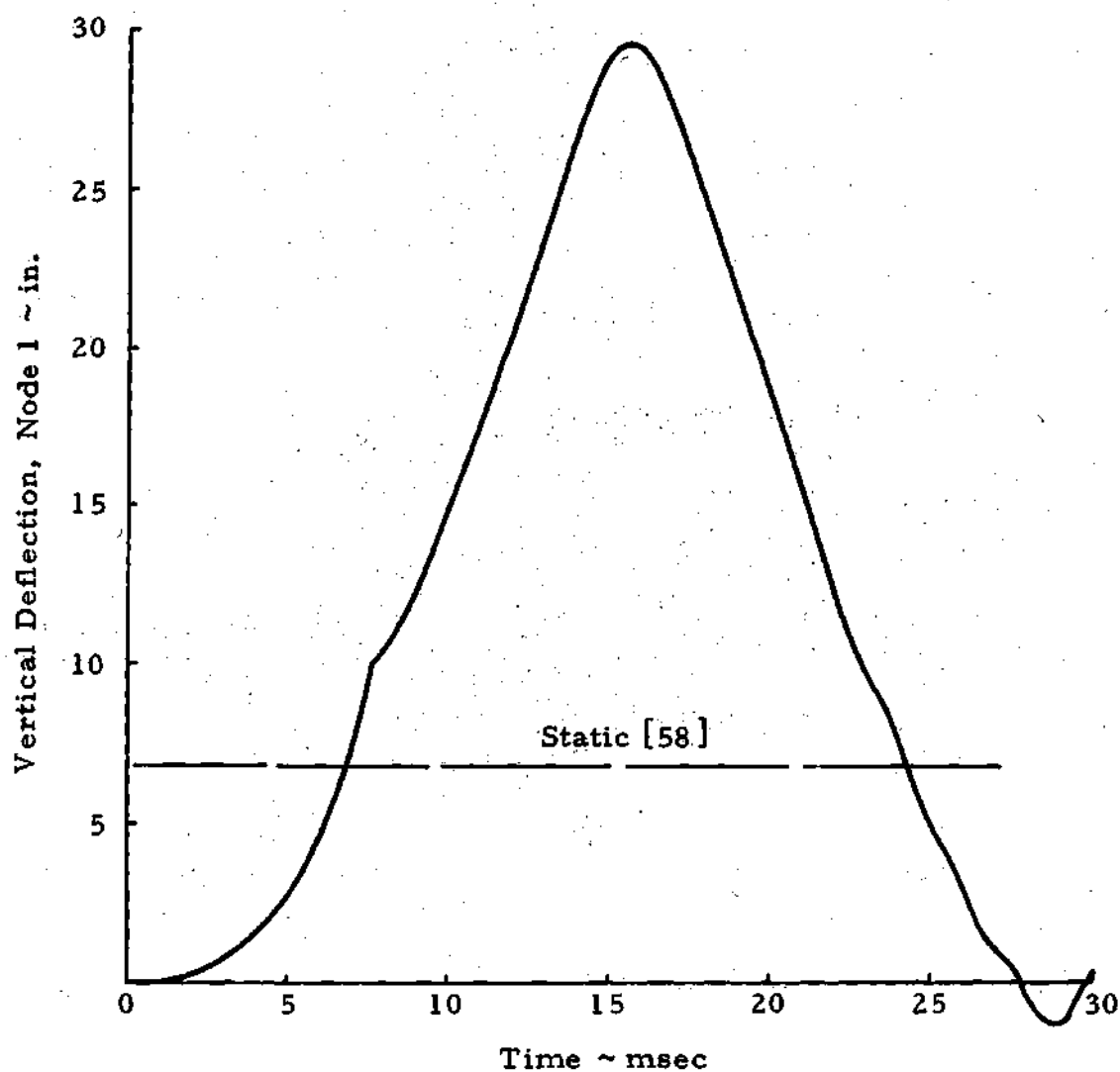
Figure 20. Time History of Vertical Displacement of Node 1. Case 2

the central node is shown. From Fig. 19 we can see that the membrane continues to inflate, balloon-like, until t = 15.82 msec and then rebounds past the initial position as shown at t = 29.08 milliseconds. At t = 15.82 msec the vertical displacement of the central node is seen to be 29.6 in.; thus for case 2, the dynamic magnification factor (6.43) is μ = 4.35.

Case 3. The loading differs from case 2 in that a sinusoidally varying pressure is applied at t = 0.004 seconds. The effect of this superposed pressure variation can be seen in the vertical deflection time history of the central node, shown in Fig. 21. Here it can be seen that, although the pressure begins to vary at t = 4 msec, the "snap-through" into a round balloon still happens at about t = 8 msec as it did for case 2. Also, the maximum deflection occurs at almost the same time as it did in case 2, but it is over 4 in. less--the dynamic magnification factor for this case is μ = 3.73. Membrane profiles at various times are shown in Fig. 22 for this case. Figure 23 shows perspective views of the deformed finite-element mesh calculated at various times for the case 3 loading. Successive views shown in Fig. 23 were calculated every millisecond for 22 milliseconds.

Thirty minutes on the UNIVAC 1108 were required to complete 2200 time integration steps. A 16mm film was made and the frames presented in Fig. 23 are from that film.
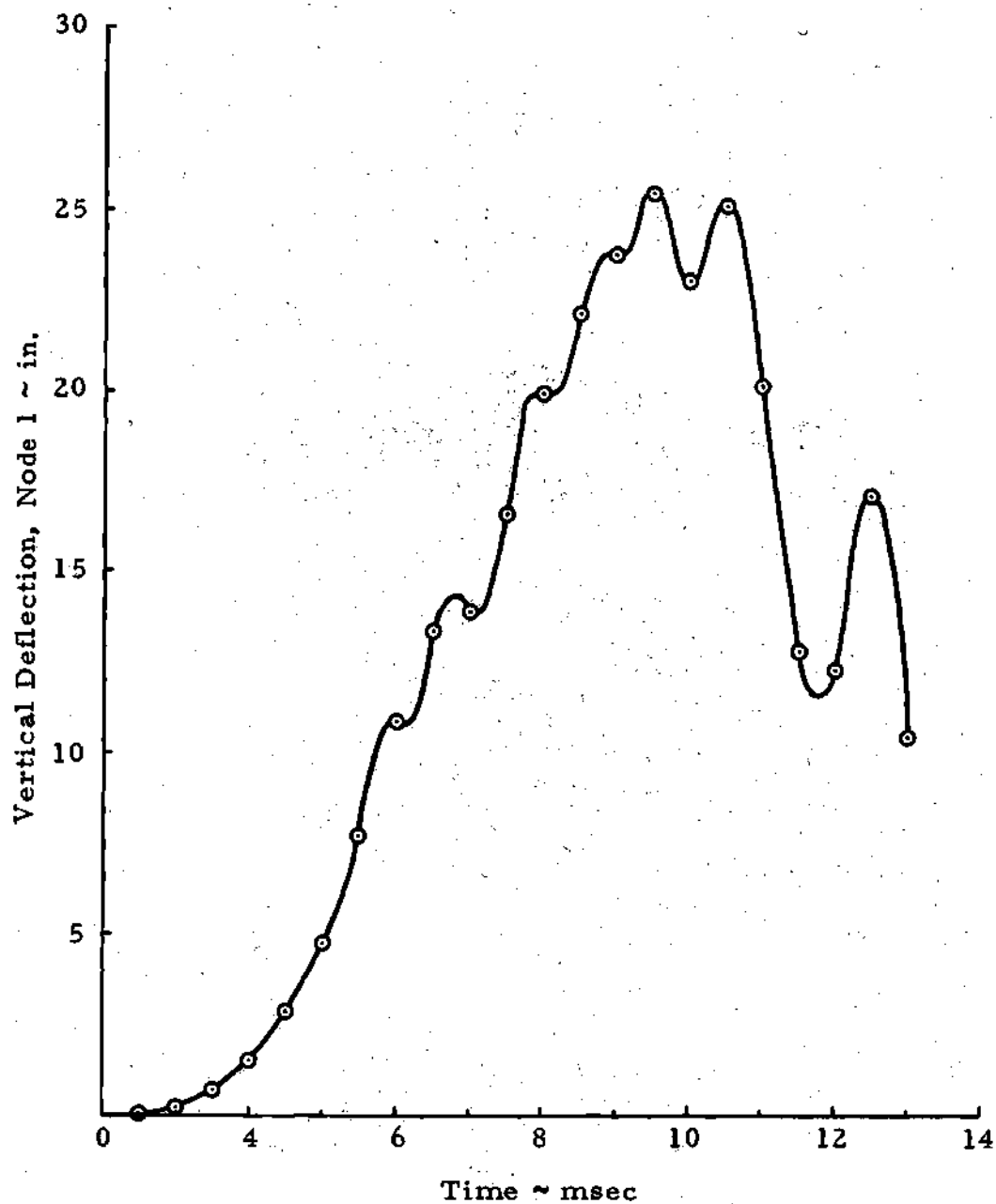
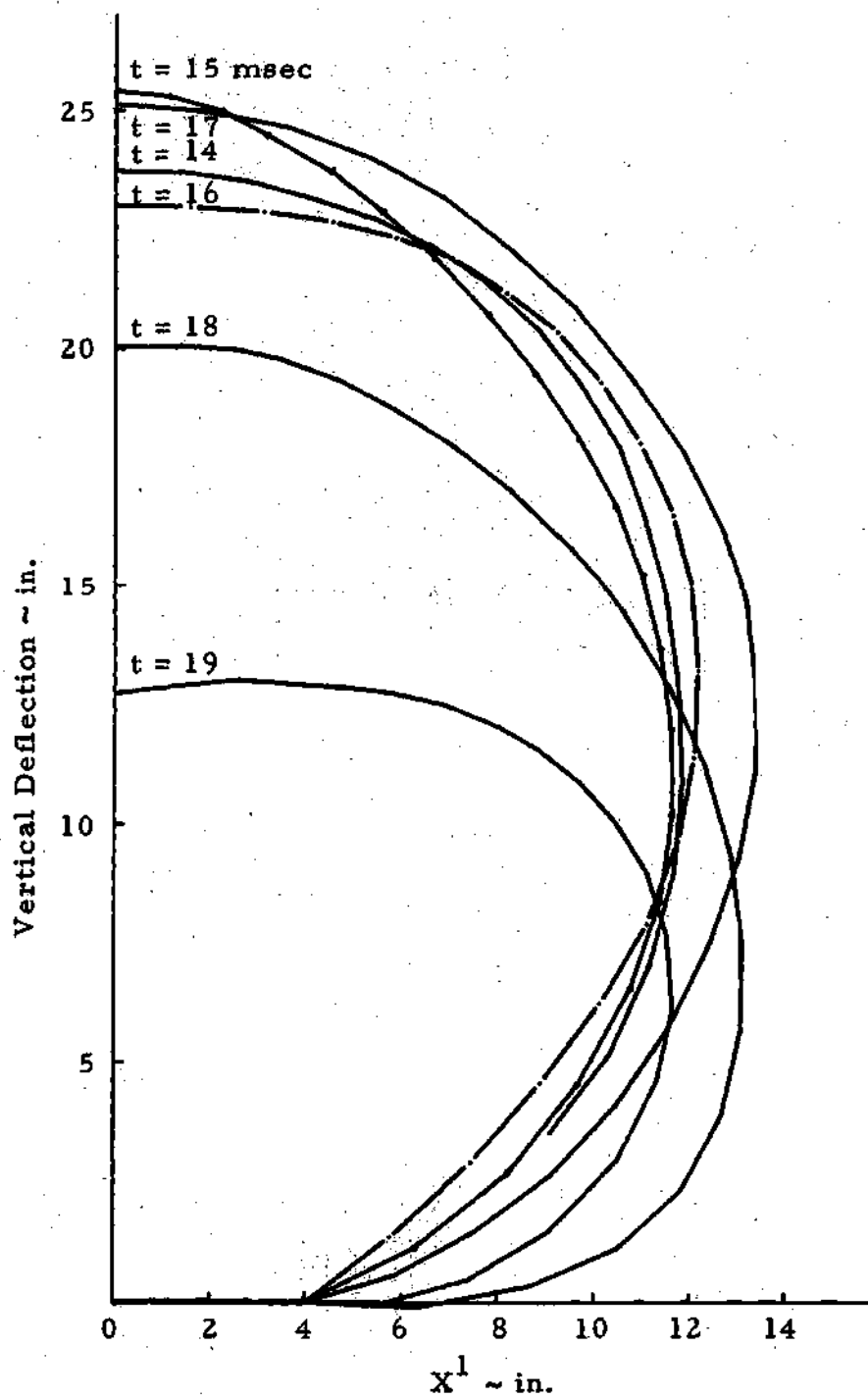Figure 21. Time History of Vertical Displacement of Node 1. Case 3

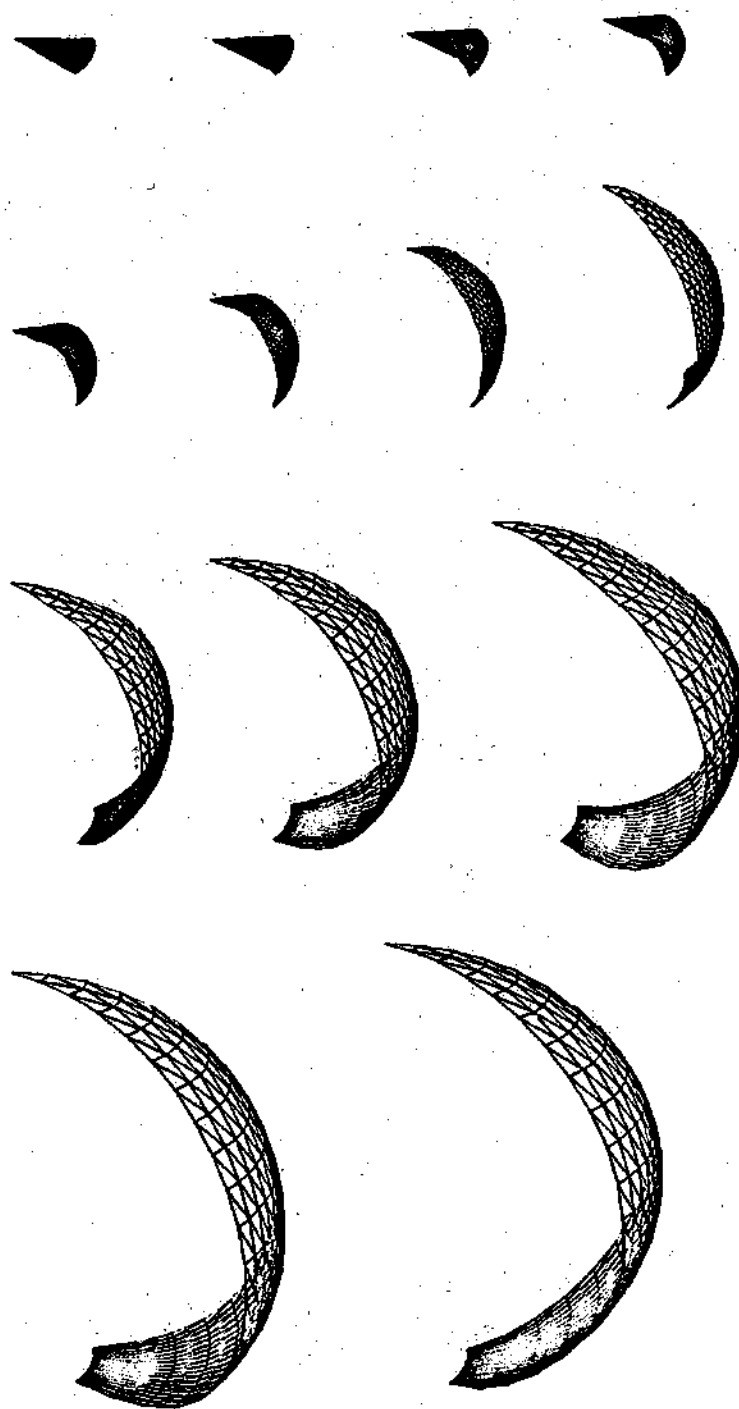Figure 22. Deformed Profiles of Circular Membrane. Case 3

Figure 23. Perspective Views of Deformed Finite-element Mesh.
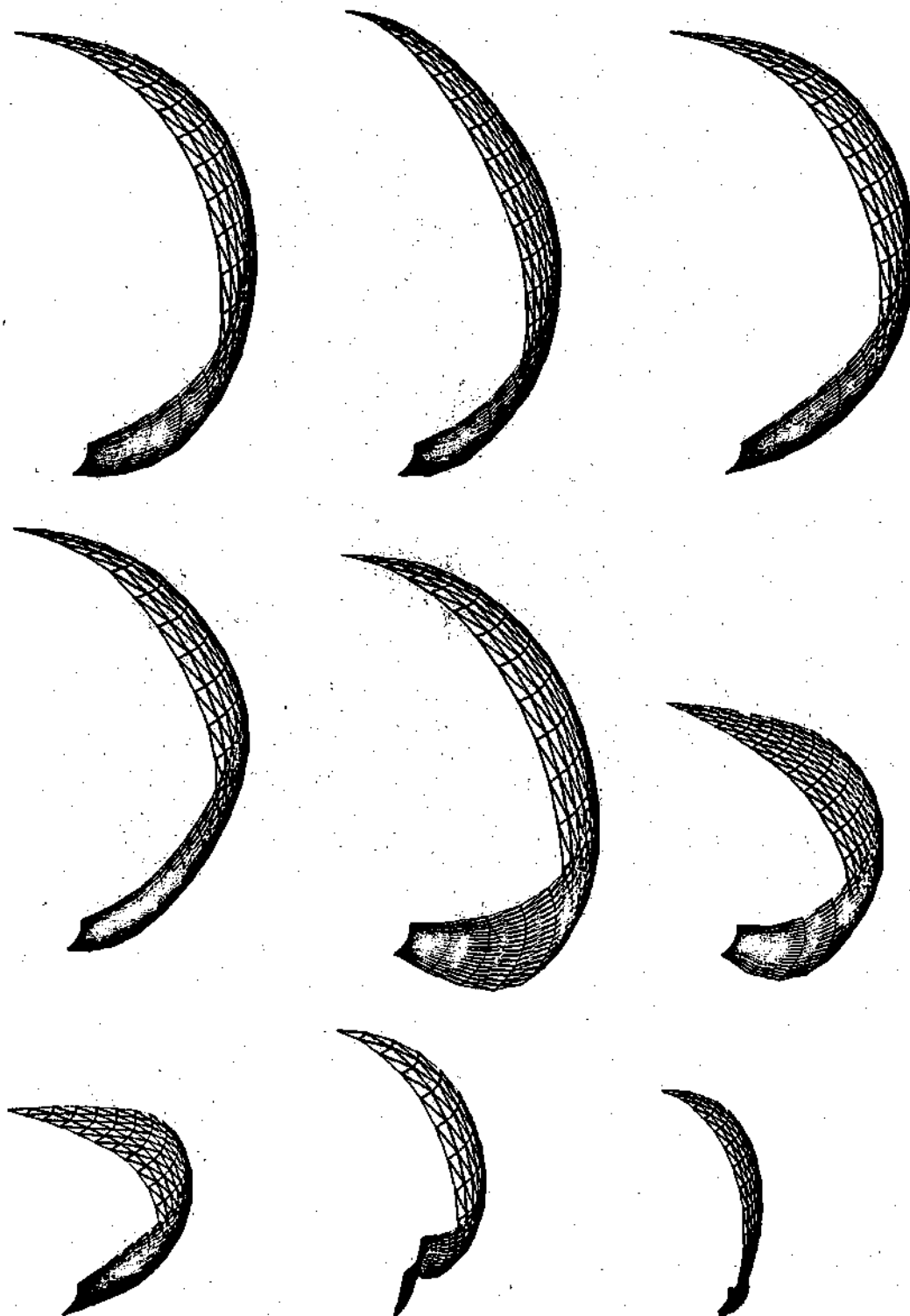Case 3 (Sheet 1 of 2)

Figure 23. Perspective Views of Deformed Finite-element Mesh.
Case 3 (Sheet 2 of 2)

CHAPTER VII

SUMMARY AND CONCLUSIONS

7.1 Summary

The objective of this research was to develop approximate methods for the quantitative analysis of the dynamic response of arbitrary elastic bodies at finite strain. Finite element models of thin incompressible hyperelastic membranes are developed, which involve large systems of second-order nonlinear differential equations in nodal displacements.

One dimensional versions of these equations are first solved using a variety of time integration schemes in conjunction with the successful extension of the finite-element method to one-dimensional elastodynamic problems with finite strain. Qualitative arguments and studies of various cases confirm that shock waves can develop, even in cases in which smooth initial data are prescribed. Using the one-dimensional finite element equations, it was possible to verify numerically the theoretical estimate (X_{CR}, t_{CR}) for evolution of a shock wave from Lipschitz continuous initial data. In the presence of shocks, the standard integration schemes are ineffective, and it is necessary to seek an integration scheme adequate for shock propagation studies.

A new explicit integration scheme, which combines features of the Lax-Wendroff method and finite elements, is developed and used successfully to study the formation, reflection, and propagation of shock and acceleration waves in hyperelastic rods. A number of cases are studied numerically.

Motivated by the absence of any convergence criteria or numerical stability criteria for finite-element approximations of nonlinear hyperbolic equations, a study of these equations for the subject class of problems is initiated. Therein, a rigorous analysis of numerical stability and convergence of finite element approximations of nonlinear hyperbolic equations is given. Precise stability criteria and error estimates are derived. It is shown that while lumped and consistent mass finite-element models have the same convergence rate in natural energy norms, the lumped mass model is numerically more stable.

The investigation then returns to two- and three-dimensional membrane problems. A number of cases are considered while apparently represent the first solution of any type to problems of this kind.

7.2 Conclusions

From the work done in this research and examining the results of the numerical examples, the following conclusions were reached:

1. The finite-element method can be successfully used to solve elastodynamic problems with finite strain.

2. The finite-element method can be successfully used for the study of the formation and propagation of shock and acceleration waves.

3. The explicit integration scheme developed in Chapter IV can be used to study the formation and propagation of weak shock and acceleration waves. The success of this scheme, as presented herein, stems from the nature of the Lax-Wendroff equations (cf., [86], p. 302) being such that they contain a built-in dissipative mechanism and hence can sometimes be used in unmodified form for shocks. However, the order of the effective dissipation is the same as the order of the truncation error, so we obtain solutions of systems of conservation laws as limits of solutions of parabolic equations as the coefficient of the dissipative term goes to zero. Since the solution converges everywhere outside the shock, it is our expectation that it will converge at the shock.

4. An essential feature of our integration scheme is that the spatial derivative in the conservation law is replaced by a difference quotient involving nodal values. By rewriting (3.16) as (3.18) and using only a linear finite-element approximation, we are able to represent all the required quantities with nodal values. If we use (3.16) with a linear finite-element approximation, the quantites required by the Lax-Wendroff equations (the stress and wave speed) are double-valued at the nodes, so that nothing is gained with this particular model.

5. The stability of the finite-element/finite-difference scheme is assured of $(h/\Delta t) > \nu_\alpha C^i_{max}(u_x)/\sqrt{2}$, where h is the minimum mesh length for the finite-element model, ν_α ($\alpha = 1, 2$) are constants, ν_1 corresponding to a consistent mass formulation and ν_2 to a lumped mass formulation, and $C^i_{max}(u_x)$ is the maximum speed of propagation of acceleration waves relative to the material for all X at time $t = i\Delta t$. Obviously, this result reduces to similar criterion obtained for linear difference approximations when C^i_{max} = constant.

6. To maintain stability for a given finite-element/difference scheme with fixed h, it is necessary to use a smaller time step for the consistent mass formulation than for the lumped mass formulation since $\nu_1 > \nu_2$!

7. Under the assumptions stated in Chapter V, the square of the L_2 norm, $\|e^i_x\|^2$, of the gradient of error of the finite-element approximation at each time step i is $O(h^2 + (\Delta t)^2)$. (Similar accuracies are obtained after R time steps in the linear case.) Uniform convergence of the error e is also obtained.

8. The same rates-of-convergence for the consistent mass formulation are obtained for the lumped mass formulation.

9. The above stepwise stability estimate was incorporated in the velocity formulated difference scheme discussed in Chapter IV. It was found that in this case, there was no increase in accuracy, stability, or

computational efficiency. It does seem, however, that a variable time-step integration scheme would be advantageous in solving problems with more than one spatial dimension.

7.3 Recommendations

The following topics are suggested areas of interest which would extend this investigation.

1. Use higher order finite-element models. Approximating the displacement gradients with linear finite-element models is roughly equivalent to using a quadratic finite-element approximation for the displacement. It would be expected that higher order finite-element approximations would result in both increased accuracy and stability of the solution.

2. Consider compressible materials

3. Extend the analysis to three-dimensional bodies.

4. Obtain general numerical stability estimates for finite-element approximations of nonlinear hyperbolic equations.

5. Investigate the merits of different forms of integration schemes, where a purely artificial dissipative mechanism is introduced into the difference equations(as originally suggested by von Neumann and Richtmyer [88] and later developed for conservation laws by Lax and Wendroff [86]), used in conjunction with finite-element approximations.

6. Check the practicality of using a variable time step integration scheme, particularly for other than one-dimensional problems, to take advantage of the stepwise stability estimate.

7. Investigate the possibility of using either the two-dimensional Lax-Wendroff integration scheme described in [98] or the two-dimensional two-step Lax-Wendroff method described in [87] for the study of shock waves in elastic bodies. As reported in [98], the two-dimensional Lax-Wendroff scheme has been used by S. Burnstein in a series of highly successful calculations of shocked flows in a narrowing channel, a portion of which are described in [99].

APPENDIX

PERTURBATION STABILITY ANALYSIS

As an interesting sidelight, we study the stability of the nonlinear wave equation (3.19) using standard central differences to approximate all derivatives. To this end, we turn to the often used heuristic procedure wherein the actual solution to (3.19), $u(X,t)$, is perturbed a small amount $\epsilon(X,t)$. Incorporating the perturbed solution, $\bar{u} = u + \epsilon$, subtracting (3.19), then linearizing the result with respect to the perturbation ϵ, we seek conditions for the stability of the linearized equation. Hence, setting $\bar{u} = u + \epsilon$, we get the perturbed extension ratio

$$\bar{\lambda} = 1 + u_X + \epsilon_X = \lambda + \epsilon_X \tag{A.1}$$

and from (3.22)

$$\bar{\sigma}_X = 2[C_1(1 + 2\bar{\lambda}^{-3}) + 3C_2\bar{\lambda}^{-4}]\bar{u}_{XX} \tag{A.2}$$

Now, for ϵ small enough, i.e., for $\epsilon^2 \ll 1$, we can say

$$\bar{\lambda}^{-3} = (\lambda + \epsilon_X)^{-3} \doteq \lambda^{-3} - 3\lambda^{-4}\epsilon_X \qquad \text{(A. 3)}$$

$$\bar{\lambda}^{-4} = (\lambda + \epsilon_X)^{-4} \doteq \lambda^{-4} - 4\lambda^{-5}\epsilon_X \qquad \text{(A. 4)}$$

Then, using (A. 1), (A. 3), and (A. 4), (A. 2) can now be written, correct to $O(\epsilon_X^2)$, as

$$\bar{\sigma}_X = \sigma_X + 2u_{XX}\epsilon_X(-6C_1\lambda^{-4} - 12C_2\lambda^{-5}) \qquad \text{(A. 5)}$$

$$+ 2\epsilon_{XX}[C_1(1 + 2\lambda^{-3}) + 3C_2\lambda^{-4}]$$

Finally, after some algebra, we obtain the linearized perturbation equation in the form

$$\ddot{\epsilon} - A(u_X, u_{XX})\epsilon_X - c^2(u_X)\epsilon_{XX} = 0 \qquad \text{(A. 6)}$$

where

$$A(u_X, u_{XX}) = \frac{-12}{\rho_o}(C_1\lambda^{-4} + 2C_2\lambda^{-5})u_{XX} \qquad \text{(A. 7)}$$

and $c^2(u_X)$ is defined in (3. 27). Assuming a smooth solution to (3. 19), we can consider the product $\epsilon_X u_{XX}$ to be of second order so that

(A. 6) becomes

$$\ddot{\epsilon} - c^2 \epsilon_{XX} = 0 \tag{A. 8}$$

If the two derivatives in (A. 8) are both approximated by divided second central differences, centered at the point (X_m, t_n), for the purpose of a step-by-step numerical solution, the resultant simulation can be written in the form

$$E_{m, n+1} - 2E_{m, n} + E_{m, n-1} = d^2(E_{m+1, n} - 2E_{m, n} + E_{m-1, n}) \tag{A. 9}$$

where

$$d^2 = c^2 \left(\frac{\Delta t}{\Delta X}\right)^2 \tag{A. 10}$$

To investigate the stability of (A. 9), we seek solutions of the form

$$E_{m, n} = \beta^n e^{i\alpha m} \tag{A. 11}$$

where α and β are constants, with α real. Substituting (A. 11) into (A. 9) yields the equation

$$\beta^2 - 2\left(1 - 2d^2\sin^2\frac{\alpha}{2}\right)\beta + 1 = 0 \qquad\qquad \text{(A. 12)}$$

The question of stability lies in determining under what conditions the magnitude of β does not exceed unity for all real values of α. Thus, to prevent solutions of the type (A. 11) from growing exponentially in magnitude as n increases, we require that the discriminant of (A. 12) be less than or equal to zero

$$\left(1 - 2d^2\sin^2\frac{\alpha}{2}\right)^2 - 1 \leq 0 \qquad\qquad \text{(A. 13)}$$

and hence we must have

$$d^2 \leq \frac{1}{\sin^2\frac{\alpha}{2}} \qquad\qquad \text{(A. 14)}$$

for all real values of α. From this it follows that the condition for stability is

$$d = c(u_X)\frac{\Delta t}{\Delta X} \leq 1 \qquad\qquad \text{(A. 15)}$$

From (A. 15) we see that, as was expected from choosing an explicit temporal integration scheme to get (A. 9), we have conditional numerical stability. However, it is of interest to note that for the

nonlinear one-dimensional problem, the critical time step is dependent

upon the longitudinal extension ratio, λ. In other words, for a fixed

ΔX, the critical time step required for numerical stability is dependent

on the current state of strain. This result is clearly shown in Fig. 24

for a Mooney-Rivlin material, where we first substituted (3.27) into

(A.15) to get

$$\frac{\Delta X}{\Delta t} \geq \sqrt{\frac{2}{\rho_0} C_1 (1 + 2\lambda^{-3}) + \frac{6}{\rho_0} C_2 \lambda^{-4}} \qquad (A.16)$$

and then calculated the artificial wave speed, $\Delta X / \Delta t$, for various

values of λ with $C_1 = 24$ psi and $C_2 = 1.5$ psi. Figure 24 shows that

for the more realistic values of the artificial wave speed (say

$\Delta X / \Delta t \geq 1200$ in/sec) there are states of strain at which the numerical

solution is not stable. Conversely, for a given strain state (i.e., for

any λ) one can find a stable signal speed for the difference scheme.

(For comparative purposes, the stability curve for the more rigorous

stability estimate (5.28) is also shown in Fig. 24.)

The plausibility of this result can be argued on the following

physical basis: for the linear problem, the critical time step is related

to the shortest transit time between any two nodal points in the finite

element mesh and it is a fixed critical value. But one thing that makes

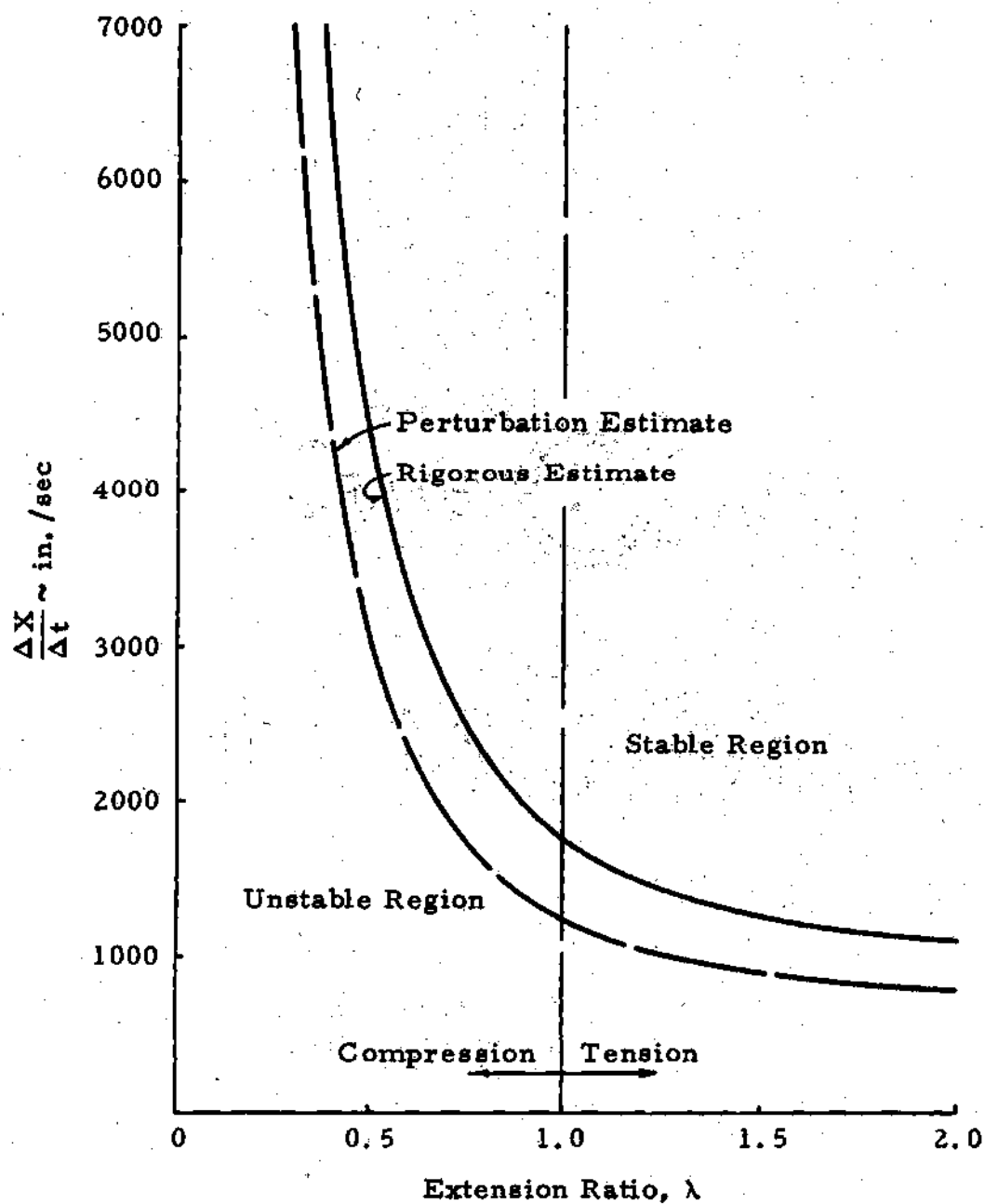a linear problem linear is being restricted to infinitesimal strains. In

Figure 24. Numerical Stability for the Longitudinal Vibration of a Rod

other words, in the linear problem, the relative displacement between

any two nodal points is very small. Now, in going to the nonlinear

problem, one might still expect the critical time step to be related to

the finite element mesh size; but here there may be an appreciable

deformation in the mesh--hence a varying value of the critical time step.

This can be seen in Fig. 24, where for increasing values of λ

(increasing distance between nodes), there is a corresponding increase

in the critical time step required for the numerical stability of the

integration scheme.

REFERENCES

1. Rivlin, R. S., "Large Elastic Deformations of Isotropic Materials, I. Fundamental Concepts (Vol. A240, pp. 459-490), IV. Further Developments of the General Theory (Vol. A241, pp. 379-397)," Philosophical Transactions of the Royal Society, 1948.

2. Adkins, J. E. and Rivlin, R. S., "Large Elastic Deformations of Isotropic Materials, X. Reinforcement by Inextensible Cords," Philosophical Transactions of the Royal Society, Vol. A248, pp. 201-223, 1955.

3. Truesdell, C. (Editor), Continuum Mechanics I: The Mechanical Foundations of Elasticity and Fluid Dynamics, Gordon and Breech, Science Publishers, Inc., 1966.

4. Shahinpoor, M. and Nowinski, J. L., "Exact Solution to the Problem of Forced Large Amplitude Radial Oscillations of a Thin Hyperelastic Tube," International Journal of Nonlinear Mechanics, Vol. 6, pp. 193-207, 1971.

5. Courant, R., "Variational Methods for the Solution of Problems of Equilibrium and Vibration," Bulletin, American Mathematical Society, Vol. 49, pp. 1-23, 1943.

6. Turner, M. J., Clough, R. W., Martin, H. C., and Topp, L. J., "Stiffness and Deflection Analysis of Complex Structures," Journal of Aerospace Sciences, Vol. 23, pp. 805-823, 1956.

7. Zienkiewicz, O. C., The Finite Element Method in Structural and Continuum Mechanics, McGraw-Hill Publishing Company Ltd., London, 1967.

8. Zienkiewicz, O. C., The Finite Element Method in Engineering Science, McGraw-Hill Book Company, New York, 1971.

9. Przemieniecki, J. S., Theory of Matrix Structural Analysis, McGraw-Hill Book Company, New York, 1968.

10. Martin, H. C., Introduction to Matrix Methods of Structural Analysis, McGraw-Hill Book Company, New York, 1966.

11. Przemieniecki, J. S., et al. (Editors), Proceedings of the First Conference on Matrix Methods in Structural Mechanics, AFFDL-TR-66-80, Wright-Patterson Air Force Base, Ohio, 1966.

12. Berke, L., et al. (Editors), Proceedings of the Second Conference on Matrix Methods in Structural Mechanics, AFFDL-TR-68-150, Wright-Patterson Air Force Base, Ohio, 1968.

13. Argyris, J. H., "On the Analysis of Complex Elastic Structures," Applied Mechanics Review, Vol. 11, No. 7, pp. 331-338, 1958.

14. Argyris, J. H., "Matrix Analysis of Plates and Shells," Ingenieur-Archiv, XXXV, pp. 102-142, 1966.

15. Singhal, A. C., "775 Selected References on the Finite Element Method and Matrix Methods of Structural Analysis," Report S-12, Civil Engineering Department, Laval University, Quebec, Jan., 1969.

16. Felippa, C. A. and Clough, R. W., "The Finite Element Method in Solid Mechanics," Proceedings, Symposia in Applied Mathematics--Numerical Solution of Field Problems, Vol. 21, 1969.

17. Oden, J. T., Finite Elements of Nonlinear Continua, McGraw-Hill Book Company, New York, 1971.

18. Oden, J. T., "Finite Element Applications in Nonlinear Structural Analysis," Proceedings of the Symposium on Application of Finite Element Methods in Civil Engineering, Vanderbilt University, Nashville, Tennessee, pp. 419-456, 1969.

19. Gallagher, R. H., Yamada, Y., and Oden, J. T., (Editors), Recent Advances in Matrix Methods of Structural Analysis and Design, University of Alabama Press, Tuscaloosa, 1971. (Proceedings, U.S.-Japan Seminar on Matrix Methods of Structural Analysis and Design, Tokyo, 1969.)

20. Oden, J. T., Clough, R. W., and Yamamoto, Y., (Editors), Advances in Computational Methods in Structural Mechanics and Design, The University of Alabama in Huntsville Press, Huntsville, 1972. (Proceedings, 2nd U.S.-Japan Seminar on Matrix Methods of Structural Analysis and Design, Aug., 1972.)

21. Knowles, J. K., "Large Amplitude Oscillations of a Tube of Incompressible Elastic Material," Quarterly of Applied Mathematics, Vol. 18, No. 1, April, 1960.

22. Knowles, J. K., "On a Class of Oscillations in the Finite-Deformation Theory of Elasticity," Journal of Applied Mechanics, Vol. 29, pp. 283-286, 1962.

23. Knowles, J. K. and Jakub, M. J., "Finite Dynamic Deformations of an Incompressible Elastic Medium Containing a Spherical Cavity," Archive for Rational Mechanics and Analysis, Vol. 18, pp. 367-378, 1965.

24. Truesdell, C. A., (Editor), Continuum Mechanics IV: Problems in Non-Linear Elasticity, Gordon and Breach, Science Publishers, Inc., New York, 1965.

25. Guo, Z. H. and Solecki, R., "Free and Forced Finite Amplitude Oscillations of an Elastic Thick-Walled Hollow Sphere Made of Incompressible Material," Archiwum Mechaniki Stosowanej, Vol. 15, pp. 424-433, 1963.

26. Wang, C. C., "On the Radial Oscillations of a Spherical Thin Shell in the Finite Elasticity Theory," Archive for Rational Mechanics and Analysis, Vol. 23, pp. 270-274, 1965.

27. Nowinski, J. L. and Wang, S. D., "Finite Radial Oscillations of a Spinning Thick-Walled Cylinder," Journal of the Acoustical Society of America, Vol. 40, No. 6, pp. 1548-1553, Dec., 1966.

28. Nowinski, J. L. and Wang, S. D., "Galerkin's Solution to a Severely Non-linear Problem of Finite Elastodynamics," International Journal of Non-linear Mechanics, Vol. 1, pp. 239-246, 1966.

29. Wang, A. S. D., "On Free Oscillations of Elastic Incompressible Bodies in Finite Shear," *International Journal of Engineering Science*, Vol. 7, No. 12, pp. 1199-1212, Dec., 1969.

30. Wang, S. D., "Large Amplitude Oscillations of Thick and Thick-Walled Elastic Incompressible Bodies," Thesis, University of Delaware, 1967.

31. Wang, S. D., "A Perturbation Method as Applied to Problems of Finite Elastodynamic Deformations," *Journal of the Franklin Institute*, Vol. 289, No. 5, May, 1970.

32. Nowinski, J. L., "On a Dynamic Problem in Finite Elastic Shear," *International Journal of Engineering Science*, Vol. 4, pp. 501-510, 1966.

33. Biot, M. A., *Mechanics of Incremental Deformation*, John Wiley & Sons, New York, 1965.

34. Green, A. E. and Adkins, J. E., *Large Elastic Deformations*, Second Edition, Oxford University Press, Oxford, 1970.

35. Demiray, H. and Suhubi, E. S., "Small Torsional Oscillations of an Initially Twisted Circular Rubber Cylinder," International *Journal of Engineering Science*, Vol. 8, pp. 19-30, 1970.

36. Green, A. E., Problems of Continuum Mechanics, *Society for Industrial and Applied Mathematics*, Philadelphia, Pa., pp. 148-154, 1961.

37. Suhubi, E. S., "Small Longitudinal Vibration of an Initially Stretched Circular Cylinder," *International Journal of Engineering Science*, Vol. 2, No. 5, pp. 509-517, Jan., 1965.

38. Seide, P., "Small Vibrations of Uniformaly Compressed Isotropic Elastic Solids," *Journal of the Engineering Mechanics Division*, ASCE, Vol. 97, No. EM4, Aug., 1971.

39. Douglas, W. J., "Natural Vibrations of Finitely Deformable Structures," *AIAA Journal*, Dec., 1967.

40. Faulkner, T. R., "Finite Dynamic Deformation of an Almost Incompressible Elastic Spherical Shell," *International Journal of Engineering Science*, Vol. 9, pp. 889-898, 1971.

41. Courant, R. and Hilbert, D., *Methods of Mathematical Physics*, Vol. II, Interscience Publishers, New York, 1962.

42. Jeffrey, A. and Taniuti, T., *Non-Linear Wave Propagation*, Academic Press, New York, 1964.

43. Bland, D. R., *Nonlinear Dynamic Elasticity*, Blaisdell, Waltham, Mass., 1969.

44. Bland, D. R., "Dilatational Waves and Shocks in Large Displacement Isentropic Dynamic Elasticity," *Journal for the Mechanics of Physics and Solids*, Vol. 12, pp. 245-267, 1964.

45. Chu, B. T., "Finite Amplitude Waves in Incompressible Perfectly Elastic Materials," *Journal for the Mechanics of Physics and Solids*, Vol. 13, pp. 17-28, 1965.

46. Collins, W. D., "One-Dimensional Non-Linear Wave Propagation in Incompressible Elastic Materials," *Quarterly Journal of Mechanics and Applied Mathematics*, Vol. 19, pp. 259-328, 1966.

47. Achenbach, J. D., "Shear Waves in Finite Elastic Strain," *Quarterly of Applied Mathematics*, Vol. 25, pp. 306-310, 1967.

48. Achenbach, J. D. and Reddy, D. P., "Shear Waves in Finite Strain Generated at the Surface of a Viscoelastic Half-Space," *International Journal of Engineering Science*, Vol. 5, pp. 527-539, 1967.

49. Nair, S. and Nemat-Nasser, S., "On Finite Amplitude Waves in Heterogeneous Elastic Solids," *International Journal of Engineering Science*, Vol. 9, pp. 1087-1105, 1971.

50. Nowinski, J. L., "On the Propagation of Finite Disturbances in Bars of Rubberlike Materials," *Journal of Engineering for Industry*, ASME, Vol. 87, pp. 523-529, 1965.

51. Reddy, D. P. and Achenbach, J. D., "Simple Waves and Shock Waves in a Thin Prestressed Elastic Rod," _Zietschrift fuer Angewandet Mathematik und Physik_, Vol. 19, pp. 473-485, 1968.

52. Lax, P. D., _Hyperbolic Systems of Conservation Laws and the Mathematical Theory of Shock Waves_, Regional Conference Series in Applied Mathematics, SIAM, Philadelphia, Pa., 1973.

53. Chen, P. J., _Growth and Decay of Waves in Solids_, in "Encyclopedia of Physics," Vol. VI a/3, Mechanics of Solids III, Springer-Verlag, New York, pp. 303-402, 1973.

54. Oden, J. T. and Poe, J., "On the Numerical Solution of a Class of Problems in Dynamic Coupled Thermoelasticity," _Developments in Theoretical and Applied Mechanics_, Vol. V, Proceedings of the Fifth Southeastern Conference on Theoretical and Applied Mechanics, 1970, Raleigh, North Carolina, Pergamon Press, Oxford, England.

55. Oden, J. T. and Armstrong, W. H., "Analysis of Nonlinear, Dynamic Coupled Thermoviscoelasticity Problems by the Finite Element Method," _International Journal of Computers and Structures_, Vol. 1, pp. 603-621, 1971.

56. Kolsky, H., "Production of Tensile Shock Waves in Stretched Natural Rubber," _Nature_, Vol. 224, No. 5226, p. 1301, Dec., 1969.

57. Oden, J. T., "Analysis of Large Deformations of Elastic Membranes by the Finite Element Method," _Proceedings, IASS Congress on Large-Span Shells_, Leningrad, 1966.

58. Oden, J. T. and Sato, T., "Finite Strains and Displacements of Elastic Membranes by the Finite Element Method," _International Journal of Solids and Structures_, Vol. 3X, pp. 471-488, 1967.

59. Oden, J.T. and Sato T., "Structural Analysis of Aerodynamic Deceleration Systems," _Advances in the Astronautical Sciences_, Vol. 24, June, 1967.

60. Oden, J.T. and Kubitza, W. K., "Numerical Analysis of Nonlinear Pneumatic Structures," _Proceedings, International Colloquium on Pneumatic Structures_, Stuttgart, Germany, pp. 82-107, 1967.

61. Stricklin, J. A., et al., "Nonlinear Dynamic Analysis of Shells of Revolution by Matrix Displacement Method," AIAA/ASME 11th Structures, Structural, Dynamics, and Materials Conference, Denver, Colorado, April, 1970.

62. Marcal, P. V., "Finite Element Analysis of Combined Problems of Nonlinear Material and Geometric Behavior," Conference on Computational Approaches in Applied Mechanics, ASME, Chicago, June, 1969.

63. Hartzman, M., "Nonlinear Dynamics of Solids by Finite Element Methods," Ph.D. Dissertation, University of California, Livermore, 1969.

64. Oden, J. T., Chung, T. J., and Key, J. E., "Analysis of Nonlinear Thermoelastic and Thermoplastic Behavior of Solids of Revolution by the Finite Element Method," Preprints of the First International Conference on Structural Mechanics in Reactor Technology, Vol. 5, Part M, Berlin, Germany, Sept., 1971.

65. Green, A. E. and Zerna, W., Theoretical Elasticity, Second Edition, Oxford University Press, Oxford, 1968.

66. Blatz, P. and Ko, W. L., "Application of Finite Elasticity Theory to the Deformation of Rubbers," Transactions of the Society of Rheology, Vol. VI, pp. 223-251, 1962.

67. Mooney, M., "A Theory of Large Elastic Deformation," Journal of Applied Physics, Vol. 11, pp. 582-592, 1940.

68. Treloar, L. R. G., The Physics of Rubber Elasticity, Second Edition, Oxford University Press, Oxford, 1958.

69. Rivlin, R. S. and Saunders, D. W., "Large Elastic Deformations of Isotropic Materials, VII. Experiments on the Deformation of Rubber," Philosophical Transactions of the Royal Society, Vol. A243, pp. 251-288, 1951.

70. Gent, A. N. and Thomas, A. G., "Forms of Stored (Strain) Energy Function for Vulcanized Rubber," Journal of Polymer Science, Vol. 28, pp. 625-628, 1958.

71. Hart-Smith, L. J., "Elasticity Parameters for Finite Deformations of Rubber-Like Materials," Zietschrift fuer Angewandte Mathematik und Physik, Vol. 17, pp. 608-625, 1966.

72. Alexander, H., "A Constitutive Relation for Rubber-Like Materials," International Journal of Engineering Science, Vol. 6, No. 9, pp. 549-563, 1968.

73. Ames, W. F., "On Wave Propagation in One-Dimensional Rubber-like Materials," Journal of Mathematical Analysis and Applications, Vol. 34, No. 1, pp. 214-222, April, 1971.

74. Truesdell, C. A. and Noll, W., The Non-Linear Field Theories of Mechanics, in "Encyclopedia of Physics," Vol. III/3, Springer-Verlag, New York, 1965.

75. Courant, R. and Friedrichs, K. O., Supersonic Flow and Shock Waves, Interscience, New York, 1948.

76. Shapiro, A. H., The Dynamics and Thermodynamics of Compressible Fluid Flow, Vol. 1, The Ronald Press Co., New York, 1953.

77. Ames, W. F., "Discontinuity Formation in Solids of Homogeneous Non-Linear Hyperbolic Equations Possessing Smooth Initial Data," International Journal of Non-Linear Mechanics, Vol. 5, pp. 605-615, 1950.

78. Lax, P. D., "Development of Singularities of Solutions of Non-Linear Hyperbolic Partial Differential Equations," Journal of Mathematical Physics, Vol. 5, No. 5, pp. 611-613, May, 1964.

79. Jeffrey, A., "The Evolution of Discontinuities in Solutions of Homogeneous Nonlinear Hyperbolic Equations Having Smooth Initial Data," Journal of Mathematics and Mechanics, Vol. 17, No. 4, pp. 331-352, 1967.

80. Key, S. W. and Beisinger, Z. E., "The Transient Dynamic Analysis of Thin Shells by the Finite Element Method," Proceedings of the Third Conference on Matrix Methods in Structural Mechanics, Wright-Patterson Air Force Base, Ohio, October, 1971.

81. Krieg, R. D. and Key, S. W., "Transient Shell Response by Numerical Time Integration," Advances in Computational Methods in Structural Mechanics and Design, Edited by J. T. Oden, R. W. Clough and Y. Yamamoto. The University of Alabama in Huntsville Press, Huntsville, 1972.

82. Scarborough, J. B., Numerical Mathematical Analysis, Fifth Edition, The Johns Hopkins Press, Baltimore, 1962.

83. Scheid, F., Theory and Problems of Numerical Analysis, Schaum's Outline Series, McGraw-Hill Book Company, New York, 1968.

84. Ralston, A., A First Course in Numerical Analysis, McGraw-Hill Book Company, New York, 1965.

85. Lax, P. D., "Weak Solutions of Nonlinear Hyperbolic Equations and Their Numerical Computation," Communications on Pure and Applied Mathematics, Vol. 7, pp. 159-193, 1954.

86. Lax, P. and Wendroff, B., "Systems of Conservation Laws," Communications on Pure and Applied Mathematics, Vol. 13, pp. 217-237, 1960.

87. Richtmyer, R. D. and Morton, K. W., Difference Methods for Initial-Value Problems, Second Edition, Interscience Tracts in Pure and Applied Mathematics, No. 4, Interscience, New York, 1967.

88. Von Neumann, J. and Richtmyer, R. D., "A Method for the Numerical Calculations of Hydrodynamical Shocks," Journal of Applied Physics, Vol. 21, No. 3, pp. 232-237, March, 1950. Reprinted in John von Neumann Collected Works, Vol. 6, Pergaman Press, pp. 380-385, 1961.

89. Hicks, D. L. and Pelzl, R., Comparison Between a von Neumann-Richtmyer Hydrocode (AFWL's PUFF) and a Lax-Wendroff Hydrocode, Air Force Weapons Laboratory, AFWL-TR-68-112, 1968.

90. Oden, J. T. and Fost, R. B., "Convergence, Accuracy, and Stability of Finite-Element Approximations of a Class of Nonlinear Hyperbolic Equations," International Journal for Numerical Methods in Engineering, Vol. 6, pp. 357-365, 1973.

91. Fix, G. and Nassif, N., "On Finite Element Approximations to Time-Dependent Problems," Numeriche Mathematik (to appear).

92. Kikuchi, F. and Ando, Y., "A Finite Element Method for Initial Value Problems," Proceedings, Third Conference on Matrix Methods in Structural Mechanics, Wright Patterson Air Force Base, Dayton, 1971.

93. Fujii, H., "Finite Element Schemes: Stability and Convergence," Advances in Computational Methods in Structural Mechanics and Design, Edited by J. T. Oden, R. W. Clough, and Y. Yamamoto, The University of Alabama in Huntsville Press, Huntsville, 1972.

94. Fried, I., "Accuracy of Finite-Element Eigenproblems," Journal of Sound and Vibration, Vol. 18, pp. 289-295, 1971.

95. O'Brien, G. G., Hyman, M. A., and Kaplan, S., "A Study of the Numerical Solution of Partial Differential Equations," Journal of Mathematics and Physics, Vol. 29, pp. 223-251, 1951.

96. Mikhlin, S. G., Mathematical Physics, An Advanced Course, North-Holland Publishing Co., Amsterdam, 1970.

97. Oden, J. T., "Approximations and Numerical Analysis of Finite Deformations of Elastic Bodies," in Nonlinear Elasticity, Academic Press, New York, 1973.

98. Lax, P. D. and Wendroff, B., "Difference Schemes for Hyperbolic Equations with High Order of Accuracy," Communications on Pure and Applied Mathematics, Vol. 17, pp. 381-398, 1964.

99. Burnstein, S. Z., Numerical Calculations of Multidimensional Shocked Flows, New York University, Courant Institute of Mathematical Sciences, Research Report NYO 10433, 1963.

VITA

Ronald Burett Fost

I was born on March 30, 1937, in Oklahoma City, Oklahoma, the son of Burett and Lillus Fost. I received my primary and secondary education in Oklahoma City, graduating from Classen High School in May, 1955. I attended the University of Oklahoma from 1955 to 1957, majoring in Architecture. In September, 1957, I transferred to Oklahoma State University where I majored in Architectural Engineering. I received the degree of Bachelor of Architectural Engineering in 1961 and the degree of Master of Architectural Engineering in 1962, both from Oklahoma State University. Also in 1962, my military obligation was completed, as I had been an active member of the Oklahoma National Guard since 1954.

After graduating in 1962, I accepted employment with the Lockheed Aircraft Corporation, California Division. At Lockheed, I participated in their work-study program wherein I was a full-time (six hours per semester) graduate student at the University of California at Los Angeles for two years. Late in 1965, I transferred to Lockheed's Georgia Division in Marietta, Georgia. After satisfying the state residency requirements, I enrolled at Georgia

Institute of Technology in September, 1967, as a graduate student in the School of Engineering Mechanics. I received my M. S. in Engineering Mechanics in 1970. In 1971, I was given permission to conduct my thesis research for the Ph. D. degree in absentia at the Research Institute of the University of Alabama in Huntsville, under the supervision of Professor J. T. Oden. With the research essentially completed in December, 1972, I accepted part-time employment with Teledyne Brown Engineering in Huntsville, Alabama. I became a permanent employee there in March, 1974.

During the time I was at Georgia Tech, I received an NDEA Fellowship. I was also a graduate research assistant for four years and a graduate teaching assistant for two years. At the University of Alabama in Huntsville, I received a Research Assistantship from the Themis contract sponsored by the U. S. Air Force Office of Scientific Research.